Predicted and Measured Arrival Rates of Meteors over Forward-Scatter Links

Robert Stanley Mawrey
March 1991

Submitted in partial fulfilment of the requirements for the degree of Doctor of Philosophy in the Department of Electronic Engineering, University of Natal.

Abstract

Investigations into currently accepted methods of modelling variations in the arrival rate of meteors over forward-scatter meteor links have revealed some shortcomings. In these investigations, particular emphasis is placed on the work of Rudie due to its current acceptance in the literature. The non-uniform radiant distribution of meteors measured by Davies and modelled by Rudie, is critically examined and predictions using these models are compared with measured results taken over two forward-scatter links in the Southern Hemisphere. A new, alternative method of including the effect of non-uniform radiant distributions on the predicted arrival rate of meteors is given. The method used by Rudie to model Davies' measured radiant distribution is shown to be unnecessarily complicated and a simpler alternative is given. Furthermore, Rudie's distribution is shown not to be derived from a particular set of Davies' results as implied by Rudie.

Other non-uniform distributions of meteors are also investigated. Comparisons between monthly-averaged daily cycles of measured and predicted arrival rates of meteors for a midpath and an endpath meteor link are used to reveal the validity and limitations of the published distributions. A new graphical method is used to aid in determining the validity and limitations of the non-uniform distributions.

Discrepancies in the published predicted and measured annual variations in the arrival rate of meteors are investigated. Contrary to recently published information, predicted annual variations in the arrival rate of meteors for meteor radiants close to the ecliptic are shown to be comparable to measured results.

Preface

The author was born in Durban on 30 April, 1964. The author's involvement in meteor-scatter communications began in 1985 as a final year B.Sc. Eng. student in the Department of Electronic Engineering at the University of Natal, Durban. In 1986 he registered as a M.Sc. Eng. student at the university of Natal and joined the Meteor-Scatter Research team to investigate meteor-scatter receiver design. This investigation resulted in a greater and greater involvement in the measurement of meteor-scatter reflections and the author submitted a thesis in June 1988 entitled "A Meteor Scatter Measurement System". The M.Sc. Eng. degree was awarded with distinction in August 1988.

The research work described in this thesis was performed in the Department of Electronic Engineering, University of Natal, Durban, under the supervision of Professor Anthony D. Broadhurst. These studies represent original work by the author and have not been submitted in any form to another university. Where use has been made of the work of others, it has been duly acknowledged in the text.

Acknowledgements

I would like to take this opportunity to thank a few of the many people that I have had the pleasure of working with during this thesis project:

Paul Rodman for his invaluable assistance with software support and advice without whom any modifications to the Meteor Prediction Model would have been impossible;

Peter Handley for his extremely professional management of the Meteor-Scatter programme;

David Fraser for his moral support and friendship throughout this project;

Stuart Melville for cooperation and assistance in the papers we co-authored;

Professor A. D. Broadhurst for his assistance with the completion of this thesis;

James Larsen for his permission to continue development of the Meteor Prediction Model and for his suggestion of this topic of investigation;

Rod Radford for his tireless running of the measurement system and for always being willing to go the extra mile;

Gernot Larsen for his generous offer of office space for two years and for bearing all the inconvenience that his offer entailed.

I would like to thank the Foundation for Research and Development, Salbu (Pty) Ltd) and the University of Natal for their support. In particular, I would like to thank Mr Dave Larsen of Salbu (Pty) Ltd for supporting the Meteor-Scatter Research Project.

Last, but not least, I would like to thank my family for all their support and especially my wife, Alison, for all her understanding during the difficult times of thesis preparation.

Table of Contents

List of Figures

List of Tables

Chapter 1

Introduction

1.1 Meteor-burst communications

The use of naturally occurring ionization trails left by meteors[1] burning up in the earth's upper atmosphere to communicate cheaply and reliably over long distances is now an established communication technique. Every day billions of meteoroids[1], in orbit around the sun, collide with the earth's atmosphere. The meteors burn up at heights ranging between 80 and 120 kilometres above the earth's surface forming trails of ionization tens of kilometres long with an initial diameter of approximately one metre. The meteor ionization trails or meteor trails may be used to reflect radio waves between two points on the earth's surface. The curvature of the earth's surface limits the separation between the two points to a maximum of approximately 2000 kilometres. Very high frequency radio waves, rather than high frequency radio waves, are typically used for communication purposes to avoid interference caused by ionospheric reflections. The duration of the reflected signal is limited by diffusion of the ionized trail, but is sufficiently long to support burst-mode data communication.

The birth of the concept of the reflection of radio waves off meteor trails or meteor-scatter can be traced back to the late 1920's and early 1930's. Although

1 The term *meteor* is a general term used to describe the whole phenomenon associated with the entry into the earth's atmosphere of a particle from space. A *meteoroid* is an object moving in interplanetary space which, on entering the earth's atmosphere, produces the phenomenon of a meteor. For simplicity, the term meteor in this thesis includes the term meteoroid.

most of the basic theory of meteor-scatter propagation was developed during the 1950's, the development of practical communication systems was limited by the available technology. One of the earliest data communications systems was the JANET test system developed by the Defense Research Board of Ottawa during the 1950's. (See *Forsyth et al.* [1957].) The improvement in electronic technology enabled the data processing and data storage limitations of the early test systems to be overcome and one of the first commercial systems to be implemented was the Snopak telemetry (SNOTEL) system described by *Barton and Burke* [1977]. Since the late 1970's there has been considerable renewed interest in meteor-burst communications when it became apparent that it offered a reliable and cheap method of communication that, in particular circumstances, offered advantages over other communications techniques such as satellites. Applications of some of the more recent systems include remote data gathering, teletype, facsimile, vehicle tracking and back-up for military early warning radar systems. For further reading, one of the most recent summaries of meteor-burst communications has been given by *Yavus* [1990].

1.2 Modelling meteor-burst communications

Modelling any type of communications technique is essential to understand and optimise its performance. To aid in the design, implementation and understanding of meteor-burst communications and propagation, theoretical models have been developed and implemented since the 1950's by *James and Meeks* [1956], *Hines* [1956] and *Rudie* [1967]. As mentioned by *Weitzen* [1986] and *Mawrey* [1990], the complexity of the meteor-burst communications channel requires the implementation of sophisticated computer-based meteor prediction models. A description of the development of computer-based prediction models is presented in Chapter 2. One of the most important parameters affecting communications performance is the arrival rate of meteor trails useful for communication over a forward-scatter link. (The term *forward-scatter* is used here to describe reflection

via meteor trails between two separated points on the earth's surface, as opposed to *back-scatter* where the transmission and reception points are coincident.) In order to predict the arrival rate of meteors the most sophisticated meteor prediction models include the effect of the following parameters:

- Path location, orientation and geometry
- Transmitter power, receiver sensitivity, and operating frequency
- Antenna polar patterns and antenna polarization
- Galactic and local noise sources
- Physical characteristics of meteor trails
- Meteor showers
- Non-uniform distribution of meteors intercepting the earth

The axial rotation of the earth, the orbital rotation of the earth around the sun, and a non-uniform distribution of meteors intercepting the earth, are the three primary factors resulting in variations in the arrival rate of meteor trails. In order to model these effects accurately, it is necessary to have a model of the distribution of meteors intercepting the earth and to incorporate the effects of this distribution of meteors on the arrival rate of meteor trails useful for communication over forward-scatter links.

1.3 Problem Statement

Investigations into currently accepted methods of predicting the arrival rate of meteors over forward-scatter links have revealed the following problems:

- There appears to be a lack of information regarding the validity of the currently available measured distributions of meteors intercepting the earth.
- Discrepancies exist regarding the accepted annual variation in the arrival rate of meteors intercepting the earth and therefore also over a forward-scatter link.

- Limitations exist with the method used by *Rudie* [1967] to model the distribution of meteors in space and also to incorporate the effects of the distribution on the arrival rate of meteors over a forward-scatter link. Limitations with Rudie's techniques are significant since Rudie's technique has received recent acceptance by *Weitzen* [1986], *Larsen and Rodman* [1988], and *Desourdis et al.* [1988].

1.4 Thesis summary and claims

Currently available measured radiant distributions of meteors are presented in Chapter 2. A summary of existing methods of predicting the arrival rate of meteors over forward-scatter links is given, as well as some comparisons between published predicted and measured variations in the arrival rate of meteors. Discrepancies between published, measured and predicted annual variations in the annual arrival rate of meteors are also presented.

A summary of the technique used in this thesis to calculate the arrival rate of meteor trails useful for communication over a forward-scatter link is given in Chapter 3. A new, alternative method of incorporating the effect of a non-uniform distribution of meteors on the arrival rate of meteors is proposed.

An investigation into the distribution of meteors presented by *Rudie* [1967], which were based on the measurements performed by *Davies* [1957], is presented in Chapter 4. The limitations of the apparent method used by Rudie to generate a distribution based on Davies' results are given. A new, alternative, and far simpler method of using Davies' results is proposed.

In order to verify the validity of the radiant distributions of meteors presented in Chapter 2, comparisons between measured and predicted arrival rates of meteors over a forward-scatter link in the Southern Hemisphere are given in Chapter 5. A new graphical method of determining which region of a particular radiant

distribution contributes to the arrival rate of meteors over the forward-scatter link, for a particular system, time of day, and time of year is proposed. This is useful to determine the validity of parts of the various distributions. The annual variation in the arrival rate of meteors intercepting the earth is also estimated using the measured and predicted annual variations in the arrival rate of meteors over the forward-scatter link for the two different systems. The estimated annual variation obtained using the two systems is compared with the published results presented in Chapter 2 and conclusions are drawn regarding the actual annual variation of meteors intercepting the earth. Finally, an overall conclusion is given in Chapter 6.

Chapter 2

Radiant distributions and modelling the arrival rate of meteors

The current state and development of modelling variations in the arrival rate of meteors over forward-scatter links is described in this chapter. Due to the dependence of variations in the arrival rate of meteors over forward-scatter links on non-uniform distributions, published non-uniform radiant distributions are described in some detail. Problems and limitations with the current state of modelling variations in the arrival rate of meteors are also mentioned.

2.1 Measured non-uniform density distributions of sporadic meteors

The distribution of meteor radiants intercepting the earth may be described in terms of an ecliptical coordinate system illustrated in Figure 2-1. The ecliptical coordinate system may be defined as a right handed cartesian system with its origin at the centre of the earth and its axis pointing in the direction of the earth's motion (apex), the direction of the sun and the direction perpendicular to the ecliptic plane (plane of the earth's motion around the sun). The direction of meteor radiants in ecliptical longitude, λ, and latitude, β, relative to the apex is shown in Figure 2-1. The effect of the earth's motion on the apparent direction of a meteor radiant is illustrated in Figure 2-2. As a result of the vector addition of the earth's orbital velocity, V_e, and a meteor's velocity, V_h, relative to the sun, a meteor will appear to come from direction, R_g, with velocity, V_g, relative to the

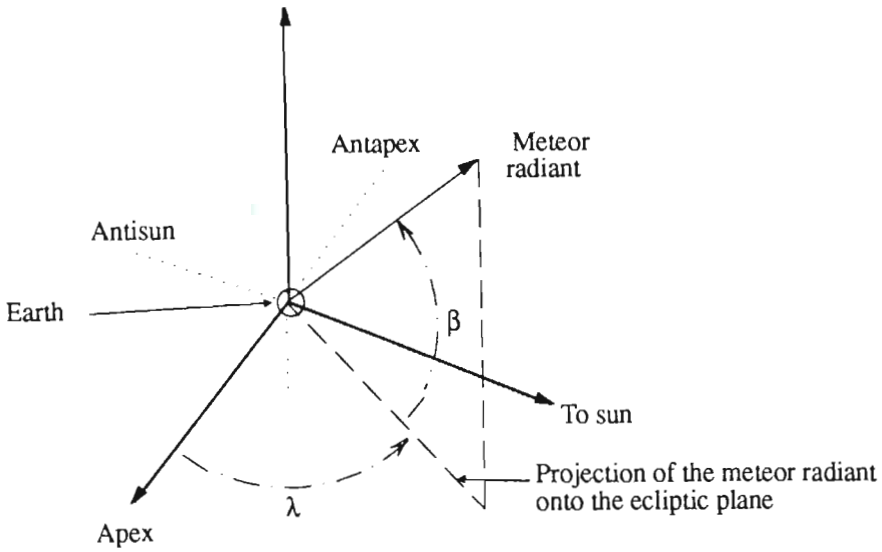

Figure 2-1 Meteor radiant given in ecliptical longitude, λ, and latitude, β, relative to the apex of the earth's way.

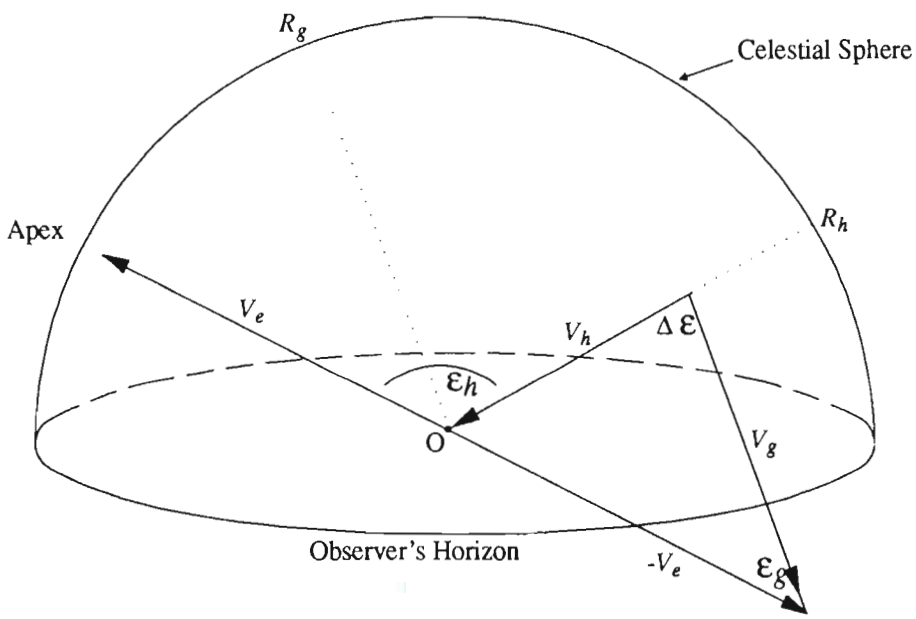

Figure 2-2 Apparent change in direction of a meteor radiant as seen by an observer on the earth

observer on the earth at O. The effect of the earth's gravitational attraction and the earth's rotation have been ignored. R_g and R_h respectively, are the geocentric and heliocentric meteor radiants.

Measurements of meteor velocities and radiants have shown that most meteors intercepting the earth travel in the same direction as the earth travels around the sun *Hawkins* [1956], *Davies* [1957], *Southworth and Sekanina* [1975]. The vector addition of the earth's orbital velocity and a meteor's velocity results in most meteors entering the earth's atmosphere on the apex hemisphere of the earth. In heliocentric coordinates, therefore, most meteor radiants are clustered around the antapex, whilst in geocentric coordinates most meteor radiants appear to be concentrated around the apex hemisphere.

2.1.1 Hawkins' data

Between October 1949 and September 1951, approximately 240 000 sporadic meteor reflections were measured using radar at Jodrell Bank, England, 2^o 18′ W, 53^o 14′ N. (See *Lovell* [1954] and *Hawkins* [1956].) The distribution of sporadic meteor radiants was determined on a statistical basis by analysing the relative number of meteor reflections measured using two narrow-beam aerials. The results of the analysis of these measurements are shown in Figures 2-3 and 2-4. Figure 2-3 gives polar plots of the yearly-averaged distribution of meteor radiants in geocentric ecliptical longitude. "Survey 1" and "Survey 2" are the measurements between, October 1949 and September 1950, and, October 1950 and September 1951, respectively. The results showed a concentration of meteor radiants close to the ecliptic plane in the direction of the apex and at ecliptical longitudes of $\lambda_g = 65^o$ and $\lambda_g = 295^o$ known, respectively, as the sun and antisun regions. The nature of the measurements did not enable the distribution of radiants with respect to ecliptical latitude to be determined. The close corre-

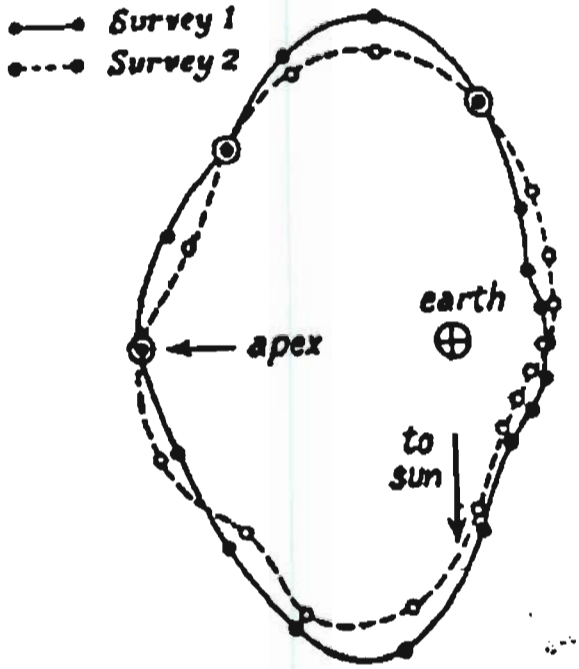

Figure 2-3 Polar plot of the observed distribution of meteor radiants in ecliptical coordinates measured by *Hawkins* [1956]. The radiants were predicted to be concentrated close to the ecliptic plane.

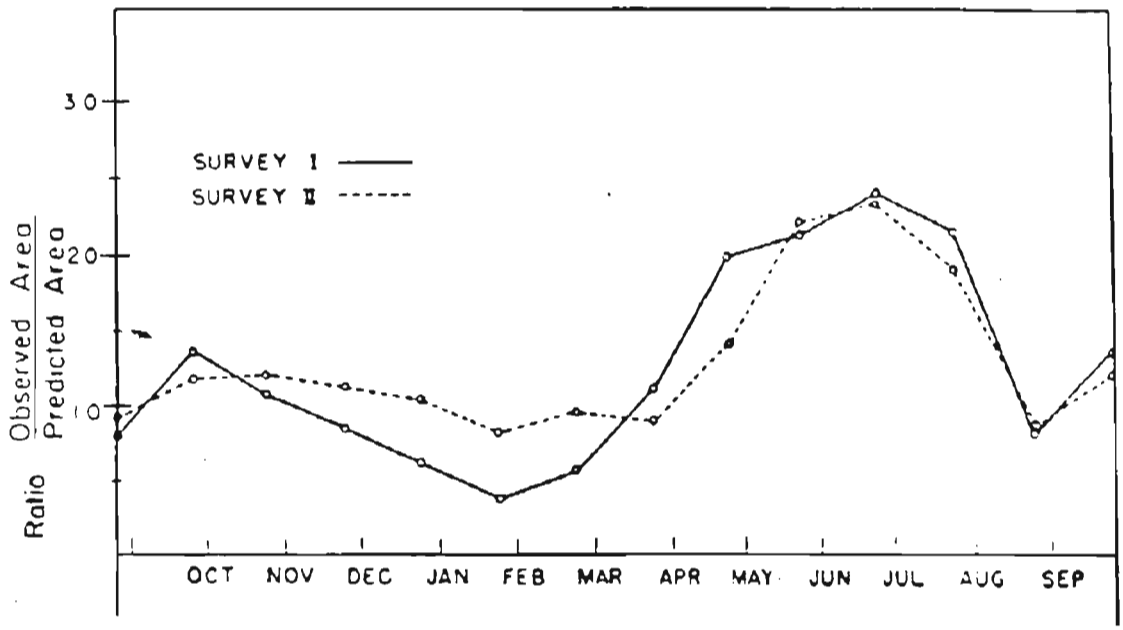

Figure 2-4 Space density of meteors along the earth's orbit measured by *Hawkins* [1956]

lation between the two surveys indicated that there was little year-to-year variation in the distribution of radiants averaged over this duration.

Comparisons of measured monthly variations with predicted results based on the yearly-averaged space density of meteors shown in Figure 2-3 indicated that the space density of meteors along the earth's orbit was not constant and varied as shown in Figure 2-4, *Hawkins* [1956]. Although not explicitly mentioned by Hawkins, the latitude at which the measurements were taken enabled few radiants south of the ecliptic to be measured, and therefore, the results presented by Hawkins consisted primarily of radiants north of the ecliptic.

2.1.2 Davies' data

Davies [1957] published the results of radar measurements of about 2400 meteors measured over 24 hour periods for one day each month between May, 1954, and April, 1955. The measurements were taken at Jodrell Bank and included velocity and direction information of individual meteors. As with the measurements taken by Hawkins, the high latitude of Jodrell Bank enabled few radiants south of the ecliptic to be measured. The measured results were presented as yearly-averaged observed ecliptical radiant distributions and as graphs of yearly-averaged orbital parameters. According to Davies, corrections were applied to the data based on two types of observational selection: certain parts of the sky were better observed than others; and the chance of a high-velocity meteor yielding a measurable trail is greater than that for a slow meteor. Although no specific details regarding selection effects due to velocity were supplied by Davies, a later reference to Davies' measurements by *McCrosky and Posen* [1961] seems to imply that each meteor was weighted by a factor of $1/V_\infty^2$, where V_∞ is the velocity of a meteor just outside the earth's atmosphere.

Davies presented the results of his measurements in a reduced form as shown in Figures 2-5 to 2-8. Figure 2-5 is a polar plot of sporadic meteor radiants in

ecliptical longitude. The results were presented as the sum of various ranges of geocentric ecliptical latitude, β_g, versus ecliptical longitude, λ_g, as shown in the figure.

Similar to Hawkins' results, Davies' results showed concentrations of meteor radiants at the apex, sun and antisun regions. Davies' results, however, were far less uniform than Hawkins' results and gave more information regarding the distribution of meteor radiants with respect to ecliptical latitude. Davies also presented the results of his measurements as distributions of orbital parameters of meteors as shown in Figures 2-6 to 2-8. Unfortunately, however, the original data used to generate these graphs was not published.

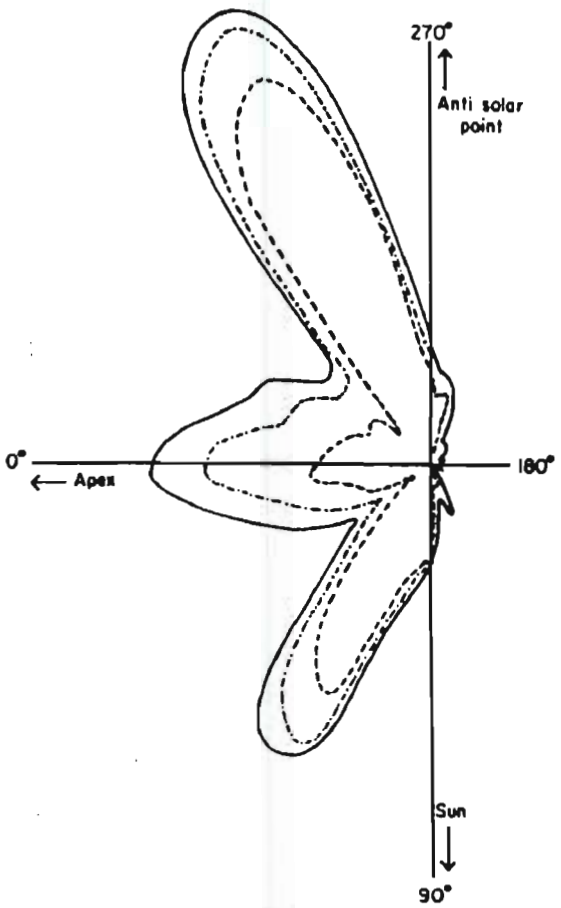

Figure 2-5 Polar plot of sporadic meteor radiants in ecliptical coordinates, corrected for observational selection: - - - - radiants within 20° of the ecliptic; – · – · radiants within 40° of the ecliptic;—— all radiants, *Davies* [1957].

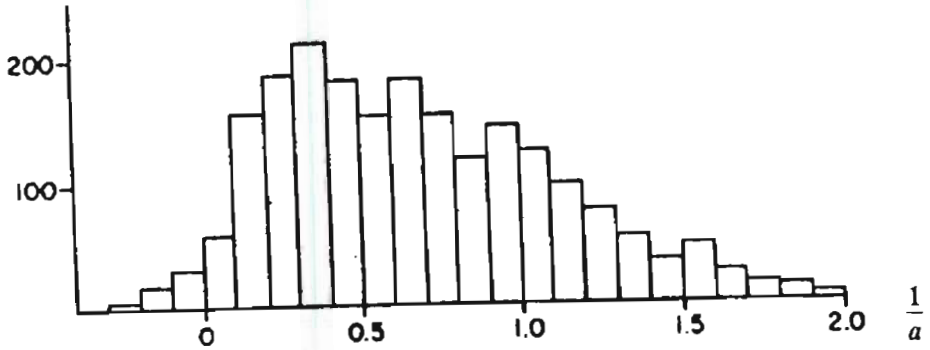

Figure 2-6 Distribution of $1/a$ for sporadic meteors, weighted for observational selection. Ordinates: Weighted number of meteors, *Davies* [1957].

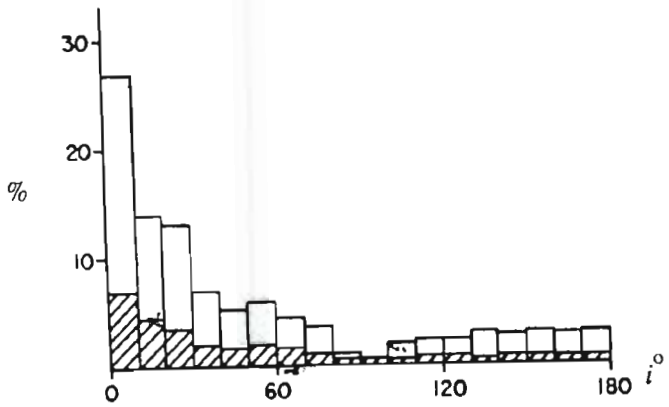

Figure 2-7 Distribution of inclination of orbits with aphelion distances greater than 3 AU. Orbits with aphelion distances greater than 10 AU shown shaded, *Davies* [1957].

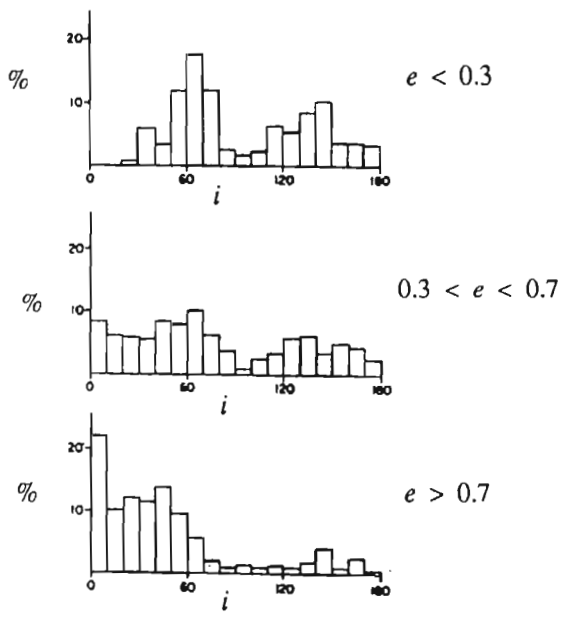

Figure 2-8 Distribution of inclination of orbits with aphelion distances less than 3 AU, *Davies* [1957].

2.1.3 McCrosky and Posen's data

McCrosky and Posen [1961] presented, amongst other parameters, the geocentric velocity and radiants of 2529 meteors, of which approximately 400 were shower meteors. The meteors were photographed from New Mexico between February, 1952, and July, 1954, as part of the Harvard Meteor Project. McCrosky and Posen's data has been converted to an observed radiant distribution which is given as a contour plot of meteor radiants in geocentric ecliptical coordinates in Figure 2-9. The absence of radiants in the direction of the sun is due to the photographic nature of the measurements. The meteor radiants appear concentrated north of the ecliptic due to observational selection. As with the previous distributions, meteor radiants are concentrated at the antisun and apex regions. McCrosky and Posen's data also provides information regarding the velocity distribution of meteors, which is given in Section 2.3.

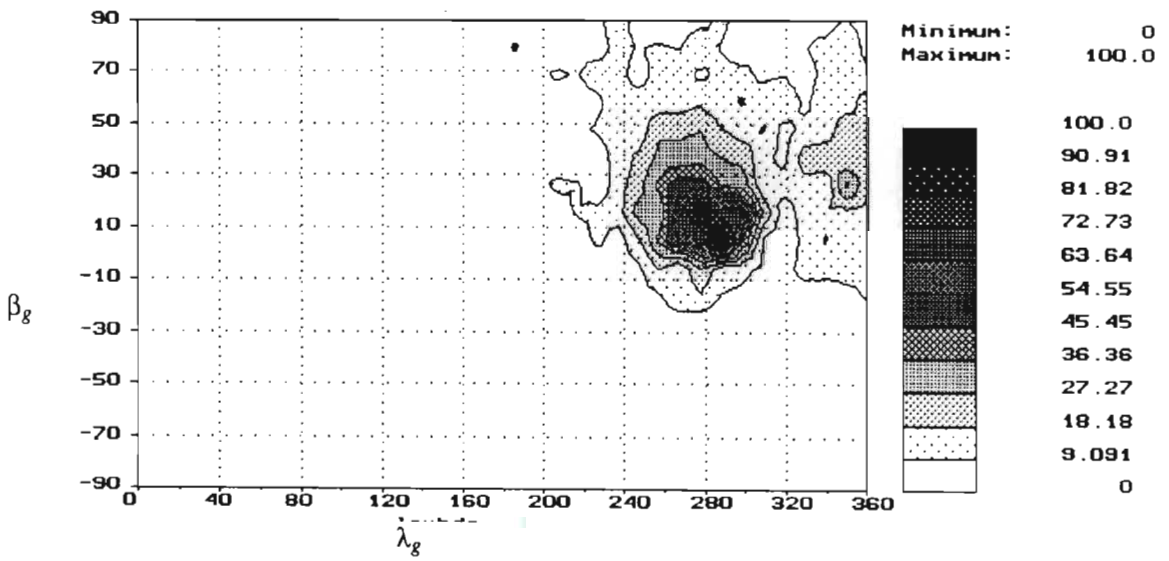

Figure 2-9 Photographic observed distribution of meteors extracted from *McCrosky and Posen* [1961].

2.1.4 Harvard data

Southworth and Sekanina [1975], presented the results of eight-station radar measurements of approximately 20 000 meteors taken during the year 1968 as part of the Harvard Meteor Project. Results of measurements of approximately 20 000 meteors taken from 1961 to 1965 were also presented. The radar stations were situated in Illinois, approximately 40^{o} N, 90^{o} W. A more detailed description of the system may be found in *Cook et al.* [1972].

The Harvard data was presented in a number of forms: unweighted; weighted to give "equal mass in the atmosphere"; and weighted to provide the space distribution of meteors. The unweighted results of the 1968 measurements are presented as a contour plot of relative radiant density in geocentric ecliptical coordinates in Figure 2-10. The 1961 to 1965 results are not presented here, but comparison between the two sets of data revealed a close similarity, which indicated that the year-to-year variation in the yearly-averaged radiant distributions was small.

Due to the concentration of meteors at high latitudes, it appears that the data has not been corrected suitably for the effects of antenna selection. This observation is supported by the following quote from *Sekanina,* [1970], p 460:

> *"Also, the highly anisotropic sensitivity of the antenna system introduces selection effects that entirely mask the actual frequency distribution of meteors over the sky. It would be extremely difficult, if not impossible, to evaluate these selection effects."*

In support of the previous distributions, the data does, however, exhibit peaks at the apex and antisun regions.

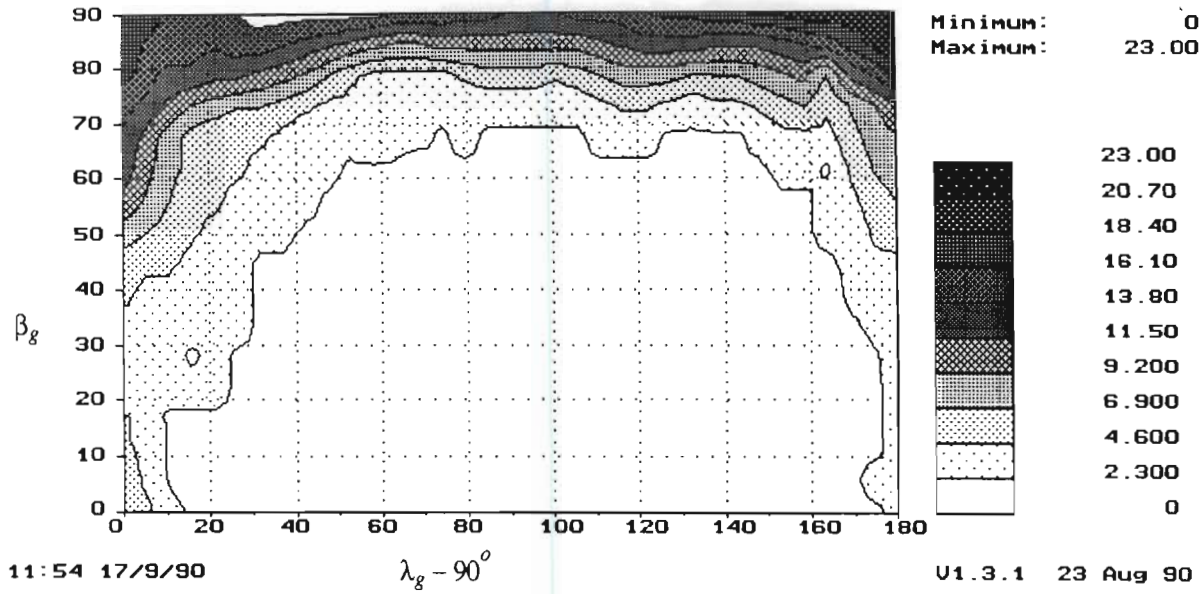

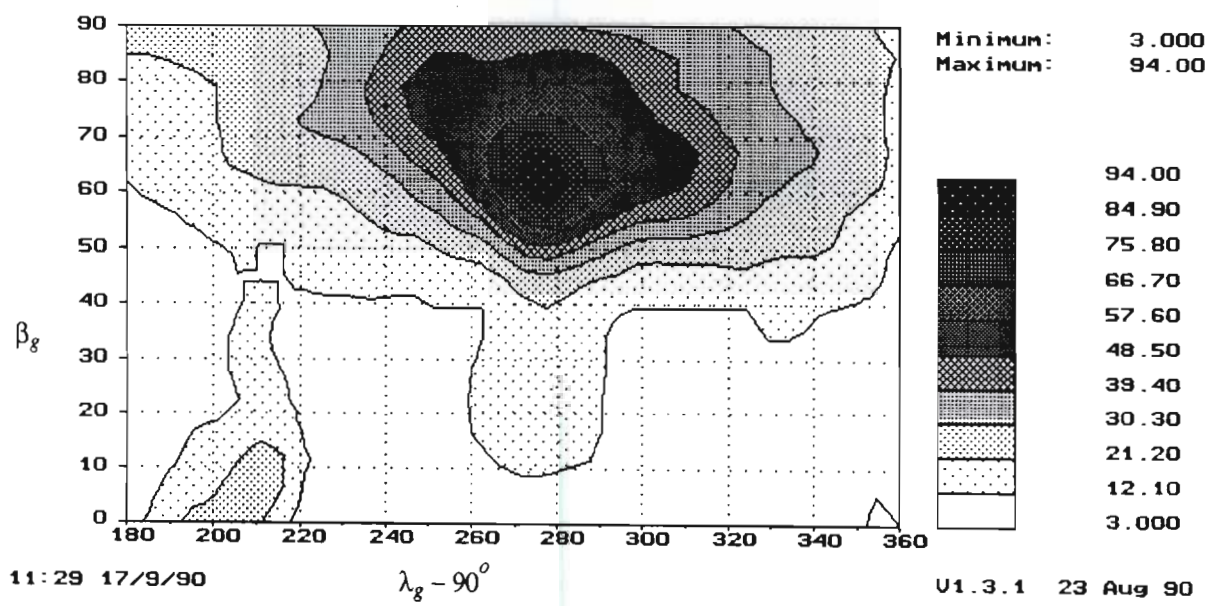

Figure 2-10 Observed radiant density of meteors measured as part of the Harvard meteor project, *Southworth and Sekanina* [1975].

2.1.5 Pupyshev's data

Tabulated monthly distributions of meteors in geocentric coordinates presented in *Pupyshev et al.* [1980], have been made available to the author by personal correspondence. Unfortunately, however, the original document is apparently classified and is not available to the author. Based on the title of Pupyshev's reference, the method of measurement is assumed to be radar and the data has been assumed to be in the form of a radiant density of meteors. Pupyshev's data represents the only measured distribution of meteors radiants known to the author that includes a relatively equal distribution of radiants north and south of the ecliptic. Although no reference is available to the author, personal discussion arising from the *Milcom 90 Conference* indicated that the results were based on measurements taken at Mogadishu, Somalia, Africa, and possibly also in the USSR. A reference to measurements taken at Mogadishu from December, 1968, to May, 1970, is given by *Svetashkova,* [1987].

The data have been reproduced as contour maps for each month of the year in Figures 2-11 to 2-22. The data contoured in Figures 2-11 to 2-22 were divided into cells 7.5^{o} square, and the density of each cell was smoothed by averaging with the adjacent cells. Even after smoothing the data, it is clear that the distributions are rough. It is not known how many meteors were used to generate each distribution. Since the original monthly-averaged data appeared to be rough, a yearly-averaged distribution has been generated from the monthly-averaged data. The yearly-averaged distribution of meteors is presented in Figure 2-23. Consistent with previous distributions, the yearly-averaged distribution of meteors shows similar concentrations at the antisun and apex regions. High concentrations of meteor radiants, however, are also found at the north and particularly the south ecliptic poles.

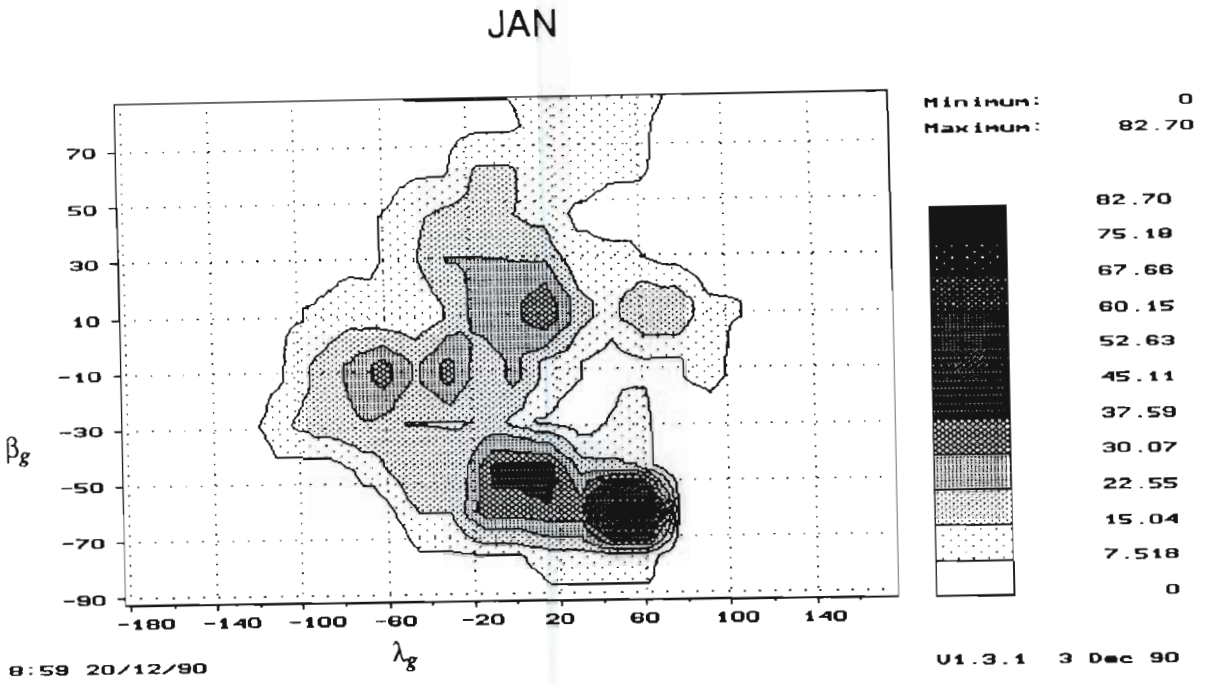

Figure 2-11 Contour map of the relative density of meteor radiants for January in geocentric ecliptical coordinates measured by *Pupyshev et al.* [1980]

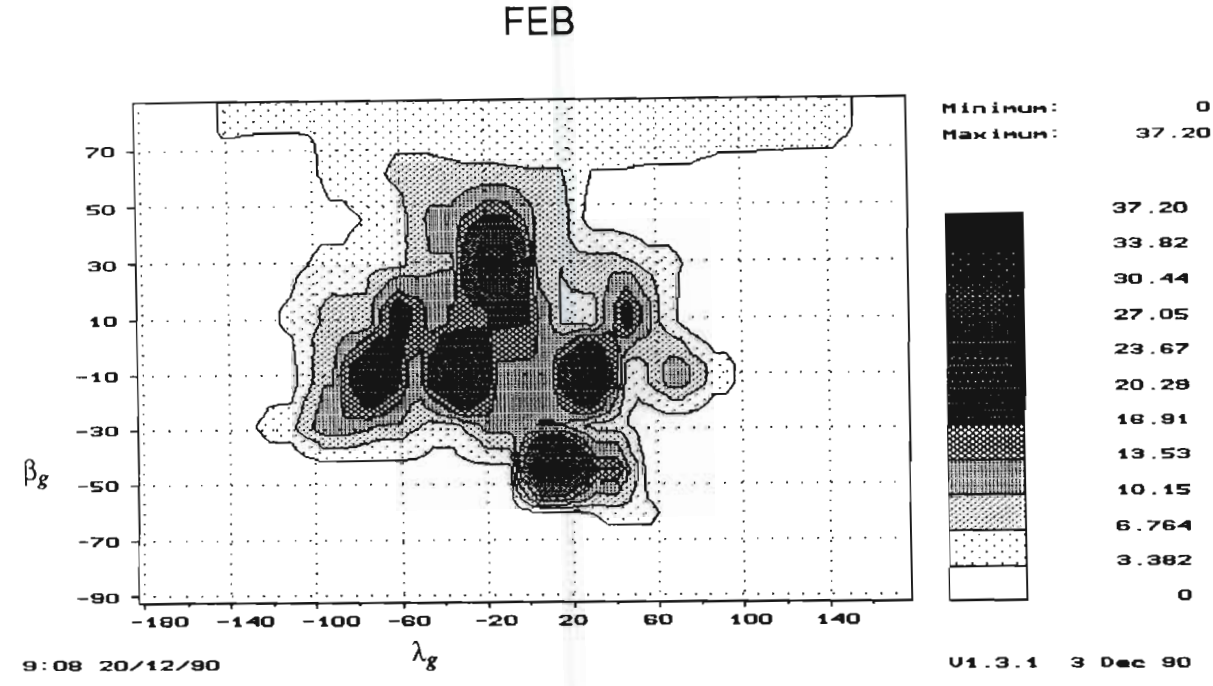

Figure 2-12 Contour map of the relative density of meteor radiants for February in geocentric ecliptical coordinates measured by *Pupyshev et al.* [1980]

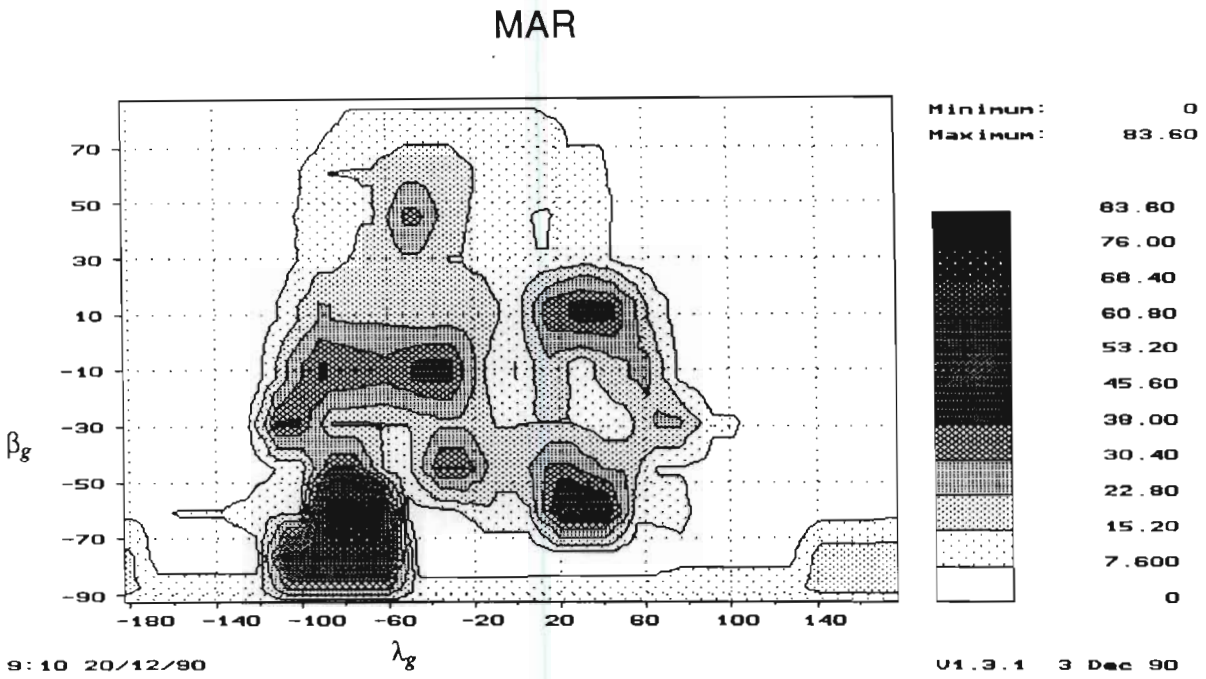

Figure 2-13 Contour map of the relative density of meteor radiants for March in geocentric ecliptical coordinates measured by *Pupyshev et al.* [1980]

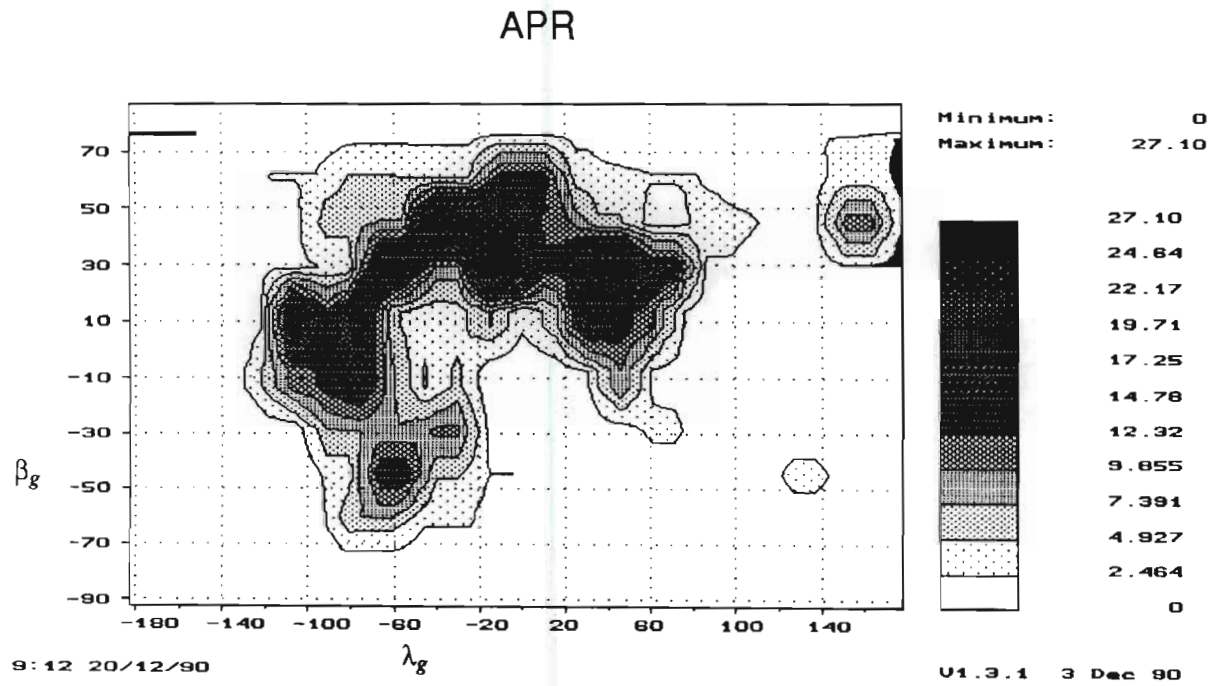

Figure 2-14 Contour map of the relative density of meteor radiants for April in geocentric ecliptical coordinates measured by *Pupyshev et al.* [1980]

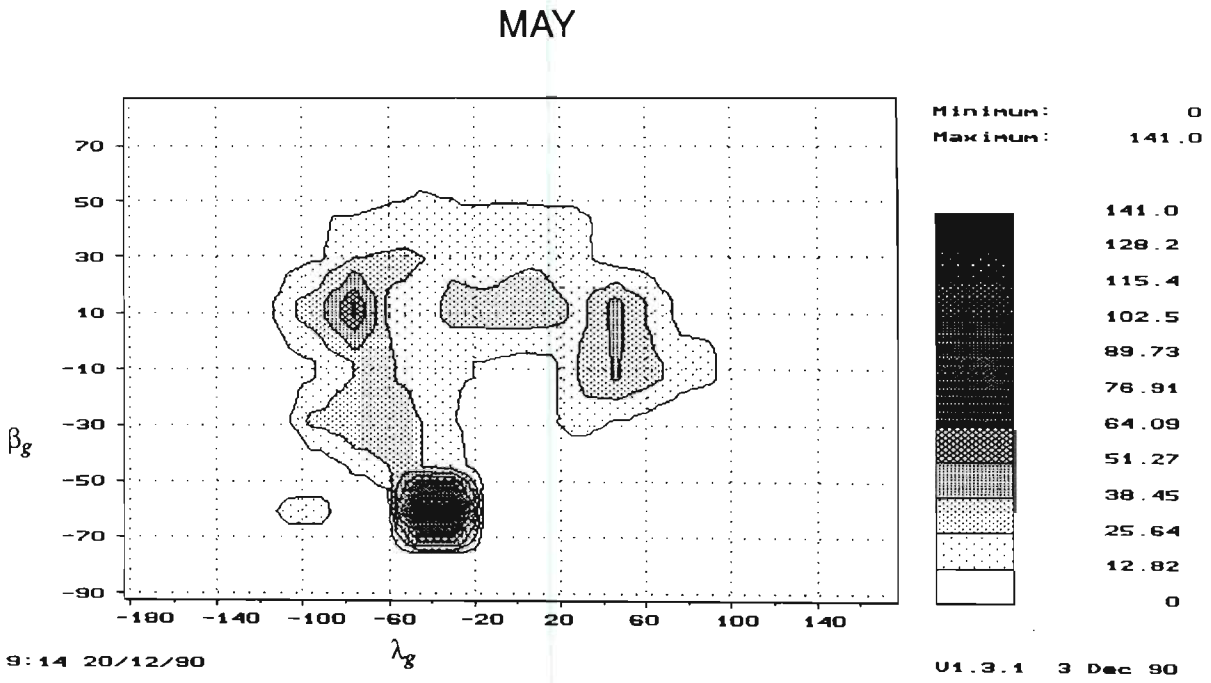

Figure 2-15 Contour map of the relative density of meteor radiants for May in geocentric ecliptical coordinates measured by *Pupyshev et al.* [1980]

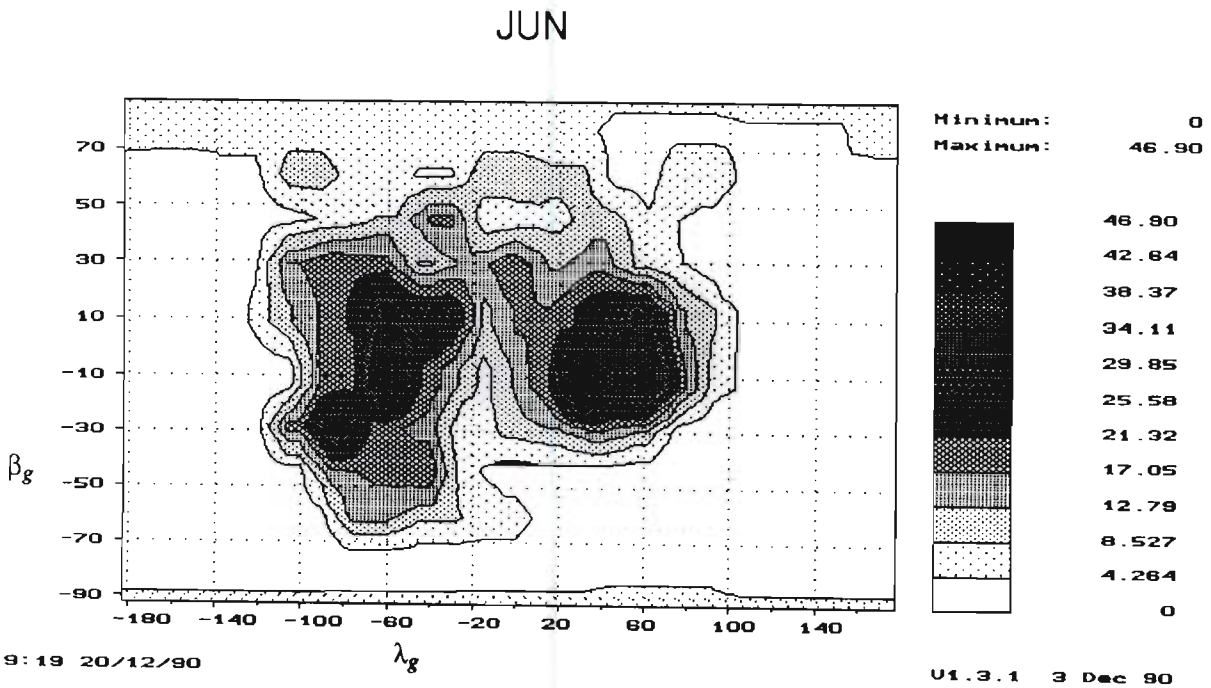

Figure 2-16 Contour map of the relative density of meteor radiants for June in geocentric ecliptical coordinates measured by *Pupyshev et al.* [1980]

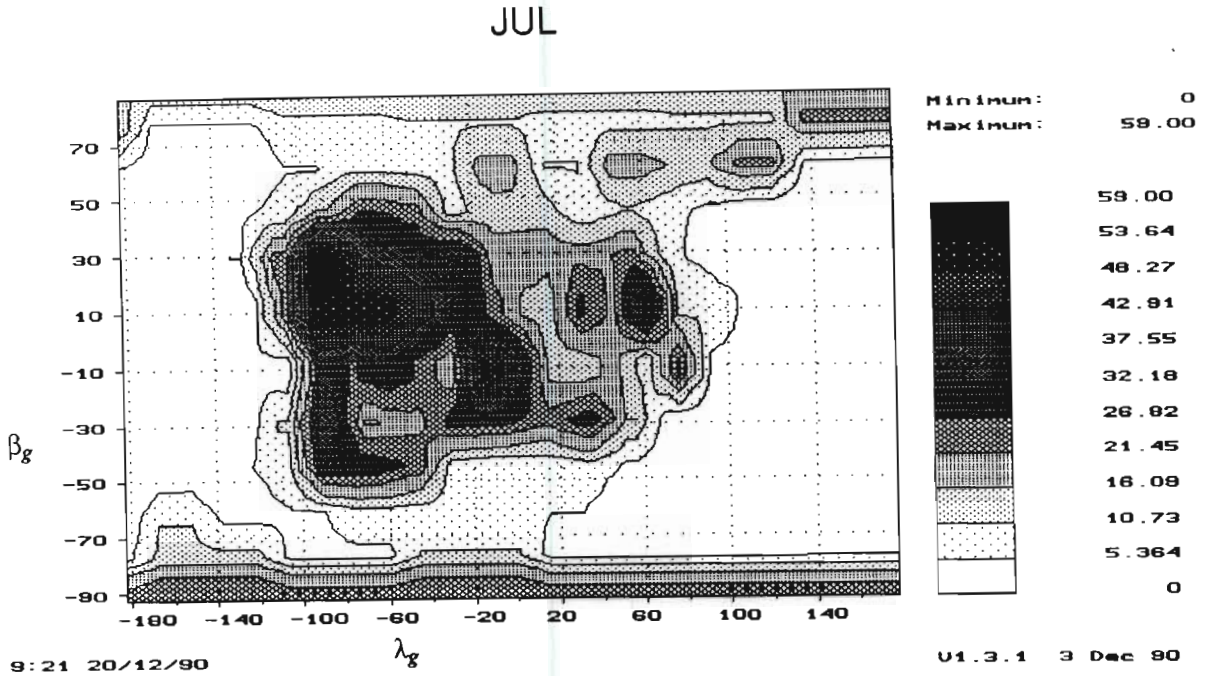

Figure 2-17 Contour map of the relative density of meteor radiants for July in geocentric ecliptical coordinates measured by *Pupyshev et al.* [1980]

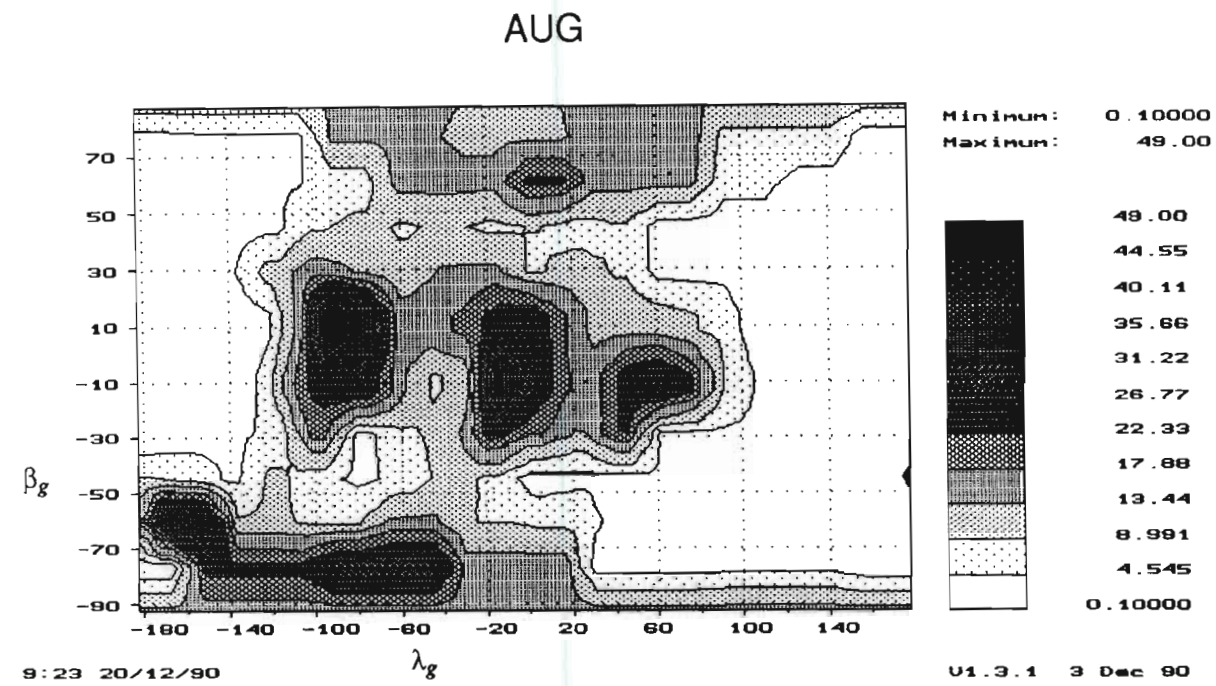

Figure 2-18 Contour map of the relative density of meteor radiants for August in geocentric ecliptical coordinates measured by *Pupyshev et al.* [1980]

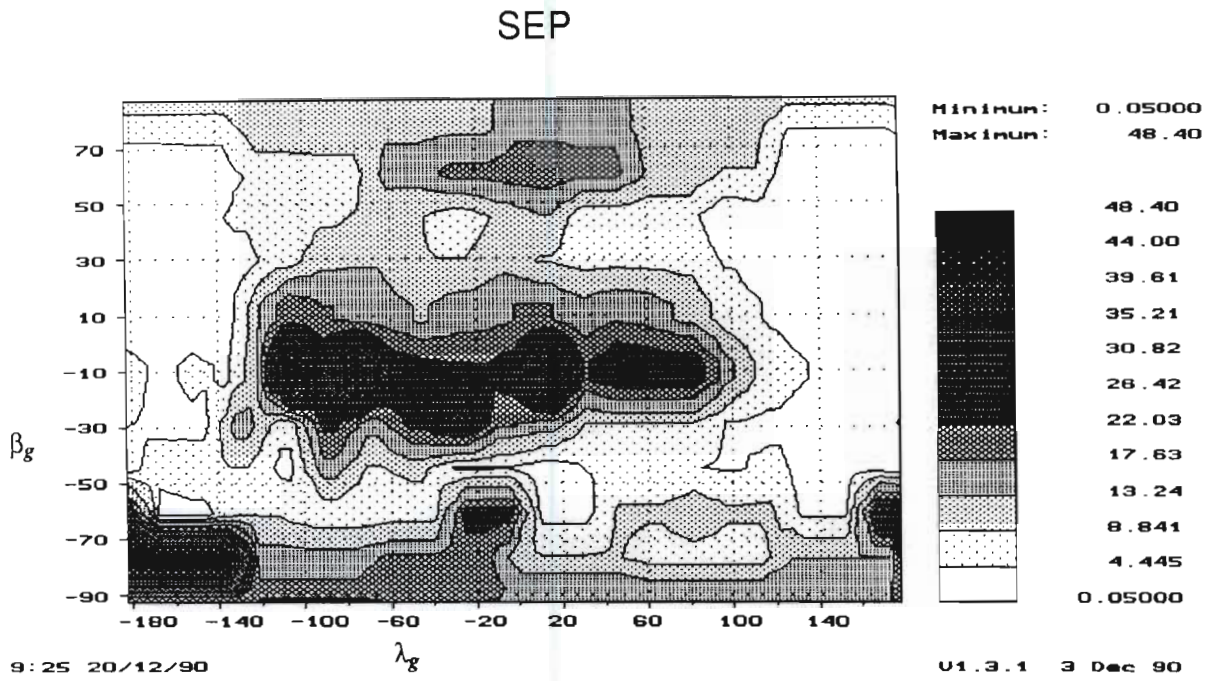

Figure 2-19 Contour map of the relative density of meteor radiants for September in geocentric ecliptical coordinates measured by *Pupyshev et al.* [1980]

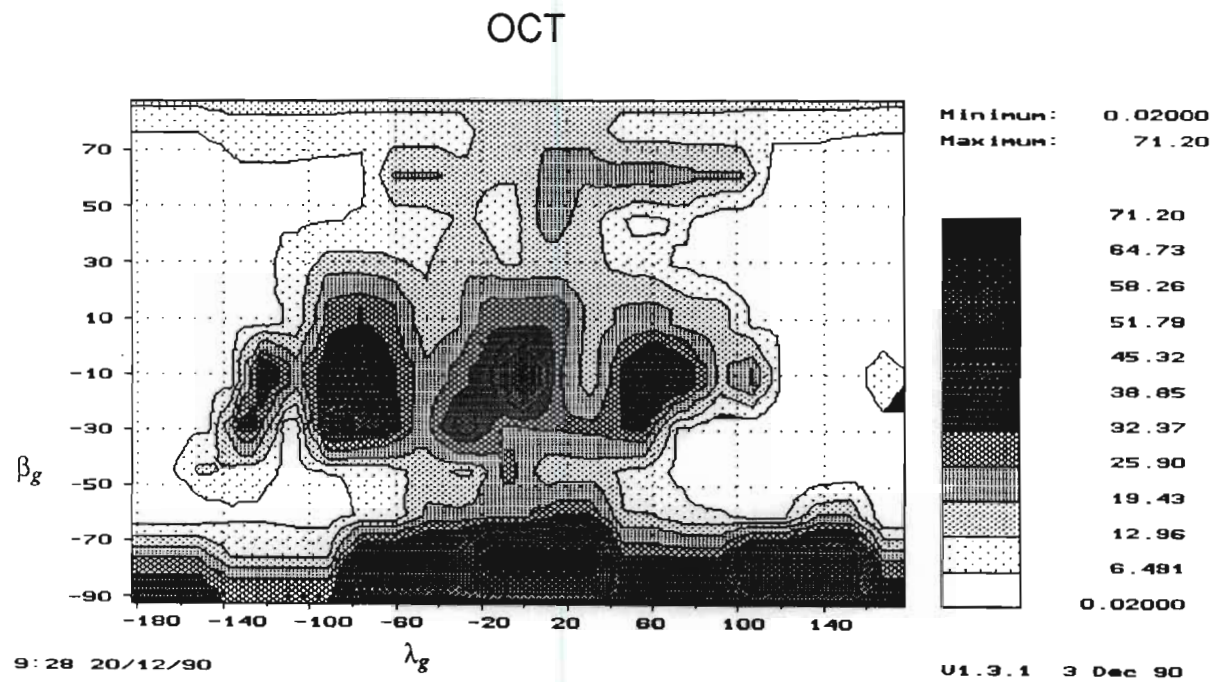

Figure 2-20 Contour map of the relative density of meteor radiants for October in geocentric ecliptical coordinates measured by *Pupyshev et al.* [1980]

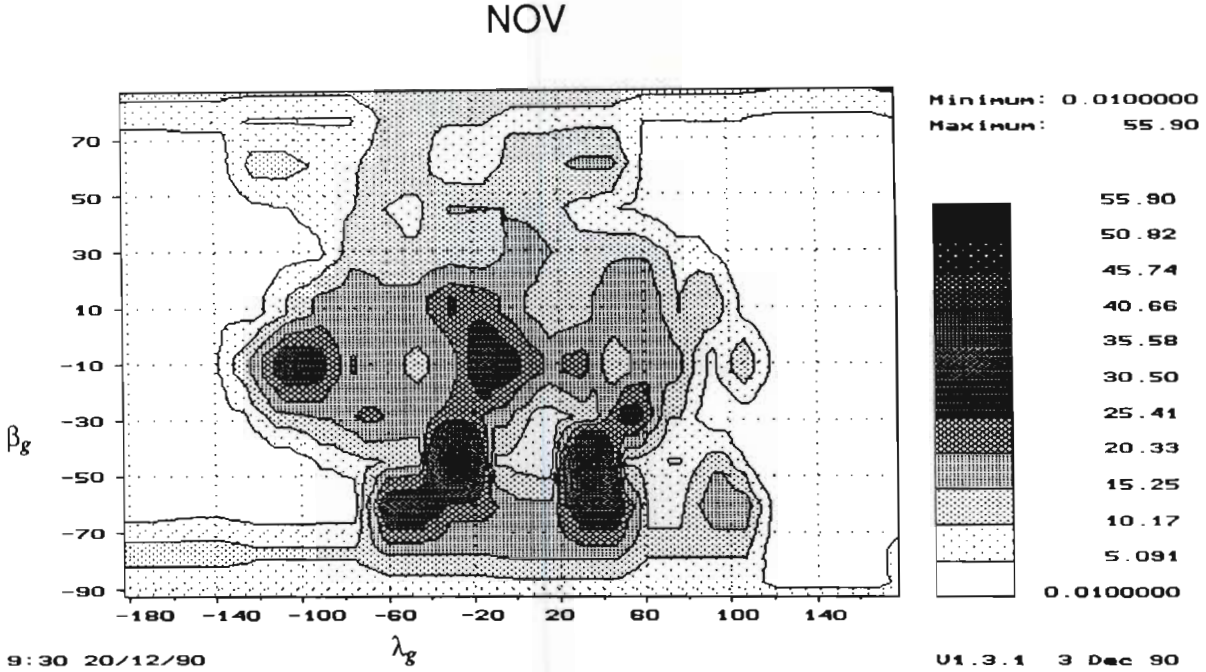

Figure 2-21 Contour map of the relative density of meteor radiants for November in geocentric ecliptical coordinates measured by *Pupyshev et al.* [1980]

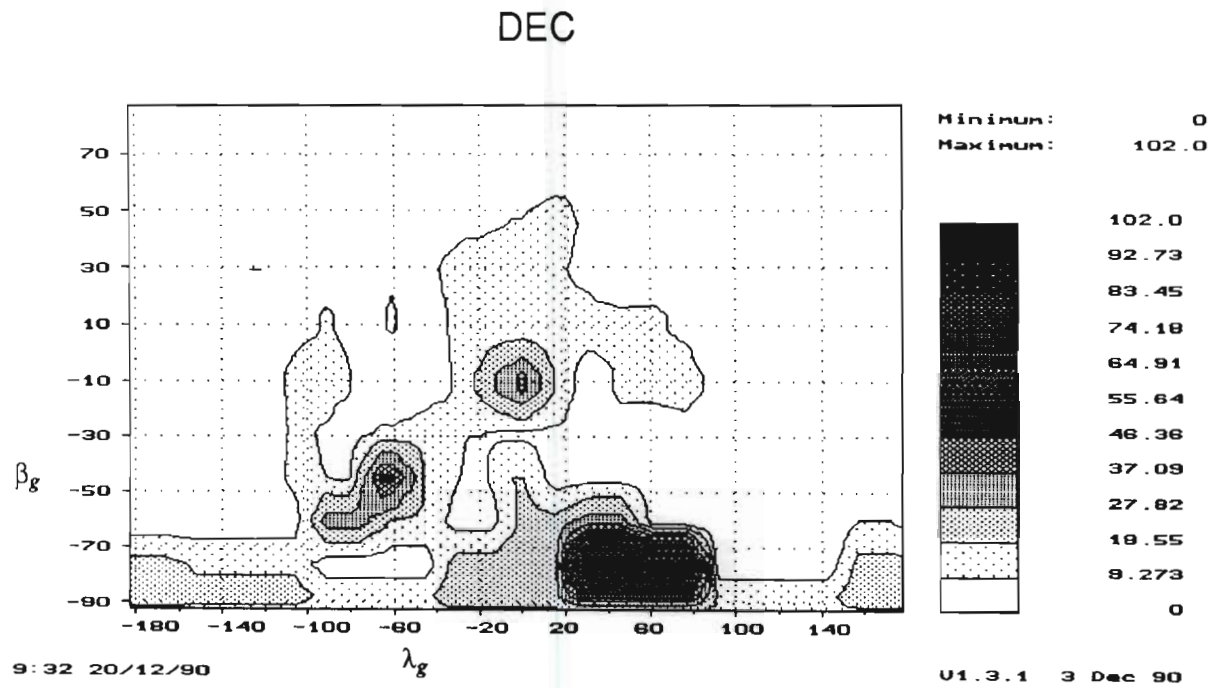

Figure 2-22 Contour map of the relative density of meteor radiants for December in geocentric ecliptical coordinates measured by *Pupyshev et al.* [1980]

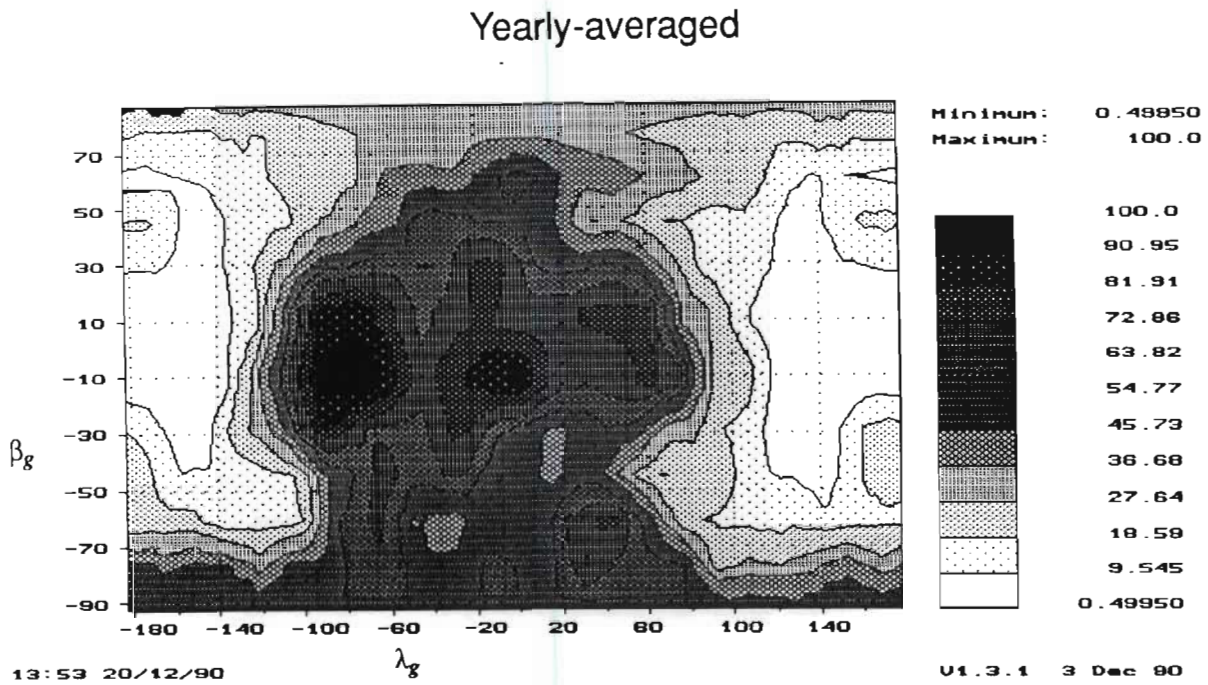

Figure 2-23 Contour map of the yearly-averaged relative density of meteor radiants in geocentric ecliptical coordinates measured by *Pupyshev et al.* [1980]

2.2 Ecliptical orbital distribution simulated by Rudie

An ecliptical orbital density distribution of meteors was simulated by Rudie using the results presented by Davies. The orbital distribution was simulated as closed form equations that are reproduced in Table 2-1. A contour plot of Rudie's simulation based on the equations in Table 2-1 is given in Figure 2-24. No derivation of these equations was given by Rudie. The only information regarding the origin of these equations was the following quote from Rudie's thesis, *Rudie* [1967] p 68:

> *"The orbital distribution described by Figures 3-6 through 3-8 can be simulated. A simulation is given in Table I, where* $N_h(\lambda', \beta')$ *is the relative polar density of sporadic meteor orbits in ecliptic coordinates."*

Rudie's Figures 3-6 to 3-8 correspond to Figures 2-6 to 2-8 and Rudie's Table I corresponds to Table 2-1.

Table 2-1 Rudie's simulation of the orbital distribution of meteors, *Rudie* [1967].

$N_h(\lambda_h, \beta_h)$	λ_h	β_h
$\frac{-0.56\,CNB + [(0.56\,CNB)^2 + 2.24\,CNA]^{1/2}}{2\,CNA}$	$0^o \le \lambda_h < 40^o$ $320^o \le \lambda_h < 360^o$	$\lvert\beta_h\rvert \le 90^o$
$\frac{-0.944\,CNB + [(0.944\,CNB)^2 + 2.828\,CNA]^{1/2}}{2\,CNA}$	$40^o \le \lambda_h < 60^o$ $300^o \le \lambda_h < 320^o$	$\lvert\beta_h\rvert \le 90^o$
$\frac{-1.25\,CNB + [(1.25\,CNB)^2 + 2.5\,CNA]^{1/2}}{2\,CNA}$	$60^o \le \lambda_h < 80^o$ $280^o \le \lambda_h < 300^o$	$\lvert\beta_h\rvert \le 90^o$
0	$80^o \le \lambda_h < 100^o$ $260^o \le \lambda_h < 280^o$	$\lvert\beta_h\rvert \le 12^o$
0.5	$80^o \le \lambda_h < 100^o$ $260^o \le \lambda_h < 280^o$	$12^o < \lvert\beta_h\rvert \le 90^o$
$\frac{-0.3\cos\beta_h + [(0.3\cos\beta_h)^2 + 4\sin^2\beta_h]^{1/2}}{2\sin^2\beta_h}$	$100^o \le \lambda_h < 110^o$	$\lvert\beta_h\rvert \le 90^o$
$\frac{-0.22\cos\beta_h + [(0.22\cos\beta_h)^2 + 4\sin^2\beta_h]^{1/2}}{2\sin^2\beta_h}$	$110^o \le \lambda_h < 210^o$	$\lvert\beta_h\rvert \le 90^o$
$\frac{-0.9\cos\beta_h + 9[(0.3\cos\beta_h)^2 + 4\sin^2\beta_h]^{1/2}}{4\sin^2\beta_h}$	$210^o \le \lambda_h < 260^o$	$\lvert\beta_h\rvert \le 90^o$
$CNA = \frac{1 - 2\sin\beta_h\cos\beta_h}{2}$	$CNB = 0.707(\sin\beta_h + \cos\beta_h)$	

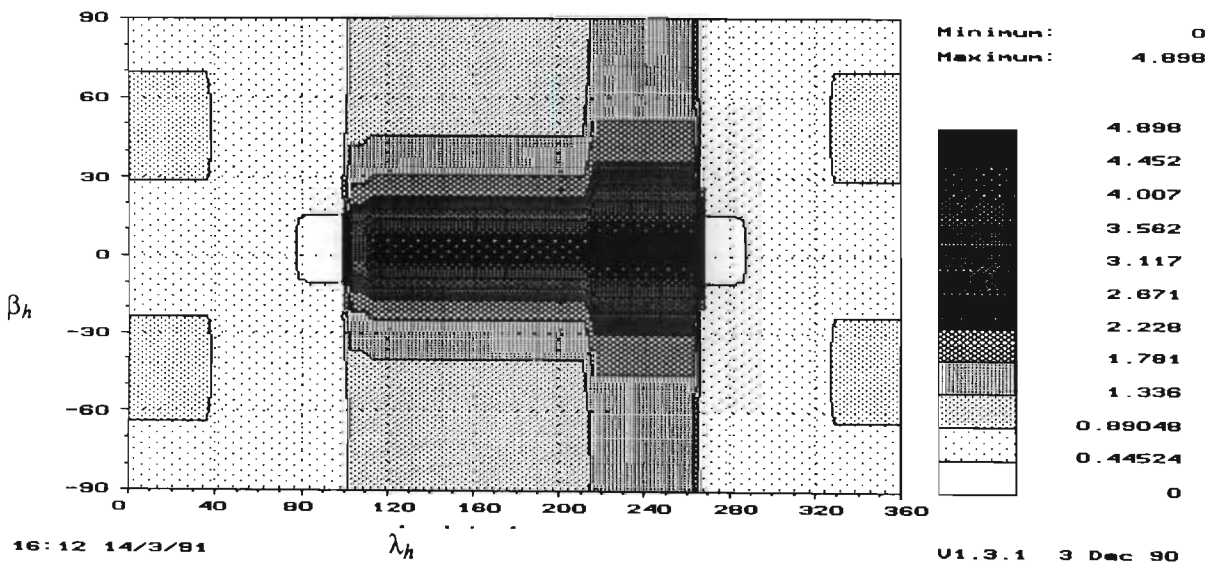

Figure 2-24 Contour map of Rudie's orbital simulation of meteors.

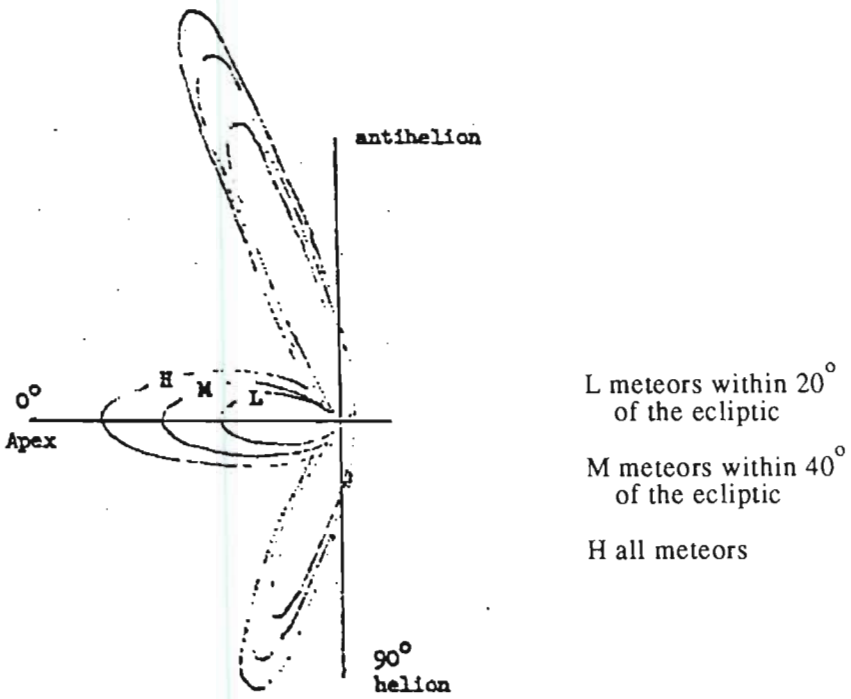

Figure 2-25 Observed distribution of meteors given by *Rudie* [1967].

In support of his simulated orbital distribution, Rudie compared results obtained from his so called "orbit-radiant" transformation with Davies' measured results of Figure 2-5. Rudie's results are reproduced in Figure 2-25. As mentioned by Rudie, there are only two minor deviations between the results when compared as polar plots as shown in Figures 2-5 and 2-25. The widths of the regions of intense radiant activity near the sun and antisun in Figure 2-25 are narrower than those in Figure 2-5, and the locations of those regions differ by about ten degrees. As will be shown later, the similarity between the results does not, however, necessarily imply that the Rudie's orbital distribution is an accurate representation of the actual orbital distribution, but simply serves to show that combination of Rudie's orbital simulation and transformation produces a result that is similar to the actual observed result.

2.3 Velocity distribution of sporadic meteors

As will be shown in the following chapter, the velocity distribution of meteors is an important parameter in determining the arrival rate of meteors over a forward-scatter link. Unfortunately, however, very little published information on this parameter is available.

Radar measurements of meteor velocities have shown that the majority of meteors travel in elliptical orbits around the sun with an average heliocentric velocity of approximately 35 kilometres per second, *Davies* [1957], *McKinley* [1961]. The only presentation of the velocity distribution of meteors versus position on the celestial sphere known to the author was by *Andrianov and Pupyshev* [1972]. Based on the measurements taken by McCrosky and Posen and by radar measurements of 2200 meteors taken from April to May, 1965, and October, 1966, at Kazan, USSR, Andrianov and Pupyshev presented distributions of geocentric velocities for sixteen regions on the celestial sphere. Although statistically a small sample set, analysis of the radar measurements and McCrosky and Posen's data revealed no clear seasonal or latitudinal dependence of geocentric velocity on the elongation angle, ε_g. Differences between the radar and photographic measurements were found, as might be expected, due to the different selection effects inherent in the two types of measurement. Unfortunately the reproduction of the graphical data presented by Andrianov and Pupyshev available to the author is of very poor quality and is therefore not reproduced here. McCrosky and Posen's original data is however available and has been analysed by the author. A contour map of the relative density distribution of geocentric velocity versus geocentric elongation angle extracted from *McCrosky and Posen* [1961] is presented in Figure 2-26.

McCrosky and Posen's measurements confirm the expected maximum and minimum geocentric velocities of approximately 11 and 72 kilometres per second limited by the escape velocities of the earth and sun respectively. The regions of

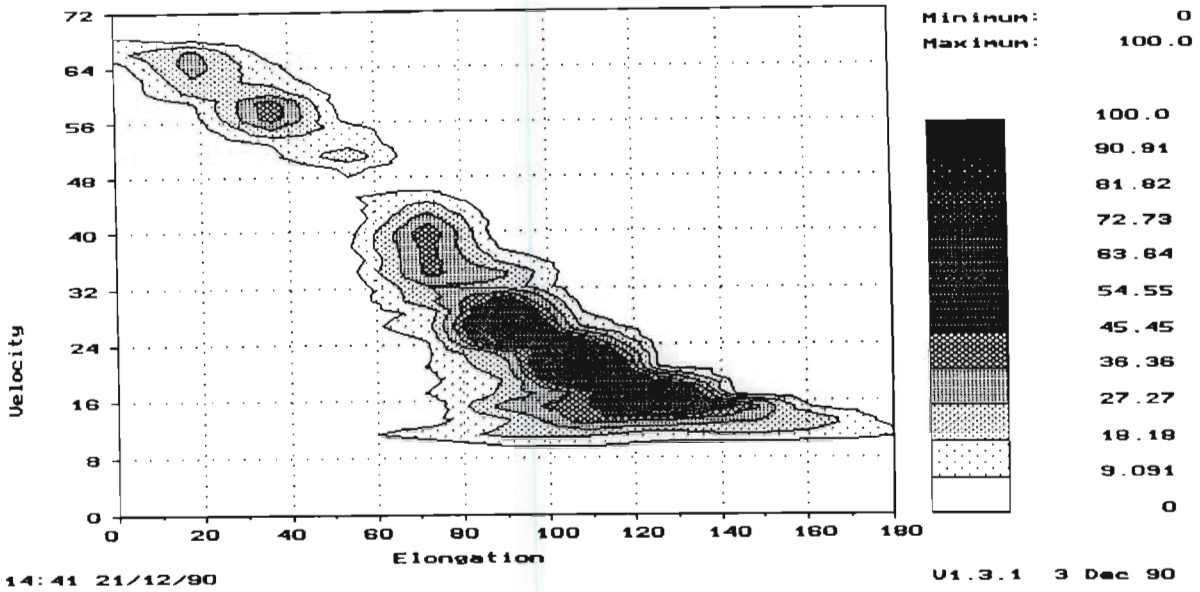

Figure 2-26 Contour map of the relative density distribution of geocentric velocity versus geocentric elongation angle extracted from data given in *McCrosky and Posen* [1961]

high contribution also correlate well with the expected mean heliocentric velocity of 35 kilometres per second.

2.4 Predicting the arrival rate of meteors over forward-scatter links

As mentioned by *Mawrey* [1990], the modelling of meteor-scatter links to predict communication performance has received renewed interest during the last decade. One of the most important parameters affecting communication performance is the arrival rate of meteors over a forward-scatter link. The theory and measurements published since the late 1940's have been combined in the form of advanced computer-based prediction models. The recent computer-based prediction models may be divided into two broad categories. The first category, which includes the models by *Haakinson* [1983], *Sachs* [1984] and *Felber et al.* [1985], is based on the assumption that the arrival rate of meteors for any arbitrary link can be predicted by scaling data from known reference links. The second

category includes the models by *Brown* [1985], *Weitzen* [1986], *Larsen and Rodman* [1988] and *Desourdis et al.* [1988] that use the theory of the physical properties of meteors, as well as the effects of a non-uniform distribution of meteors intercepting the earth.

2.4.1 Development of meteor prediction models

Using the geometrical tangential requirements of forward-scattering from underdense meteor trails, the characteristics of the power received from an underdense trail, and the assumption that a meteor trail only acts as a useful radiator when at least half its principal Fresnel zone is ionized, *Eshleman and Manning* [1954] calculated the relative contribution of parts of the meteor region to forward-scatter communication. Based on the assumption of a uniform geocentric distribution of meteors intercepting the earth, Eshleman and Manning's results showed that, primarily due to geometrical requirements, regions of high contribution occurred either side of the path between the transmitter and receiver with a null along the path midpoint between the regions of high contribution. Due to the assumption of a uniform distribution of meteors, Eshleman and Manning's method was unable to predict any variations in the arrival rate of meteors.

The first predictions of variations due to the effect non-uniform radiant distributions on the arrival rate of meteors over forward-scatter links were presented by *Hines* [1956] and *James and Meeks* [1956]. Using an alternative method of predicting the relative contribution of various sky regions, *Hines* [1955], *Hines and Pugh* [1956], *Hines* [1956] published predicted daily variations in forward-scattered meteor signals based on the assumption that sporadic meteor radiants could be modelled as a diffuse concentration of radiants centered on the apex of the earth's way. Details of the distribution used by Hines were not given. By improving the method of calculating the relative contribution of parts of the meteor region developed by Eshleman and Manning, and by developing an approximate technique of including Hawkins' non-uniform radiant distribution,

James and Meeks [1956] presented comparisons between predicted and measured daily cycles of meteors. The poor correlation between the predicted and measured daily cycles obtained by James and Meeks was subsequently improved by *James* [1958] who modelled Hawkins' radiant distribution as a three-point concentration of radiants along the ecliptic at the apex, sun and antisun peaks as measured by *Hawkins* [1956] and *Lovell* [1954].

Rudie [1967] improved on the previous method of modelling the arrival rate of meteors by generating a distribution of meteors that approximated Davies' measured distribution. Besides incorporating the effect of a non-uniform distribution of meteors, Rudie also used an alternative method of calculating the relative contribution of parts of the meteor region. Rudie's model was the first published model to include a non-uniform distribution with potential contributions across the entire celestial sphere. Investigations by the author have revealed some problems with Rudie's technique that are discussed in greater detail in Chapter 4.

The importance of investigating Rudie's method in greater detail is illustrated by the fact that three out of the four recently developed advanced prediction models, namely, the models by *Weitzen* [1986], *Larsen and Rodman* [1988], and *Desourdis et al.* [1988], are based on Rudie's method of calculating the effect of Davies' non-uniform radiant distribution on the arrival rate of meteors. Brown's model uses an approximation of Hawkins' distribution.

Although the effect of non-uniform distributions is of primary importance in this thesis it is important to note that the recent computer based prediction models offer significant improvement over the previous models. One of the primary reasons for this is the incorporation of more of the underlying physical parameters and theory into an integrated prediction tool. Detailed descriptions of the recent prediction models are given in the literature.

As part of the investigation into predicted and measured arrival rates of meteors, the meteor prediction model developed by Larsen and Rodman has been further developed by the author.

2.4.2 Comparisons between predicted and measured variations in the arrival rate of meteors

The non-uniform distribution of meteor radiants intercepting the earth results in predicted variations in the arrival rate of meteors over a particular meteor-scatter link. In the case of the yearly-averaged non-uniform distributions of meteors in geocentric ecliptical coordinates given in the previous section, predicted daily and seasonal variations may be seen to be due to changes in position of the particular link relative to the geocentric ecliptical coordinate system. The daily rotation of the earth about its axis and an anisotropic distribution of meteors in geocentric ecliptical coordinates results in a daily cycle of meteors, whilst the tilt of the earth's axis relative to the ecliptic plane similarly results in a seasonal or annual variation in meteor arrival rates.

Few published comparisons between measured and predicted variations in the arrival rate of meteors exist. *James* [1958] presented comparisons between predicted results based on a three-point approximation to Hawkins' radiant distribution and measured daily variations in the arrival rate of meteors for three different meteor links. Although a reasonable agreement between the measured and predicted results was obtained, the approximate nature of the radiant distribution used by James limited the accuracy of the predicted results. *Rudie* [1967] demonstrated the feasibility of his prediction technique by demonstrating the effect of his non-uniform distribution on relative meteor activity on the meteor region. Rudie did not, however, integrate over the sky region to compare measured and predicted variations in the arrival rate of meteors directly. Using Rudie's technique *Weitzen* [1986] compared measured and predicted monthly-averaged daily variations in the arrival rate of meteors for two different links.

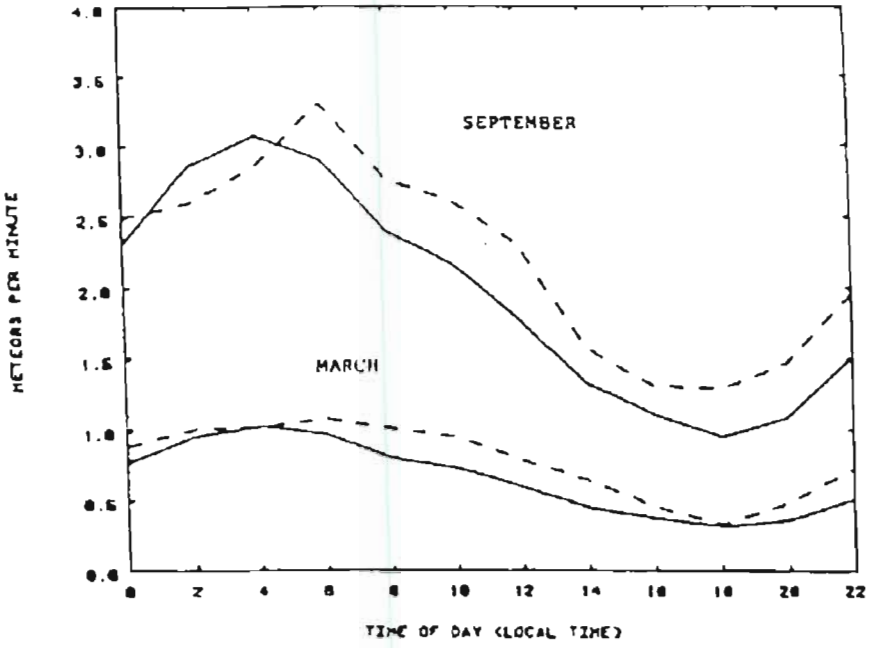

Figure 2-27 Arrival rate of meteors (meteors/min) for a 960 km mid-latitude link (solid lines) and predicted results for March and September (broken lines). *Weitzen* [1986]

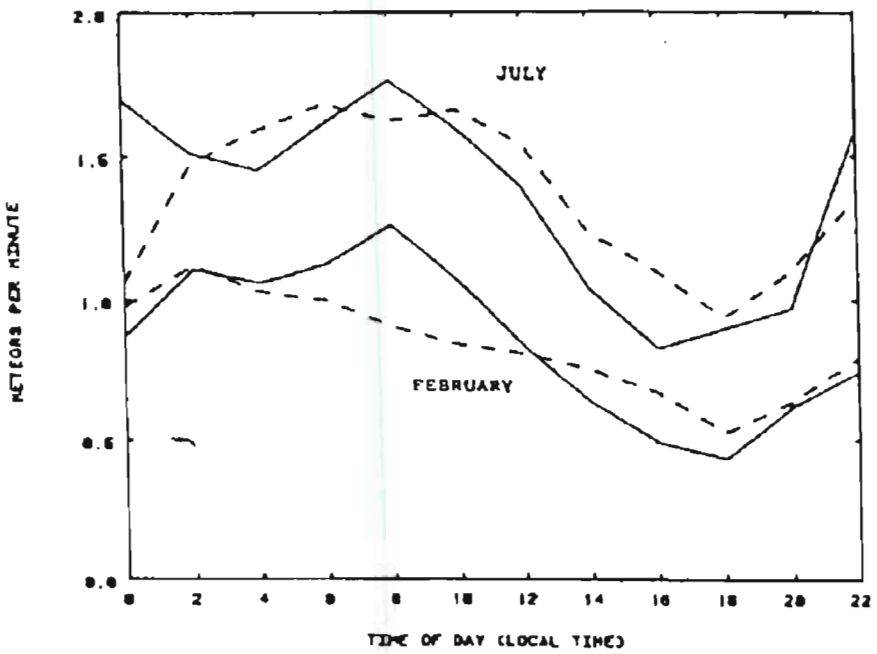

Figure 2-28 Arrival rate of meteors (meteors/min) for a 1260 km high-latitude link (solid lines) and predicted results for February and July (broken lines). *Weitzen* [1986]

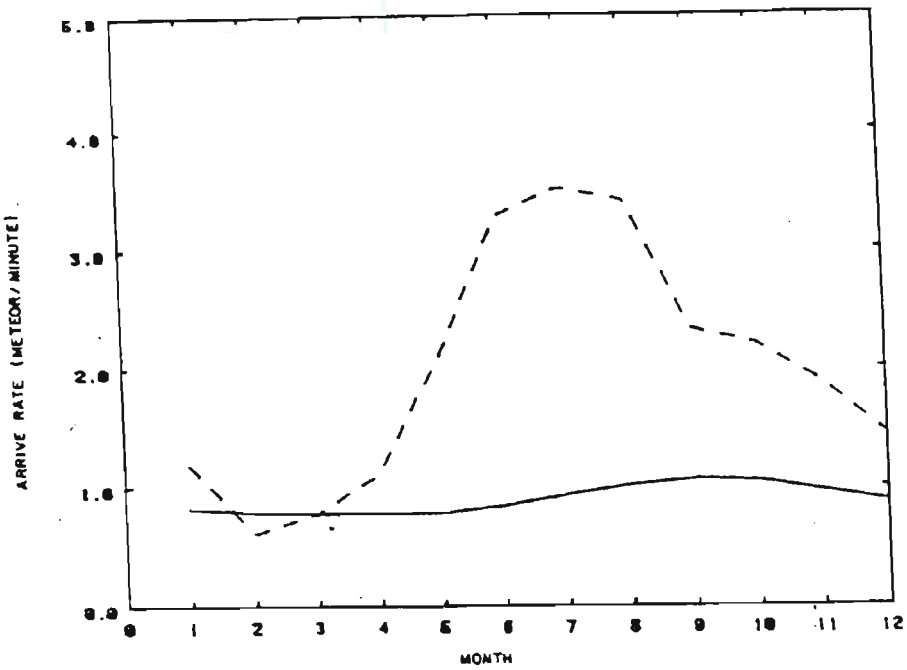

Figure 2-29 Monthly meteor arrival rate prediction with (broken line) and without (solid line) the effect of shower meteors considered according to *Weitzen* [1986]

Weitzen's comparisons are reproduced in Figure 2-27 and 2-28. The correlation between Weitzen's measured and predicted results is good, although, from *Weitzen* [1986], it appears that the predicted results have been scaled according to an expected seasonal variation in meteor arrival rates. According to *Weitzen* [1986] seasonal variations in the number of meteors predicted by considering only sporadic meteors do not correspond to observed data and additional factors are required. Variations in monthly meteor arrival rate with and without the effect of meteor showers predicted by Weitzen are reproduced in Figure 2-29. The source of these predictions was not given by Weitzen, although it appears that the solid line is based on a prediction using Rudie's distribution whilst the dotted line appears very similar to the annual variation measured by *Hawkins* [1956]. As mentioned by *Mawrey* [1990] and described in greater detail later, the inclusion of an annual scaling factor can only be approximate, since the effect of showers and the variation in the radiant distribution will vary from link to link

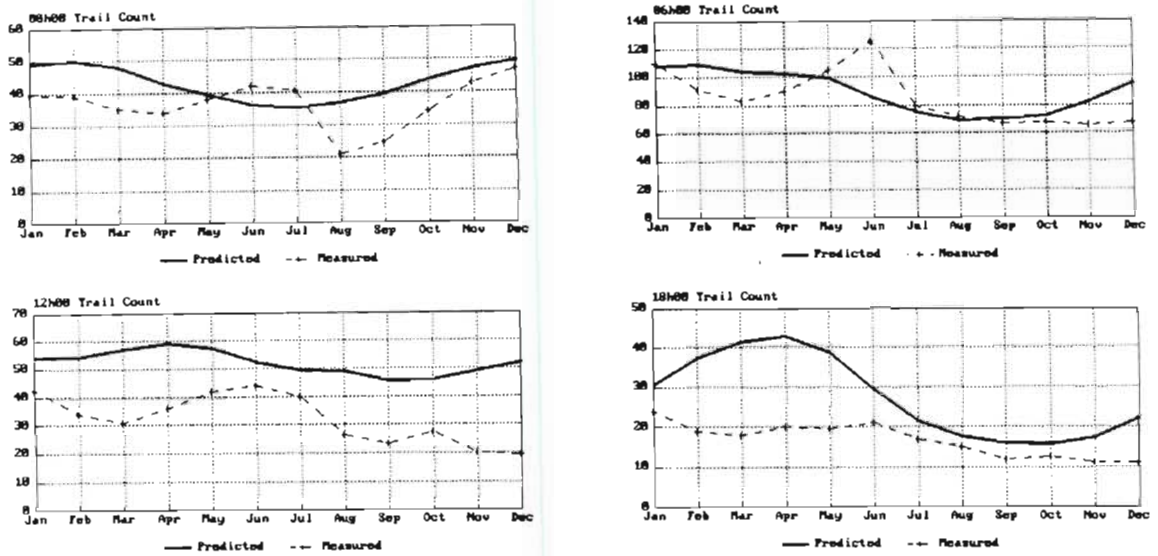

Figure 2-30 Comparison between predicted and measured annual variation in the monthly-averaged hourly arrival rate of meteors for a forward-scatter link in the Southern Hemisphere given by *Mawrey* [1990].

depending on factors such as geographical location and other link parameters. Hawkins' measured yearly variation of the relative number of meteors intercepting the earth was also initially adopted by *Brown* [1985] but was subsequently found to be inappropriate by *Steffancin and Brown* [1986]. The only direct comparison between predicted and measured annual cycles of meteors over a forward-scatter link known to the author was given by *Mawrey* [1990]. The predicted results using Rudie's radiant distribution and measured results taken in the Southern Hemisphere are reproduced in Figure 2-30. These results will be analysed in greater detail later but it is important to note at this stage that, contrary to some predictions, there was no large annual variation in the measured arrival rate of meteors.

2.4.3 Published annual variations in the arrival rate of meteors

Summaries of published annual variations in the arrival rate of meteors have been presented by *McKinley* [1961] and *Keay* [1963]. *McKinley* [1961] presented mean annual variation of meteor rates measured by naked-eye visual observations, telescopic visual observations, forward-scatter radio observations and back-scatter radio observations. The annual cycle of meteors presented by McKinley is shown in Figure 2-31. Including the results presented by *McKinley* [1961], *Keay* [1963] presented further annual variations in the arrival rate of meteors recorded at mid-northern latitudes. The annual variations of meteors were scaled for easy comparison and are reproduced in Figure 2-32.

Forward-scatter cycles have been extracted from papers by *Vogan and Campbell* [1957], *Sinno* [1979] and *Srirama Rao et al.* [1983]. The cycle extracted from

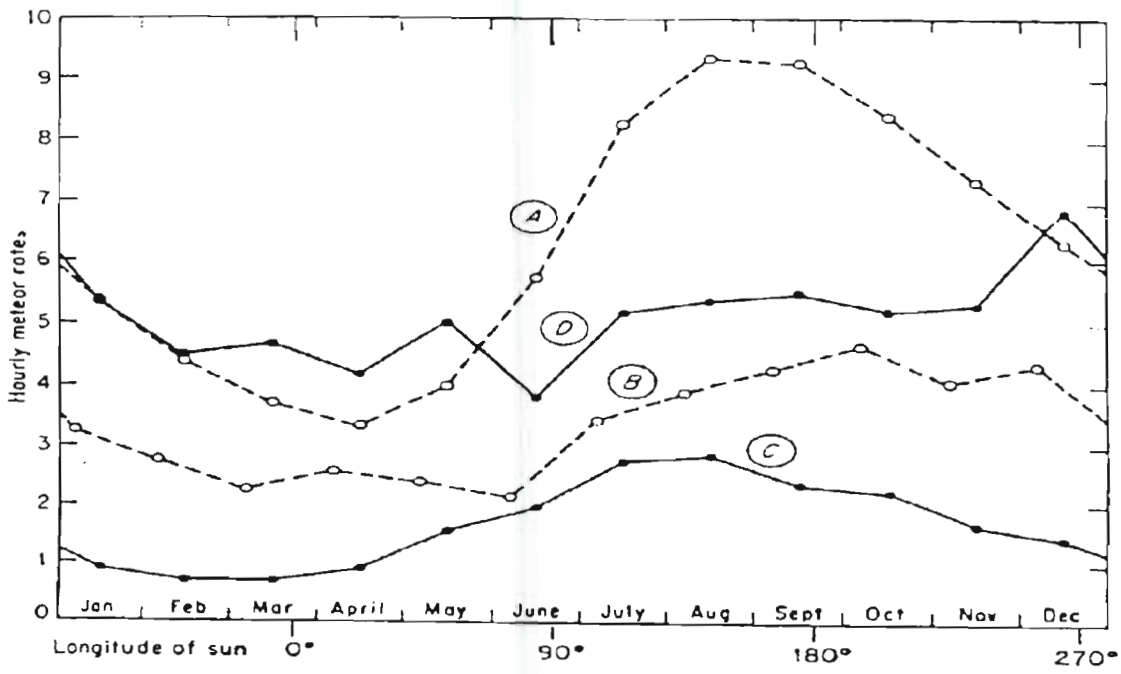

Figure 2-31 Annual cycles of meteors given by *McKinley* [1961]. Curve A, naked-eye visual observations. (*Murakami* [1955].) Curve B, telescopic visual observations. (*Kresáková and Kresák* [1955].) Curve C, forward-scatter radio observations. Multiply ordinate scale by 20. (*Vogan and Campbell* [1957].) Curve D, back-scatter radio observations. Multiply ordinate scale by 2. (*Weiss* [1957].)

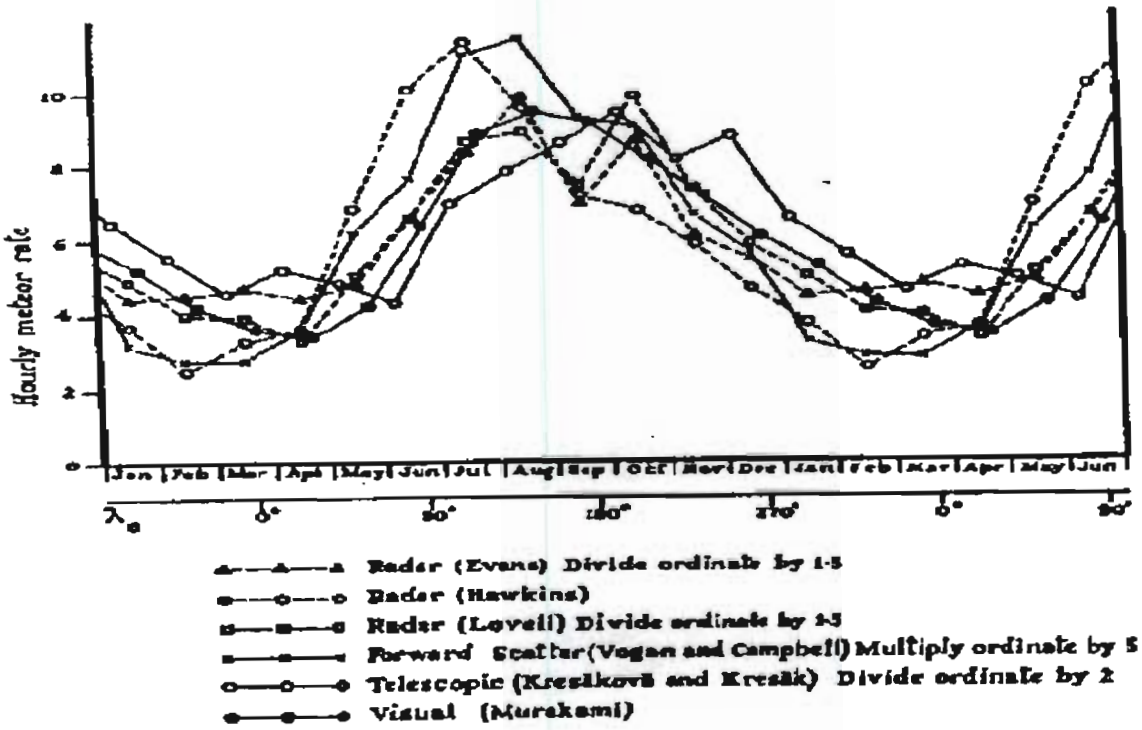

Figure 2-32 The annual variation in the arrival rate of meteors recorded at mid-northern latitudes presented by *Keay* [1963]

Vogan and Campbell is also given in Figures 2-31 and 2-32. In order to obtain a comparison between the different systems the published data was extracted graphically to obtain the monthly average where it was not specified. The monthly average for each system was then normalized to the mean for each annual cycle. The normalized annual cycles for the forward-scatter measurements are given in Figure 2-33.

The annual variation in the arrival rate of meteors in both hemispheres was compared by *Keay* [1963]. The results of this comparison are presented in Figure 2-34, which gives the normalized results of Figure 2-32 and radar back-scatter measurements measured by Keay in the Southern Hemisphere at a latitude of 43 $\frac{1}{2}^{o}$. As mentioned by Keay, the slight difference in amplitudes of the Northern and Southern hemisphere cycles measured at approximately the same absolute

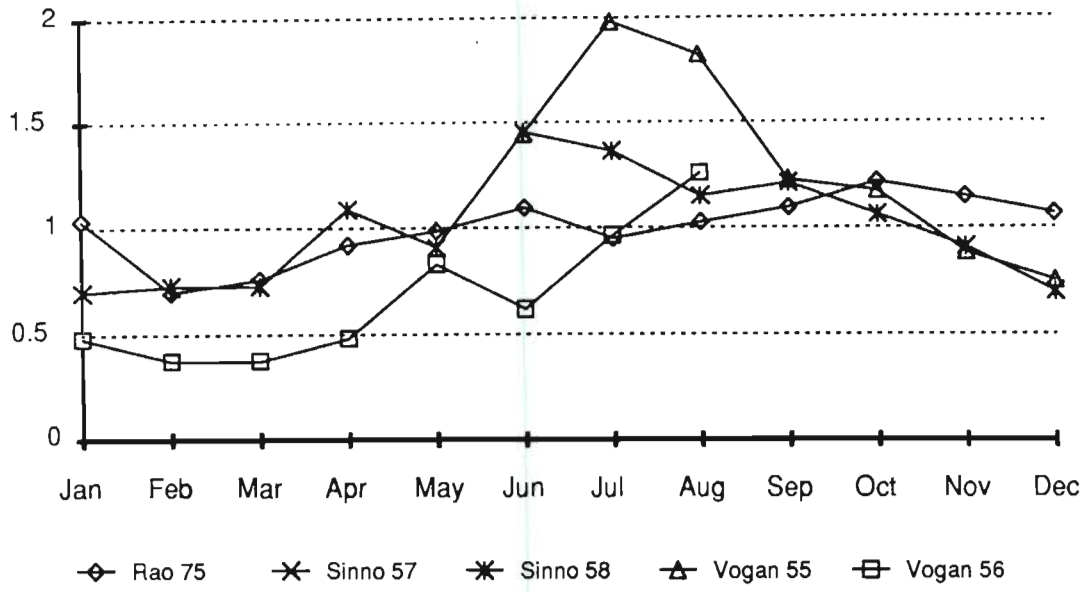

Figure 2-33 Some normalised annual variations in the arrival rate of meteors measured over forward-scatter links.

latitude indicated that there was also a slight annual variation in the density of meteors intercepting the earth. Comparisons between predictions of the annual variation of meteors using a three-point radiant distribution, similar to the distribution presented by *James* [1958], and measured annual variations of meteors indicated the annual variation in the density of meteors intercepting the earth had the form given in Figure 2-35, *Keay* [1963].

As mentioned by *Keay* [1963] the results presented in Figure 2-35 vary significantly from the annual variation in the number of meteors intercepting the earth presented by *Hawkins* [1956] that is reproduced in Figure 2-4. Based on the apparent current acceptance of Hawkins' results by *Weitzen* [1986] this discrepancy will be further investigated in Chapter 5.

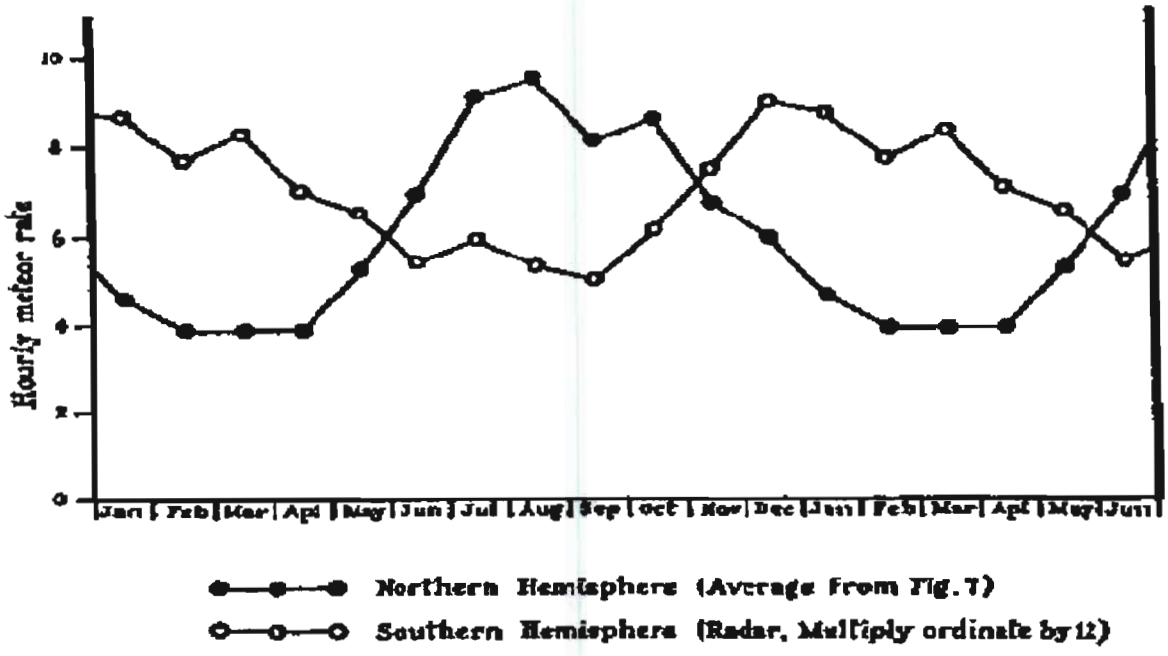

Figure 2-34 The annual variation of meteor arrival rates in both the Northern and Southern hemisphere presented by *Keay* [1963].

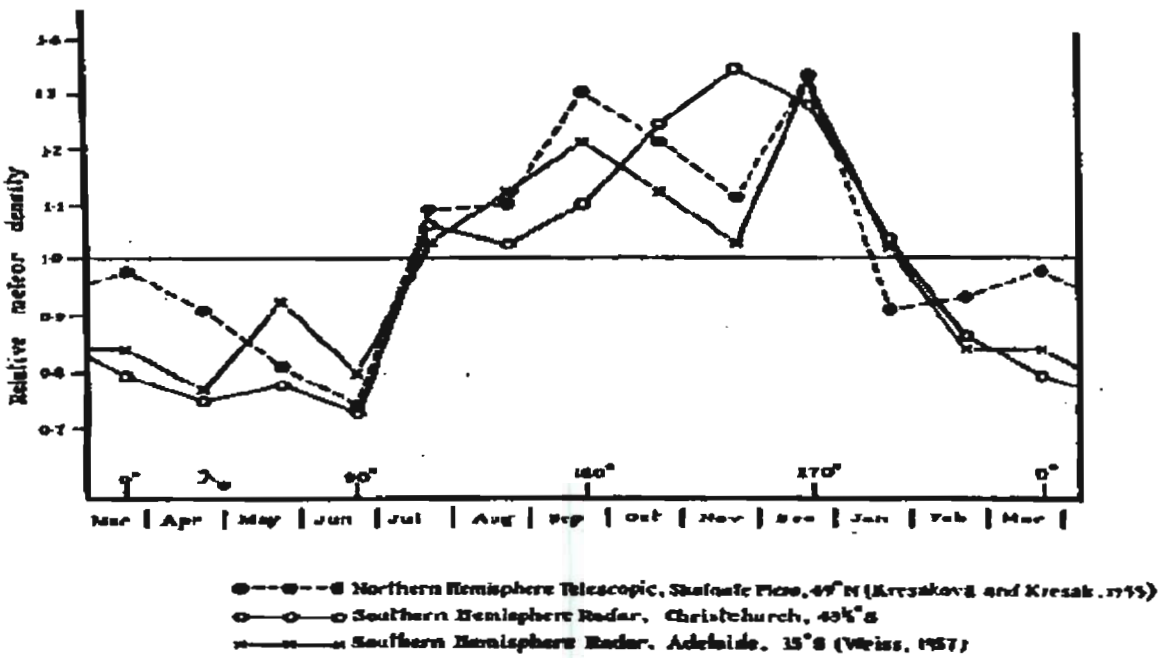

Figure 2-35 The annual variation in the arrival rate of meteors intercepting the earth based on comparisons between predicted and measured results for the Northern and Southern hemisphere presented by *Keay* [1963].

2.4.4 Published year-to-year variations in the arrival rate of meteors

Published year-to-year variations in the arrival rate of meteors have been presented or may be extracted from the data given by *Hawkins* [1956], *Ellyett and Keay* [1963], *Millman and McIntosh* [1964 & 1966] and *Southworth and Sekanina* [1975]. One of the most detailed investigations into the year-to-year variation in arrival rates was performed by *Keay and Ellyett* [1968]. Annual variations in the average hourly meteor rate from February 1963 to August 1965 presented by Ellyett and Keay are reproduced in Figure 2-36. As mentioned by Ellyett and Keay, apart from an inexplicable fluctuation in March 1964, the form of the annual variation is similar for each year. The overall level of activity varies from year to year as shown in Figure 2-36 although an even greater variation was found between data measured during 1960/61 (not shown here) and during 1963 to 1965, *Ellyett and Keay* [1964] and *Millman and McIntosh* [1964]. Subsequent investigation, *Linblad* [1967], *Ellyett* [1977], *Ellyett and Kennewell* [1980]

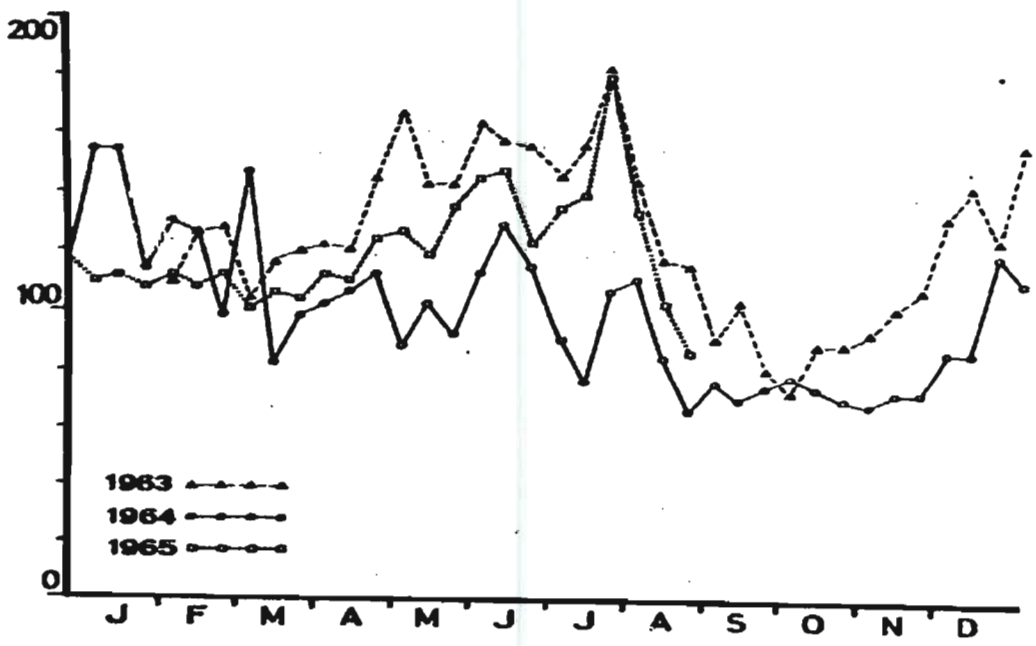

Figure 2-36 Annual variation in average hourly meteor rate between 1 February 1963 and 31 August 1965 presented by *Keay and Ellyett* [1968].

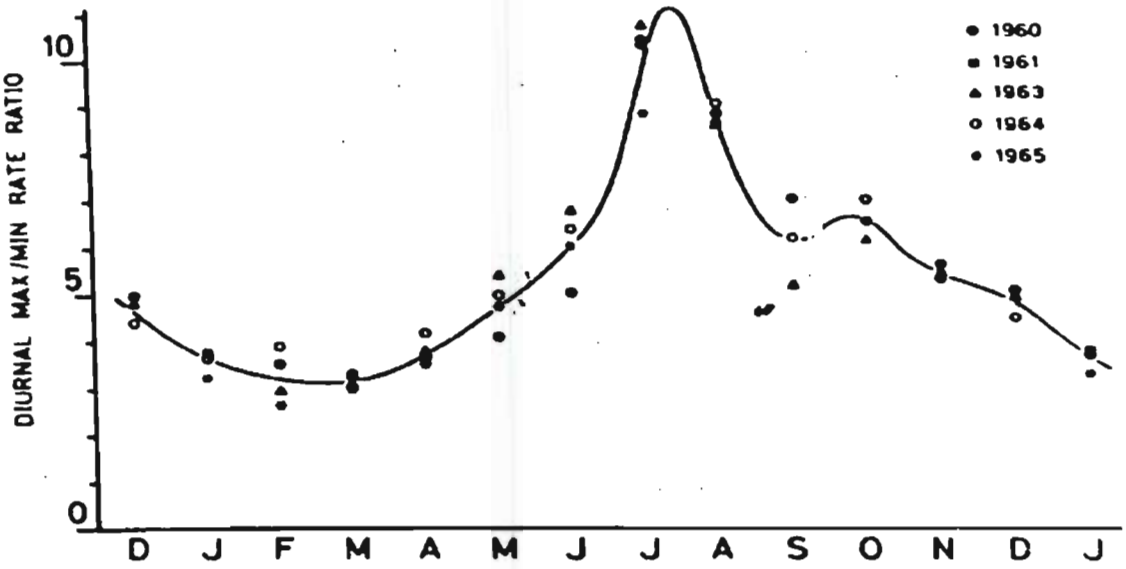

Figure 2-37 Annual variation in the diurnal ratio of maximum to minimum meteor rates presented by *Keay and Ellyett* [1968]

indicates that there may be an inverse correlation between apparent meteor arrival rates and the solar cycle due to the sun-controlled variations of atmospheric density in the meteor region.

As mentioned by Ellyett and Keay, although there is considerable variation in the extreme rates from year to year, the relative variation in rates from year to year is far smaller. This is illustrated by the ratio of minimum to maximum diurnal rates presented by *Keay and Ellyett* [1968] that is reproduced in Figure 2-37. The correlation in the year-to-year variations in the arrival rate of meteors appears to indicate that the radiant distribution of meteors remains relatively constant from year to year.

2.5 Problems and uncertainties

Of the distributions presented at the beginning of this chapter, only the distributions given by Hawkins and indirectly by Davies have been used in published models. Rudie's interpretation of Davies' distribution appears to have received the widest acceptance but no detailed analysis of the applicability or limitations of the use of this model have been published. An investigation of the validity of Pupyshev's distributions is important for a number of reasons. Firstly, no published account of the use of the distributions presented by Pupyshev for the prediction of forward-scatter variations are known to the author. Secondly, Pupyshev's distributions are the only known distributions that consist of a large proportion of radiants south of the ecliptic, and thirdly, Pupyshev's distributions are the only distributions known to the author that provide monthly-averaged rather than yearly-averaged distributions.

Besides the need for a more detailed analysis of the presently used radiant distributions based on comparisons between measured and predicted data, the contradiction between large predicted variations in the annual arrival rate of meteor based on Hawkins' results that appears to have some acceptance in the literature, and the relatively small variation in some of the measured results requires further examination.

As already mentioned, the general acceptance of Rudie's method of applying Davies' results also requires further attention.

Chapter 3

Calculation of the arrival rate of meteors

The technique used to calculate the arrival rate of meteors over a meteor scatter link is described in this chapter. Theory used to calculate the arrival rate of observable underdense meteors over a forward-scatter link are presented and a simple technique of including the effect of non-uniform distributions of meteors on the arrival rate of meteors is described.

The method of implementation of the theory described in this chapter as part of an advanced computer-based prediction model is also described.

3.1 The physical properties of meteors

3.1.1 Mass distribution of meteors

Based on observational data of meteors the relationship between the mass of meteors, m, and the average arrival rate of meteors, N, entering the earth's atmosphere at a particular radiant and at a particular time has been shown to be: *McKinley* [1961]

$$\frac{dN}{dm} = K'_m m^{-s} \tag{3-1}$$

where K'_m and s are constants determined by measurement.

The integrated form of the above expression is often used, namely

$$N(m) = K_m m^{1-s} = K_m m^{-k} \tag{3-2}$$

where $N(m)$ is the arrival rate of meteors, N, greater than mass, m, entering the earth's atmosphere for a particular radiant and time of day and year, K_m is a constant, and $k = s - 1$.

The above expressions are only strictly true over a limited range of mass, but are normally assumed to be accurate over the range of masses typically used for communication purposes. Some measured values of k are given in Table 3-1.

Table 3-1 Measured values of k.

k	Reference
1.3 ± 0.3	*McIntosh and Simek* [1969]
1.1	*Babadzhanov et al.* [1985]

Particular values of k may also be associated with different meteor showers and particular meteor trail families. A value of $k = 1.25$ has been used in this thesis.

3.1.2 Ionization

As a meteoroid enters the earth's atmosphere, collisions between the meteoroid and individual air particles in the atmosphere result in the kinetic energy of the meteoroid being transformed into heat, light and ionization, *McKinley* [1961]. The ionization is produced in the form of an electrically neutral tube of positive ions and electrons with an initially small radial component. The radius of the tube of ionization increases with time due to radial diffusion of the meteor trail. The amount of ionization produced is usually described as the number of electrons per unit length along the axis of the meteors path, since the radial component remains approximately constant for the duration of the trail. The electron component of the ionization is considered, since the presence of free electrons results in the radio reflective properties of meteor trails. It has been shown by *McKinley*

[1961] that the electron line density is directly proportional to the mass of the meteor and the density of the atmosphere. The relationship between electron line density, q, and height, h, above the earth's surface has been shown by *Kaiser* [1953], to be approximately

$$q = \frac{9}{4} q_{\max} \exp\left(\frac{h_{q_{\max}} - h}{H}\right)\left[1 - \frac{1}{3}\exp\left(\frac{h_{q_{\max}} - h}{H}\right)\right]^2 \qquad (3\text{-}3)$$

where

$q_{\max}$ is the maximum electron line density (ionization) in electrons per metre,

$h_{q_{\max}}$ is the height of maximum ionization above the earth's surface in kilometres, and

H is a scale height in kilometres. (H = 7 km.)

Kaiser [1953], has shown that the maximum ionization of a meteor is

$$q_{\max} = K_{q_{\max}} m \beta_i \cos^{\gamma} \zeta \qquad (3\text{-}4)$$

where

$K_{q_{\max}}$ is a constant,

m is the mass of the meteor in kilograms,

β_i is the probability that a single atom will produce a free electron,

ζ is the zenith angle [radians], and

γ is a constant typically assumed to be equal to one.

McKinley [1961], has shown that the ionization probability has the form

$$\beta_i \propto V_\infty^{k_{\beta_i}} \tag{3-5}$$

where k_{β_i} is a constant and V_∞ is the velocity of the meteor in metres per second. Various values of k_{β_i} have been published, some of which are given in Table 3-2.

Table 3-2 Values of k_{β_i}.

k_{β_i}	Reference
3 ± 1	*Davies et al.* [1959]
5	*McKinley* [1961]
4	*Verniani* [1965]

The height of maximum ionization in kilometres has been shown to be a function of meteor velocity and maximum ionization, *McKinley* [1961], and is given as

$$h_{q_{max}} = 82 + 49 \log_{10} V_\infty - 4.4 \log_{10} q_{max} . \tag{3-6}$$

3.2 Radio reflection properties

The forward-scatter radio reflection properties of meteor trails have been derived by *Eshleman* [1955] and *Hines and Forsyth* [1957]. Trails with electron line densities of less than approximately 10^{14} electrons per metre may be modelled as a line of individual electrons and are called underdense trails. Trails with an electron line density of greater than approximately 10^{14} electrons per metre have been modelled as a metallic cylinder and are called overdense trails. In order to describe the radio refection properties of these trails, the geometrical requirements for reflection via a meteor trail between two points on the earth's surface will first be described.

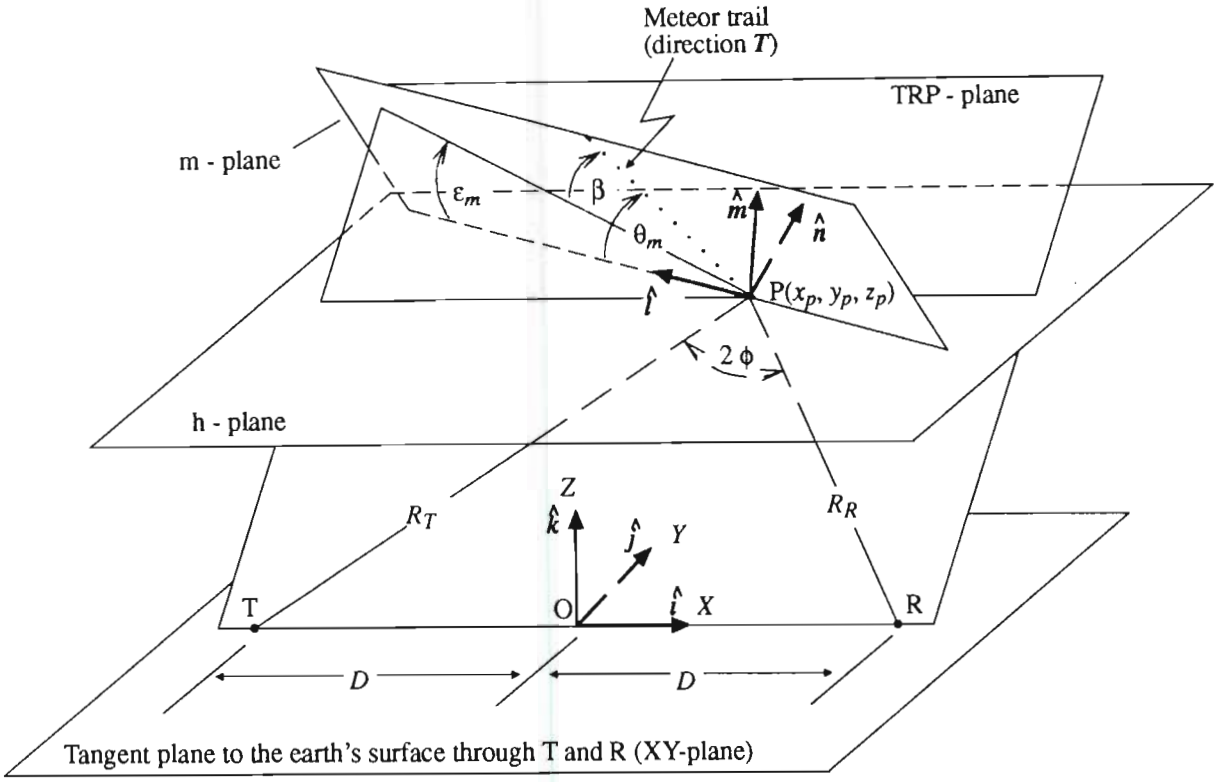

Figure 3-1 Diagram to illustrate the geometry of forward-scatter.

The geometry of forward-scatter reflection is illustrated in Figure 3-1. T and R are points on the surface of the earth, corresponding to the transmitter and receiver respectively. A plane through T and R is shown. A right-handed cartesian system is defined at the midpoint between T and R with its centre at O, and with its X and Y axis in the plane of the tangential plane through T and R. The -Z axis passes through the centre of the earth and the point O is actually beneath the earth's surface. The h-plane is a tangential plane to the earth's surface at a height, h, above the earth's surface at point P. For reflection to occur between points T and R on the earth's surface it may be shown that a meteor trail must lie in the plane of the tangent to the spheroid

$$\left(\frac{x}{x_o}\right)^2 + \left(\frac{y}{z_o}\right)^2 + \left(\frac{z}{z_o}\right)^2 = 1 \qquad (3\text{-}7)$$

where x_o and z_o are the intercepts of the spheroid with the X and Z axis respectively. The Y axis intercept is also z_o, *Rudie* [1967]. This plane is shown as the meteor-plane or m-plane in Figure 3-1. For a particular meteor, reflection between points T and R is shown in the figure to occur at point P(x_p, y_p, z_p) at the intersection of the m-plane, h-plane and TRP plane. (The TRP-plane is the plane through points T, R and P.) Point P is the centre of the region of the meteor trail contributing constructively to the amplitude of the reflected signal.

James and Meeks [1956], have shown that the normal to the spheroid at point P = (x_p, y_p, z_p) is

$$\hat{\boldsymbol{n}} = (n_x, n_y, n_z) \tag{3-8}$$

where

$$n_x = \frac{1}{2\cos\phi}\left[\, x_p\,(G_R + G_T) + D\,(G_R - G_T)\,\right]$$

$$n_y = \frac{1}{2\cos\phi}\left[\, y_p\,(G_R + G_T)\,\right]$$

$$n_z = \frac{1}{2\cos\phi}\left[\, z_p\,(G_R + G_T)\,\right], \text{ and}$$

where

$$G_R = \frac{1}{R_R} = \frac{1}{\sqrt{(D + x_p)^2 + y_p^2 + z_p^2}}, \text{ and}$$

$$G_T = \frac{1}{R_T} = \frac{1}{\sqrt{(D - x_p)^2 + y_p^2 + z_p^2}}.$$

A right-handed cartesian coordinate system with unit vectors $\hat{\boldsymbol{l}}$, $\hat{\boldsymbol{m}}$, $\hat{\boldsymbol{n}}$, and origin P, may be defined with $\hat{\boldsymbol{l}}$ and $\hat{\boldsymbol{m}}$ in the m-plane, and with $\hat{\boldsymbol{l}}$ in the direction of the

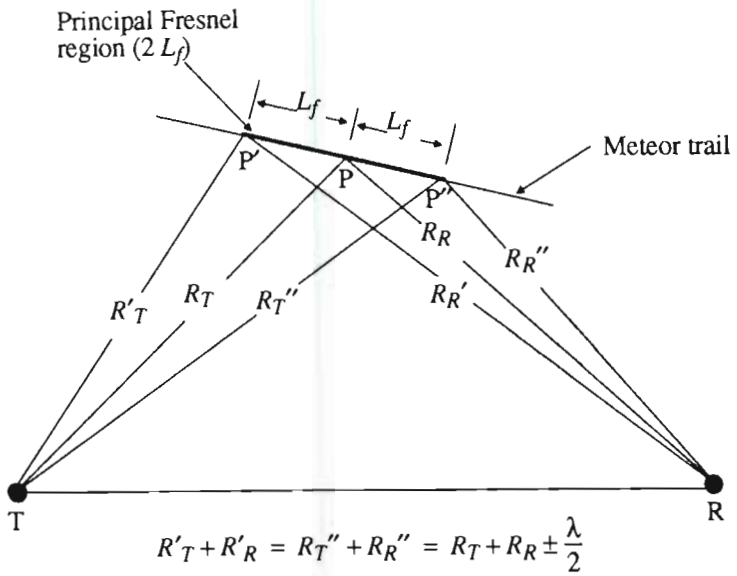

Figure 3-2 Diagram to illustrate the principal Fresnel region.

line formed by the intersection of the m-plane and the h-plane, as shown in Figure 3-1.

In order to provide reflection between T and R at point P, meteor trails must lie in the m-plane. Given meteor trail directions defined by radiant vectors, $\boldsymbol{T}$, this requirement may be described mathematically as

$$\hat{\boldsymbol{n}} \cdot \boldsymbol{T} = 0 . \tag{3-9}$$

The region along the meteor trail that provides amplitude enhancement at R (constructive interference) has a maximum path difference between T and R of half a wavelength, $\lambda/2$, at the frequency of operation. This defines a region $2L_f$ along the trail known as the principal Fresnel zone. A diagram to illustrate the principal Fresnel zone is given in Figure 3-2.

3.3 Received power

3.3.1 Underdense model

The received signal power available at a matched receiver from an underdense trail at R is, *Sugar* [1964]

$$P_R(t) = \frac{P_T G_T G_R \lambda^3 q^2 r_e^{2-} S^2}{16\pi^2 R_R R_T (R_R + R_T)(1 - \cos^2\beta \sin^2\phi)} e^{(\frac{1}{2}\tau + t_i + r_i)} \qquad (3\text{-}10)$$

where

$$\tau = \frac{\lambda^2 \sec^2\phi}{32\pi^2 d}, \; t_i = \frac{-32\pi^2 d t_o}{\lambda^2 \sec^2\phi}, \text{ and } r_i = \frac{-8\pi^2 r_o^2}{\lambda^2 \sec^2\phi}.$$

P_T is the transmitter power [watts],

G_T and G_R are the transmitting and receiving antenna gains respectively,

λ is the operating wavelength [metres],

q is the electron line density [electrons/metre],

r_e^- is the radius of an electron $\approx 2.8 \times 10^{-15}$ metres,

S^2 is the antenna polarization factor which has been described by *Rudie* [1967] and *Larsen and Rodman* [1988] (See Section 3-4.),

β is the angle between the intersection of the propagation plane and the meteor plane, and the meteor trail, as shown in Figure 3.1 [radians],

2ϕ is the angle between R_T and R_R as shown in Figure 3.1 [radians],

d is the radial diffusion constant of the meteor trail described in Section 3.1.2 [m^2/s],

$2t_o$ is the time in seconds taken to form the principal Fresnel zone, $2L_f$, and

r_o is the initial meteor trail radius in metres.

Various researchers have shown that the last three variables are a function of height and/or velocity, *Larsen and Rodman* [1988], namely:

$$\log_{10} r_o = A\,h - B \tag{3-11}$$

where h is the height in kilometres above the earth's surface.

Table 3-3 gives two different values of A and B.

Table 3-3 Values of A and B.

A	B	Reference
.075	7.2	*McKinley 1961*
.035	3.45	*Brown and Williams 1978*

Similarly, using the constants determined by *Brown and Williams* [1978], the diffusion constant is a function of height given as, *Larsen and Rodman* [1988]

$$\log_{10} d = 0.067\,h - 5.6 \tag{3-12}$$

The time taken to produce half of the principal Fresnel zone is given by *Larsen and Rodman* [1988] as

$$t_o = \frac{L_f}{V_\infty} \tag{3-13}$$

where

L_f is half the length of the principal Fresnel zone and is given by *McKinley* [1961] as

$$L_f = \left[\frac{\lambda R_R R_R}{(R_T + R_R)(1 - \cos^2\beta \sin^2\phi)} \right]^{1/2} \text{ [m].} \qquad (3\text{-}14)$$

3.3.2 Overdense model

It is generally accepted that the analytical approximation of the power received from an overdense trail is, in practice, not accurate. (See *McKinley* [1961], *Rudie* [1967], *Weitzen* [1983] and *Larsen et al.* [1990].) However, the approximate expression for the power received from an overdense trail as developed by *Hines and Forsyth* [1957] is

$$P_R(t) = \frac{P_T G_T G_R \lambda^2 S^2}{32 \pi^2 R_R R_T (R_R + R_T)(1 - \cos^2\beta \sin^2\phi)} \cdot \left[\frac{4 d t}{sec^2\phi} \ln\left(\frac{\tau_o}{t} \right) \right]^{1/2} \qquad (3\text{-}15)$$

where

$$\tau_o = \frac{r_e^- q \lambda^2 sec^2\phi}{4 \pi d} .$$

3.4 Antenna gain and polarization

The antenna gain and polarization factors G_T, G_R, and S may be calculated using the theory described by *Rudie* [1967], p 97-104, combined with the Numerical Electromagnetic Code (NEC) - Method of Moments software described by *Burke and Pogio* [1981]. No detail regarding this method will be given, suffice to say that the results obtained by NEC enable the antenna gains and polarization to be accurately calculated in three dimensional space, which enable the gain and polarization factors to be calculated at any point in the meteor region. This theory has been implemented by *Larsen and Rodman* [1988].

3.5 Observable meteor trails

Using the theory described in the previous sections, *Rudie* [1967] and *Larsen and Rodman* [1988], have shown that the arrival rate of number of underdense meteors may be calculated as

$$n(q_o) = \int_{\text{XY-plane}} \int_{z_{\min}}^{z_{\max}} \int_{\beta_{\min}}^{\beta_{\max}} \left[N(q_o, x, y, z, \beta) - N(q_t, x, y, z, \beta) \right] \, dz \, d\beta \, dx \, dy \qquad (3\text{-}16)$$

where

$n(q_o)$ is the arrival rate of meteors above the minimum detectable electron line density q_o,

$N(q_o, x, y, z, \beta)$ is the arrival rate of meteors with electron line densities greater than q_o contributed by a radiant (x, y, z, β) in the meteor region,

q_t is the transition line density between underdense and overdense trails; $\approx 0.75 \times 10^{14}$ electrons per metre, (meteor trails with an electron line density smaller than $\approx 0.75 \times 10^{14}$ electrons per metre are assumed to be underdense whilst meteor trails with an electron line density greater than $\approx 0.75 \times 10^{14}$ electrons per metre are assumed to be overdense.)

$N(q_t, x, y, z, \beta)$ is the arrival rate of meteors with electron line densities greater than q_t contributed by a radiant (x, y, z, β) in the meteor region, (The subtraction of $N(q_t, x, y, z, \beta)$ ensures that only underdense trails are included in the arrival rate calculation.)

$z_{\min}$ and $z_{\max}$ are the lower and upper limits of the meteor region at (x, y) respectively, and

β_{min} and β_{max} are the minimum and maximum angles that a meteor may have to satisfy the tangential requirements at (x, y, z).

By algebraic manipulation of Equations 3-1 to 3-15, *Larsen and Rodman* [1988], have shown that

$$N(q) = K \cos\zeta \left[\frac{\cos^{\gamma}\zeta \; V_{\infty}^{k_{\beta_i}} f(h)}{q} \right]^{k} \tag{3-17}$$

where

$$f(h) = \frac{9}{4} \exp\left(\frac{h_{q_{max}} - h}{H} \right) \left[1 - \frac{1}{3} \exp\left(\frac{h_{q_{max}} - h}{H} \right) \right]^{2}, \text{ and}$$

K is a constant dependant on radiant position, time of day and time of year. K may be derived from a particular radiant distribution of meteors as shown in Section 3.6.

From Equation 3-9, the minimum detectable line density is

$$q_o = \left[\frac{P_{R_{min}} \; 16\,\pi^2 R_R R_T (R_R + R_T)(1 - \cos^2\beta \sin^2\phi)}{P_T G_T G_R \lambda^3 r_e^2 - S^2 e^{r_i + t_i}} \right]^{1/2} \tag{3-18}$$

where

$P_{R_{min}}$ is the minimum received power [watts].

$N(q_o)$ and $N(q_t)$ may thus be found by substituting, q_o from Equation 3-18, and q_t respectively into Equation 3-17.

The previous equations may be expressed in terms of x, y, z and β using the following equations developed by *James and Meeks* [1956]:

$$\cos\zeta = \cos\Psi_m \cos\left[\frac{\pi}{2} - \varepsilon_m - \beta\right] . \tag{3-19}$$

$$\Psi_m = \sin^{-1}\left[\frac{z\,(R_T + R_R)}{\left(R_R + R_T\,(R_R + R_T)^2 - 4\,R_R\,R_T\,D^2\right)^{1/2}}\right] \tag{3-20}$$

where

Ψ_m is the angle between the z-axis and the m-plane (See Figure 3-1.), and

$$\varepsilon_m = \cos^{-1}\left[\frac{|y|}{\left(y^2 + z^2\sin^2(\phi - \lambda_1)\right)^{1/2}}\right]. \tag{3-21}$$

ε_m is the angle between the intersection of the h-plane and the m-plane, and the intersection of the TRP-plane and the m-plane (See Figure 3-1), and

$$\lambda_1 = \cos^{-1}\left[\frac{\sqrt{z^2 + y^2}}{R_T}\right] \text{ if } x > 0$$

or

$$\lambda_1 = \cos^{-1}\left[\frac{\sqrt{z^2 + y^2}}{R_R}\right] \text{ if } x \le 0 .$$

Furthermore

$$\phi = \frac{1}{2}\cos^{-1}\left[\frac{R_R^2 + R_T^2 - 4\,D^2}{2R_R R_T}\right] \tag{3-22}$$

where

$$R_R = \left[(D - x)^2 + y^2 + z^2\right]^{1/2}, \text{ and}$$

$$R_T = \left[(D+x)^2 + y^2 + z^2 \right]^{1/2}.$$

Finally

$$h = -r + \left[x^2 + y^2 + \left[z + (r^2 - D^2)^{1/2} \right]^2 \right]^{1/2}. \tag{3-23}$$

3.5.1 Average duty cycle

Sugar [1964] showed that the average duration of an underdense trail above the minimum detectable line density is

$$T = \frac{\lambda^2 \sec^2 \phi}{k\, 16\, \pi^2\, d} \tag{3-24}$$

Using Equation 3-16, the average duty cycle may therefore be calculated as

Duty cycle =

$$\int_{\text{XY plane}} \int_{z_{min}}^{z_{max}} \int_{\beta_{min}}^{\beta_{max}} \left[\left(N(q_o, x, y, z, \beta) - N(q_l, x, y, z, \beta) \right) \cdot T \right] dz\, d\beta\, dx\, dy \tag{3-25}$$

For the purposes of this thesis, however, calculation of the duty cycle is unnecessary and only the arrival rate of meteors will be considered.

3.6 Including the effect of the non-uniform radiant distribution of meteors

Extending the work of *James and Meeks* [1956], *Rudie* [1967] incorporated the effect of a detailed non-uniform distribution of meteors. Rudie's work has been implemented by *Weitzen* [1986], *Larsen and Rodman* [1988] and *Desourdis et al.* [1988]. Rudie used an analytically complicated method of including the effect

of a non-uniform distribution of meteors based on the simulated orbital distribution of meteors described in Chapter 2. As shown in Chapter 2 and later in Chapter 4, the non-uniform distribution of meteors may be completely described by using a geocentric (observed) radiant distribution in ecliptical coordinates. This section proposes a new and simpler method of including the effect of the non-uniform radiant distribution for a given link. The effect of geographic position, orientation, and time of day or year is included by referencing a meteor radiant in the link coordinates to the geocentric ecliptical longitude and latitude.

With reference to Equation 3-16 and Figure 3-1, the effect of the non-uniform radiant density on the relative number of meteors, N, seen at a particular (x, y, z, β) may be included by assuming that $K = C\,\delta_g$ in Equation 3-17 where δ_g is the non-uniform radiant density and C is a scaling constant. The relationship between a meteor radiant in terms of (x, y, z, β) and ecliptical longitude λ_g and latitude β_g may be found as follows.

The equation defining the surface with a constant height, h, above the earth's surface, in terms of the $\hat{i}, \hat{j}, \hat{k}$, coordinate system in Figure 3-1, is

$$z = f(x, y) = \sqrt{(h+r)^2 - x^2 - y^2} - \sqrt{r^2 - D^2} \qquad (3\text{-}26)$$

where

r is the radius of the earth, and

D is half the distance between the transmitter and receiver as illustrated in Figure 3-1.

The normal to the surface, $z = f(x, y)$, at point, $P = (x_p, y_p, z_p)$, *is*

$$\bar{n}_{hn} = -f_x(x_p, y_p)\,\hat{i} - f_y(x_p, y_p)\,\hat{j} + \hat{k} \qquad (3\text{-}27)$$

where

$$f_x(x_p, y_p) = \frac{\partial z}{\partial x}\Big|_{x_p, y_p} = \frac{-x_p}{\left[(h+r)^2 - x_p^2 - y_p^2\right]^{1/2}}, \text{ and}$$

$$f_y(x_p, y_p) = \frac{\partial z}{\partial y}\Big|_{x_p, y_p} = \frac{-y_p}{\left[(h+r)^2 - x_p^2 - y_p^2\right]^{1/2}}.$$

A vector defining the intersection of the h-plane and the m-plane is

$$\mathcal{T} = \bar{n}_{hn} \times \hat{\boldsymbol{n}}$$

$$= \begin{vmatrix} \hat{i} & \hat{j} & \hat{k} \\ -f_x & -f_y & 1 \\ n_x & n_y & n_z \end{vmatrix}$$

$$= (-f_y n_z - n_y)\,\hat{i} + (f_x n_z + n_x)\,\hat{j} + (f_y n_x - f_x n_y)\,\hat{k} \qquad (3\text{-}28)$$

The unit vector, $\hat{\ell}$, is thus

$$\hat{\ell} = \frac{\mathcal{T}}{|\mathcal{T}|} = \frac{-f_y n_z - n_y}{|\mathcal{T}|}\hat{i} + \frac{f_x n_z + n_x}{|\mathcal{T}|}\hat{j} + \frac{f_y n_x - f_x n_y}{|\mathcal{T}|}\hat{k} = l_x\hat{i} + l_y\hat{j} + l_z\hat{k}$$

(3-29)

where

$$|\mathcal{T}| = \left[(-f_y n_z - n_y)^2 + (f_x n_z + n_x)^2 + (f_y n_x - f_x n_y)^2\right]^{1/2}$$

A right-handed coordinate system may be defined as

$$\hat{m} = \hat{n} \times \hat{l} = \begin{vmatrix} \hat{i} & \hat{j} & \hat{k} \\ n_x & n_y & n_z \\ l_x & l_y & l_z \end{vmatrix} = (n_y l_z - n_z l_y)\hat{i} - (n_x l_z - n_z l_x)\hat{j} + (n_x l_y - n_y l_x)\hat{k}$$

(3-30)

As shown in Figure 3-1, the radiant of a meteor may be defined in terms of the $\hat{l}, \hat{m}, \hat{n}$ coordinate system, and hence the $\hat{i}, \hat{j}, \hat{k}$, coordinate system. Let T be the trail radiant where

$$T = \hat{m} \sin\theta_m + \hat{l} \cos\theta_m$$

$$= (m_x \sin\theta_m + l_x \cos\theta_m)\hat{i} + (m_y \sin\theta_m + l_y \cos\theta_m)\hat{j} + (m_z \sin\theta_m + l_z \cos\theta_m)\hat{k}$$

(3-31)

and $\theta_m = \varepsilon_m + \beta$ is the angle between the intersection of the m-plane and the h-plane, and the meteor radiant.

The transformation matrix relating the $\hat{i}, \hat{j}, \hat{k}$, coordinate system to the geocentric ecliptical coordinate system $\hat{i}_g, \hat{j}_g, \hat{k}_g$, where $\hat{i}_g, \hat{j}_g$, and $\hat{k}_g$ are the right-handed unit vectors in the direction of the apex, sun and perpendicular to the ecliptic plane defining the ecliptical coordinate system on the 23 September is given as, *James* [1958]

$$A =$$

$$\begin{bmatrix} \sin\psi \sin\delta_a + \sin l_a \cos\delta_a \cos\psi & \sin l_a \sin\delta_a \cos\psi - \sin\psi \cos\delta_a & -\cos\psi \cos l_a \\ \sin\sigma \cos l_a \cos\delta_a - \cos\delta_a \cos\psi \sin\delta_a + \cos\sigma \sin l_a \cos\delta_a \sin\psi & \cos\sigma \cos\psi \cos\delta_a + \sin\sigma \cos l_a \sin\delta_a + \cos\sigma \sin l_a \sin\delta_a \sin\psi & \sin\sigma \sin l_a - \cos\sigma \sin\psi \cos l_a \\ \sin\sigma \cos\psi \sin\delta_a + \cos\sigma \cos l_a \cos\delta_a - \sin\sigma \sin l_a \cos\delta_a \sin\psi & \cos\sigma \cos l_a \sin\delta_a - \sin\sigma \cos\psi \cos\delta_a - \sin\sigma \sin l_a \sin\delta_a \sin\psi & \cos\sigma \sin l_a + \sin\sigma \sin\psi \cos l_a \end{bmatrix}$$

$$= \begin{bmatrix} A_{11} & A_{12} & A_{13} \\ A_{21} & A_{22} & A_{23} \\ A_{31} & A_{32} & A_{33} \end{bmatrix} \tag{3-32}$$

where

δ_a is the azimuth angle measured from north clockwise to the X-axis so that $0 \leq \delta_a < 180^o$,

l_a is the latitude of the midpoint between T and R. (In the northern hemisphere $l_a > 0$ and in the southern hemisphere $l_a < 0$.),

σ is $23^o27'$, the angle between the earth's axis and the ecliptic normal, and

ψ is the nutation angle which is equal to $\omega_d t_d$ where t_d is the elapsed time in solar days since noon of September 23 and ω_d is the rotation of the earth per solar day; ω_d is 360.9856 degrees per day.

Including the motion of the earth around the sun, the radiant of the meteor in terms of the geocentric ecliptical coordinate system given in Figure 2.1 is thus

$$\boldsymbol{T}_g = \boldsymbol{A}\,\boldsymbol{T} \begin{bmatrix} \cos\varphi_R & \sin\varphi_R & 0 \\ -\sin\varphi_R & \cos\varphi_R & 0 \\ 0 & 0 & 1 \end{bmatrix} = \begin{bmatrix} \boldsymbol{T}_{g_x} \\ \boldsymbol{T}_{g_y} \\ \boldsymbol{T}_{g_z} \end{bmatrix} \tag{3-33}$$

where φ_R is equal to $\left[\frac{t_d}{366} 2\pi + \frac{\pi}{2} \right]$ radians.

The geocentric ecliptical latitude and longitude corresponding to a particular meteor radiant $\boldsymbol{T}$ is thus

$$\lambda_g = \tan^{-1}\left[\frac{-T_{g_x}}{T_{g_y}}\right], \text{ and} \tag{3-34}$$

$$\beta_g = \tan^{-1}\left[\frac{T_{g_z}}{\left(T_{g_x}^2 + T_{g_y}^2\right)^{1/2}}\right]. \tag{3-35}$$

3.7 Meteor showers

As mentioned by *Weitzen* [1986] and *Mawrey* [1990], shower meteors can have a major effect on the arrival rate of meteors during the duration of a particular shower. As mentioned by *Mawrey* [1990], the distinction between sporadic and shower meteors is difficult to determine and the majority of sporadic meteor distributions are bound to include a small shower component. A quantitative method of distinguishing between shower and sporadic meteors was given by *Southworth and Hawkins* [1963], but for the purposes of this thesis, shower meteors will be limited to the well known major meteor showers listed in Table 3-4.

As is the case in Table 3-4 meteor shower radiants are often described in terms of right ascension, α, and declination, δ. The duration of the showers in Table 3-4 is the time during which the activity of the shower is greater than one-quarter the peak value. As mentioned by *McKinley* [1961], there are large variations in

Table 3-4 The major meteor showers, *McKinley* [1961].

Shower Name	Duration	Right Ascension	Declination	Hourly Rate
Quadrantids	1-4 Jan.	231 °	+50 °	50
Corona Australids	14-18 Mar.	245	-48	5
Virginids	Mar. 5-Apr. 2	190	00	<5
Lyrids	19-24 Apr.	272	+32	5
Eta Aquarids	Apr. 21-May 12	336	00	20
Arietids	May 29-June 19	45	+23	60
Zeta Perseids	1-17 June	62	+24	40
Ophuichids	17-26 June	260	-20	20
Beta Taurids	June 24-July 5	87	+20	20
Capricornids	July 10-Aug. 5	315	-15	20
Southern Delta Aquarids	July 21-Aug. 15	339	-17	20
Northern Delta Aquarids	July 15- Aug. 18	339	00	10
Pisces Australids	July 15-Aug. 20	340	-30	20
Alpha Capricornids	July 15-Aug. 20	309	-10	5
Southern Iota Aquarids	July 15-Aug. 25	338	-15	10
Northern Iota Aquirids	July 15-Aug. 25	331	-6	10
Perseids	July 25-Aug. 17	46	+58	50
Kappa Cygnids	18-22 Aug.	290	+55	5
Orionids	18-26 Oct.	95	+15	20
Southern Taurids	Sept. 15-Dec. 15	52	+14	5
Northern Taurids	Oct. 15-Dec. 1	54	+21	5
Leonids	14-20 Nov.	152	+22	5
Phoenicids	Dec. 5	15	-55	50
Geminids	7-15 Dec.	113	+32	50
Ursids	17-24 Dec.	217	+80	15

shower activity from year to year, and the values given in the table are intended to indicate long term averages only.

As pointed out by *James and Meeks* [1956], a shower meteor with a radiant T will satisfy the tangential requirements at point (x, y, z) as long as the following expression is satisfied:

$$x\,T_x + y\,T_y + z\,T_z + \left[\frac{R_R - R_T}{R_r - R_T}\right] D\,T_x = 0. \tag{3-36}$$

A method of converting from right ascension and declination to $\boldsymbol{T}$ is *James* [1958]:

$$T_x = \sin\zeta \cos(\delta_a - A) \tag{3-37}$$

$$T_y = \sin\zeta \sin(\delta_a - A) \tag{3-38}$$

$$T_z = \cos\zeta \tag{3-39}$$

where

A is the azimuth angle of the meteor radiant measured from north to east.

The azimuth angle and zenith of the meteor radiant may be found as follows:

$$\cos A = \frac{\sin\delta - \sin l_a \cos\zeta}{\cos l_a \sin\zeta} \tag{3-40}$$

$$\cos\zeta = \sin l_a \sin\delta + \cos l_a \cos H \cos\delta \tag{3-41}$$

where

δ is the right ascension of the radiant, and

H is the hour angle.

The relationship between right ascension, α, and hour angle is approximately:

$$H = 99.40^o + \Delta + 0.9856\, d + 15.041\, n - \alpha \tag{3-42}$$

where

d is the number of days since January 1,

n is the number of hours since midnight, and

Δ is the number of degrees that the path midpoint is east of the standard time meridian.

The above equations enable the effect of individual meteor showers to be included in the calculation of the total arrival rate of meteors. For the purposes of this thesis, however, meteor shower contributions will not be included. As described later in Chapter 5, in general, this does not cause a significant error if monthly-averaged meteor rates are calculated.

3.8 Noise sources

The effect of man-made and galactic noise sources may included by modelling the effect of external noise sources on the receiver's noise floor, *Mawrey* [1988], p 132. The effect of environmental noise on the received signal-to-noise ratio is:

$$\frac{S_i}{N_i} = \frac{P_R}{B_n k_b (T_i + T_e)} \tag{3-43}$$

where

S_i is the receiver's input signal power [W],

N_i is the receiver's input noise power [W],

T_i is the environmental noise temperature received by the antenna [K],

T_e is the effective input noise temperature of the receiver [K],

B_n is the receiver's noise bandwidth [Hz], and

k_b is Boltzmann's constant (1.381×10^{-23} J/K).

The environmental noise temperature at the frequencies used in forward scatter communication is primarily a combination of man-made, atmospheric and galactic noise, *Mawrey* [1988]. The contribution due to galactic noise is computed

by integrating the receiver polar pattern over the region of the galactic noise map generated by NASA *Taylor* [1973]. It may be seen from Equation 3-43 that the minimum received power of Equation 3-18 is affected by the received signal-to-noise ratio requirement.

3.9 Computer-based prediction model

The equations described in the previous sections have been implemented as part of an advanced meteor-scatter prediction model. Modifications to the prediction model have been specified by the author as part of the investigation into variations in the arrival rate of meteors over forward-scatter links. These specifications include the simpler method of incorporating the effect of non-uniform radiant distributions described in Section 3-6, as well as the incorporation of the radiant distributions described in Chapter 2. Other involvement by the author in the development of the meteor prediction model was the specification of methods of predicting the effects of shower meteors as well as the effects of galactic noise contributions. A detailed description of the capabilities of the meteor prediction model may be found in *Larsen and Rodman* [1988] and *Rodman* [1989].

3.9.1 Implementation of the arrival rate calculations

For the purposes of this thesis only a subset of the capabilities of the meteor prediction model is required, namely, the calculation of the arrival rate of underdense meteors over a forward-scatter link as well as the measured database facilities described in Chapter 5.

The calculation of the arrival rate of underdense meteors is performed by software implementation of the equations described in the previous sections. This calculation essentially consists of numerical integration of Equation 3-16. The total arrival-rate of meteors is calculated by summing over the contribution of points in the meteor region. The position of the points in the meteor region are typically

chosen to be ten kilometres apart. The contribution at each point in the meteor region is calculated as described by the inner two integrals of Equation 3-16. This integration is also performed numerically. The effect of a non-uniform distribution of meteors may be included using the the technique described in Section 3-6.

In order to concentrate on the effect of non-uniform distributions of meteors on the arrival rate of meteors, the effect of as many variables and constants whose values are presently uncertain, and whose effect on the relative variation in the arrival rate of meteors was found to be minimal, were not included. This resulted in the time taken to form the first Fresnel zone, $2t_o$, and the initial trail radius, r_o, of Equation 3-10 being assumed equal to zero. In order to be directly compared with measured data, the effect of galactic noise contributions on the predicted arrival rate of meteors was also not included, since the method of data processing described in Chapter 5 effectively removes the effects of noise on the measured arrival rate of meteors.

Chapter 4

Rudie's orbital distribution and Davies' data

This chapter investigates the widely accepted distribution of meteor radiants presented by *Rudie* [1967]. Investigations into Rudie's method of modelling the distribution of meteor radiants reveals the limitations of this technique. A new, alternative method of extrapolating Davies' data is proposed.

4.1 Rudie's orbital distribution

As mentioned in Chapter 2, an investigation into Rudie's method of deriving an orbital distribution based on Davies' results has revealed some limitations. Rudie claimed that the orbital distribution described by Davies' Figures 2-6 to 2-8 could be simulated, and that if the simulation was realistic, then a radiant distribution derived from it should compare favourably with Davies' radiant distribution shown in Figure 2-5. As no derivation of the simulation given by Rudie is available, a more detailed investigation into Rudie's technique is performed. The results of this investigation show that the orbital parameters given by Davies were not sufficient to derive the simulation given by Rudie and that Rudie's orbital simulation could, therefore, only have been derived from Davies' radiant distribution.

The following subsection briefly describes the orbital parameters of meteor orbits in order to develop the necessary background for describing the transformation

from distributions of meteor orbital parameters to a density distribution of meteor radiants.

4.1.1 Orbital parameters of meteor orbits

Application of Newtonian physics and Kepler's laws show that a meteor, with a velocity of less than the escape velocity of the sun, will travel in an elliptical path around the sun. The elliptical orbit of a meteor, m, travelling around the sun, S, is shown in Figure 4-1.

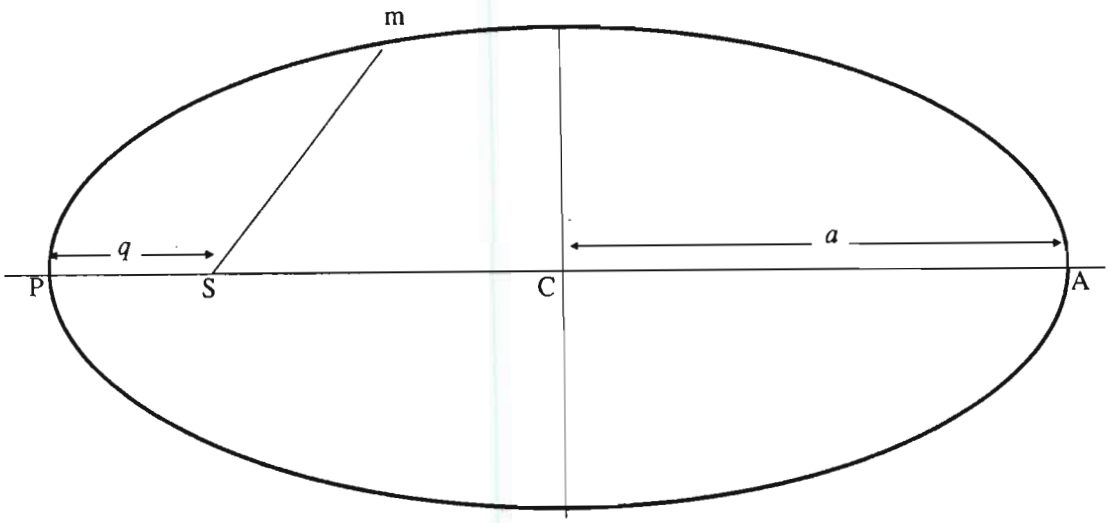

Figure 4-1 Elliptical orbit of a meteor travelling around the sun.

Following standard astronomical convention the elliptical orbit of a meteor may be defined using the following parameters, *Porter* [1952]:

a is the *semi-major axis* CP = CA that defines the size of the meteor orbit,

e is the *eccentricity* of the ellipse that may be defined as the ratio CS:CP

q is the *perihelion* distance (SP) and is equal to $a(1 - e)$, and

q' is the *aphelion* distance (SA) which is equal to $a(1 + e)$.

The *inclination*, i, is used to relate the plane of a meteor's orbit with the plane of the earth's orbit as shown in Figure 4-2. The plane of the earth's orbit is usually

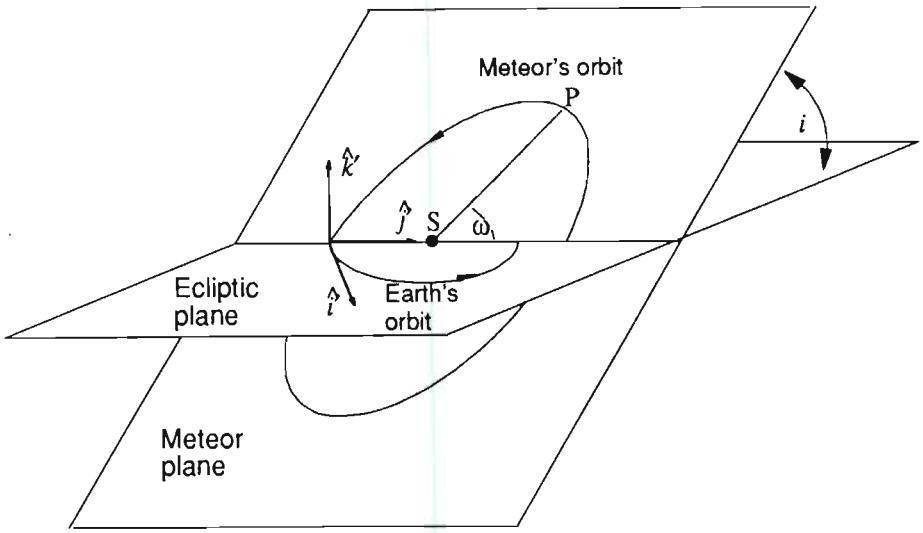

Figure 4-2 Ecliptical coordinate system.

known as the *ecliptic* plane. ω, the *argument of the perihelion*, is the angle between the ecliptic plane and the axis SP. Figure 4-2 illustrates an *ecliptical coordinate system* with the $\hat{i}'$, $\hat{j}'$ and $\hat{k}'$ axis pointing in the direction of the tangential direction of the earth's motion, the sun and perpendicular to the ecliptic plane, respectively.

In order to intercept the earth, a meteor must satisfy certain combinations of meteor orbital parameters, *a*, and, *e*. By inspection of Figure 4-1, and because the earth follows a close approximation to a circular orbit, it may be seen that meteors with a perihelion distance greater than the distance from the sun to the earth, or meteors with an aphelion distance less than the distance from the sun to the earth, cannot intercept the earth. Thus for a meteor to intercept the earth:

$$q = a(1-e) \leq 1 \text{ AU, and}$$
$$q' = a(1+e) \geq 1 \text{ AU,} \qquad (4\text{-}1)$$

where one AU (Astronomical earth unit.) is the earth's distance from the sun. This may be rearranged as:

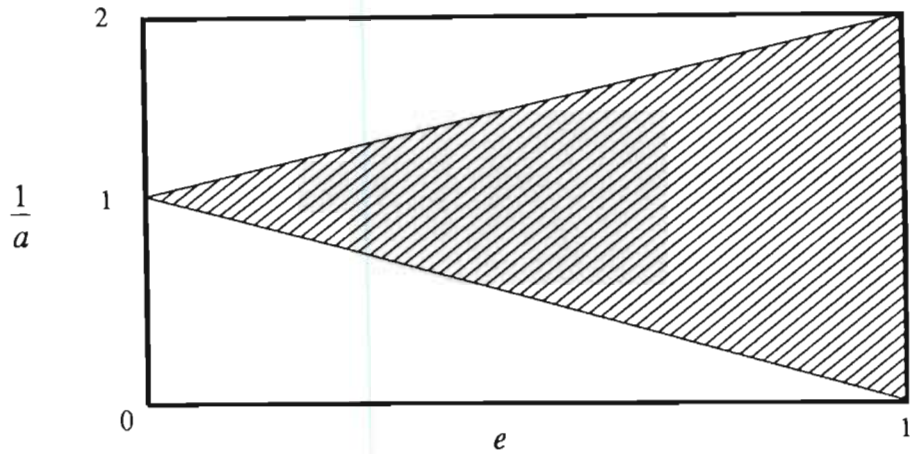

Figure 4-3 Range of possible orbital parameters of meteors $1/a$ and e that intercept the earth (shaded region).

$$\frac{1}{a} \leq (1+e), \text{ and } \frac{1}{a} \geq (1-e), \text{ where } 0 < e < 1, \text{ and } 0 < \frac{1}{a} < 2.$$

The limits on a and e are set by geometry and the escape velocity of the sun. Figure 4-3 is a plot of possible values of $1/a$ and e that may intercept the earth.

4.2 Transformation from orbital parameters to an ecliptical orbital distribution

Given the orbital parameters a, e, and i of a meteor, and ignoring the velocity of the earth, the earth's gravitation, and the spin of the earth about its axis, it is possible to calculate the apparent direction of a meteor striking the earth in ecliptical coordinates. It may be shown, using basic celestial mechanics, *Danby* [1970], that the velocity of a meteor at the earth's distance from the sun, $r = 1\text{AU}$, (See Figure 4-4.) is:

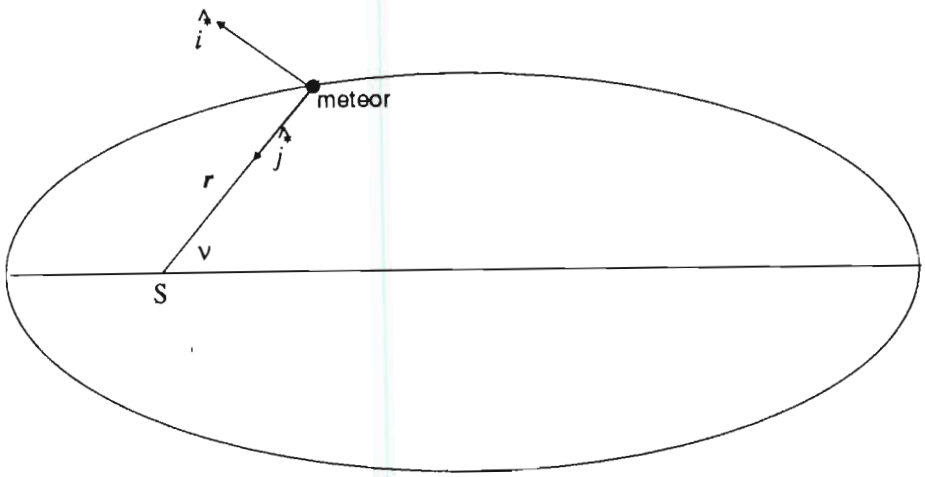

Figure 4-4 Velocity components of a meteor.

$$\frac{d\mathbf{r}}{dt} = r\frac{d\nu}{dt}\hat{i} + \frac{dr}{dt}\hat{j} \tag{4-2}$$

where $\frac{dr}{dt} = e\frac{\sqrt{a\,G\,M}}{r}\sin E$, $\frac{d\nu}{dt} = \frac{\sqrt{G\,M\,a\,(1-e^2)}}{r^2}$,

$E = \pm\cos^{-1}\left[\frac{1-\frac{r}{a}}{e}\right]$, G is the gravitational constant, and M is the mass of the sun.

The rotation of the meteor plane onto the ecliptic plane through the inclination, i, is thus:

$$(\hat{i},\hat{j},\hat{k}) = (\hat{i}^*,\hat{j}^*,\hat{k}^*)\begin{bmatrix} 0 & 1 & 0 \\ \cos i & 0 & -\sin i \\ \sin i & 0 & \cos i \end{bmatrix} \tag{4-3}$$

The radiant of the meteor relative to the sun, in terms of ecliptical longitude, λ_h, and latitude, β_h, as shown in Figure 2-1, is thus:

$$\lambda_h = \tan^{-1}\left[\frac{r\frac{dv}{dt}}{\frac{dr}{dt}} \cos i \right], \text{ and} \tag{4-4}$$

$$\beta_h = \tan^{-1}\left[\frac{r\frac{dv}{dt} \sin i}{\left[\left(\frac{dr}{dt}\right)^2 + \left(r\frac{dv}{dt}\cos i\right)^2\right]^{1/2}} \right] . \tag{4-5}$$

Given a, e and i it is thus possible to find the corresponding λ_h and β_h. It should be noted that this is not a unique transformation since contours of constant β_h may be mapped onto the $1/a$ versus e plane.

It should also be noted that a particular a, e and i maps onto (λ_h, β_h) or $(360^o - \lambda_h, \beta_h)$ depending on the value of the argument of perihelion, and whether the meteor intersected the path of the meteor on the ascending or descending node. This is of particular significance since lack of information regarding the distribution of the argument of perihelion of Davies' orbital distributions, given in Figures 2-6 to 2-8, should result in any distribution of radiants derived from Davies' orbital distributions alone having symmetry about the line of longitude through $\lambda_h = 0^o$. An inspection of Rudie's simulated orbital distributions of meteors given in Table 2-1 and Figure 2-24 does not, however, reveal symmetry about the line of longitude through $\lambda_h = 0^o$. This fact alone serves to illustrate that Rudie's simulation was not based wholly on Davies' orbital distributions of meteors alone, but also on the knowledge of the required

geocentric distribution of Figure 2-5, which exhibits asymmetry about the line of longitude through $\lambda_g = 0^o$.

Although it is clear that Rudie's orbital simulation was not based solely on Davies' orbital distributions of meteors, the derivation of the actual equations used to simulate the orbital distribution is unknown. A more detailed investigation into the information given by Davies' distributions of orbital parameters has led the author to believe that Rudie's simulation was based primarily on a knowledge of the required geocentric distribution, and that the equations of Table 2-1 were generated to provide the required geocentric polar plot of Figure 2-5, after transformation to geocentric coordinates. Rudie's transformation from a heliocentric to a geocentric radiant distribution of meteors is discussed later.

4.2.1 Extraction of an approximate heliocentric distribution from Davies' distributions of orbital parameters

In order to further illustrate the fact that the distributions of orbital parameters given by Davies' provides only limited information regarding the heliocentric distributions of meteors and that they were therefore inadequate to generate the distribution simulated by Rudie, an approximate heliocentric distribution of meteors will be derived from Davies' distributions of orbital parameters alone.

The reduced form of the data presented by Davies makes it necessary to extrapolate the data into a distribution that may be used to transform from the distribution in orbital parameters of meteors to the ecliptical orbital distribution. The extrapolation of this data can only be an approximation.

In order to perform the required transformation, Davies' results have been extrapolated into a distribution of $1/a$ verses e versus i. This extrapolation has been performed by noting that the graphs of distribution of inclinations map onto

regions on the $1/a$ versus e plane. Davies' results are divided into orbits with the following limits:

$$q' = a(1-e) > 10\text{AU},$$
$$3\text{AU} < q' = a(1-e) < 10\text{AU}, \text{ and}$$
$$q' = a(1-e) < 3\text{AU}.$$

Orbits with aphelion distances less than 3AU are further sub-divided into three groups according to eccentricity, namely: $e < 0.3$; $0.3 < e < 0.7$; and $e > 0.7$. The regions formed by these groups are illustrated in Figure 4-5.

In order to perform this extrapolation the $1/a$ versus e plane was divided into $1/a$ and e increments of 0.1. Each number on the $1/a$ versus e plane thus represents the relative number of meteors, n ($\Delta 1/a$, Δe, Δi), within each incremental region. A table of $1/a$ versus e was extracted for each range of inclination, i, given in

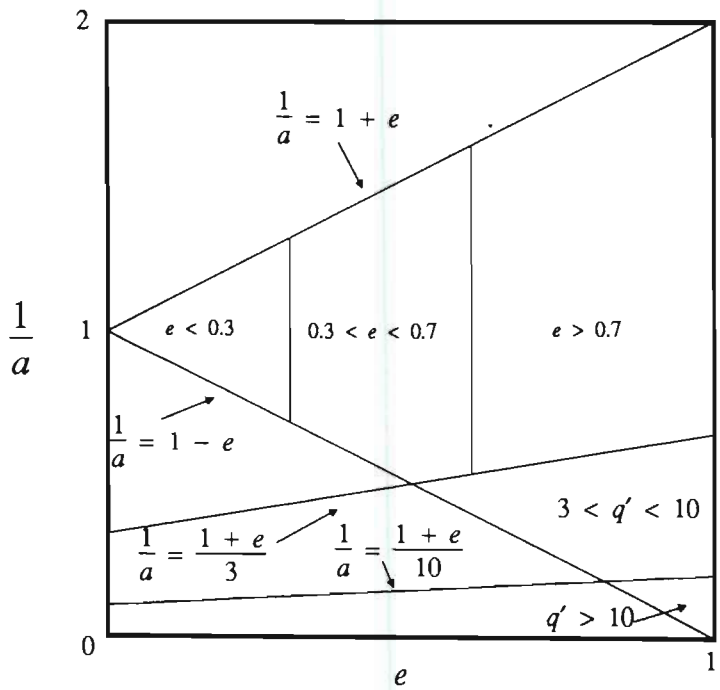

Figure 4-5 Regions on the $1/a$ versus e plane corresponding to the orbital distributions given by Davies.

Davies' results. Using Davies' distribution of the numbers of meteors versus $1/a$ shown in Figure 2-6, the assumption was made that the meteors were distributed constantly according to e as shown in Table 4-1.

The distributions of $1/a$ versus e for each range of inclination were formed by weighting the appropriate region on the $1/a$ versus e plane by the corresponding fraction of the total number of meteors at a particular inclination given in Davies' graphs.

A region in the orbital parameter space maps onto a region in heliocentric ecliptical coordinates as described in Section 4-2. An example of this transformation is illustrated in Figure 4-6.

Table 4-1 Assumed distribution of $1/a$ versus e used to extrapolate Davies' orbital data. Uniform distribution with respect to e was assumed.

$1/a$ \ e	0-0.1	0.1-0.2	0.2-0.3	0.3-0.4	0.4-0.5	0.5-0.6	0.6-0.7	0.7-0.8	0.8-0.9	0.9-1.0		Σ 1/a
0-0.1										56		56
0.1-0.2									52	104		156
0.2-0.3								37.6	75.2	75.2		188
0.3-0.4							30	60	60	60		210
0.4-0.5						20	40	40	40	40		180
0.5-0.6					13.8	27.6	27.6	27.6	27.6	27.6		152
0.6-0.7				13.8	27.6	27.6	27.6	27.6	27.6	27.6		180
0.7-0.8			10.1	20.2	20.2	20.2	20.2	20.2	20.2	20.2		152
0.8-0.9		6.8	13.6	13.6	13.6	13.6	13.6	13.6	13.6	13.6		116
0.9-1.0	7.4	14.6	14.6	14.6	14.6	14.6	14.6	14.6	14.6	14.6		142
1.0-1.1	6.4	12.8	12.8	12.8	12.8	12.8	12.8	12.8	12.8	12.8		122
1.1-1.2		5.5	11.1	11.1	11.1	11.1	11.1	11.1	11.1	11.1		94
1.2-1.3			4.8	9.6	9.6	9.6	9.6	9.6	9.6	9.6		72
1.3-1.4				4	8	8	8	8	8	8		52
1.4-1.5					3.1	6.2	6.2	6.2	6.2	6.2		34
1.5-1.6						5.1	10.2	10.2	10.2	10.2		46
1.6-1.7							3.7	7.4	7.4	7.4		26
1.7-1.8								3.2	6.4	6.4		16
1.8-1.9									4.7	9.3		14
1.9-2.0										8		8

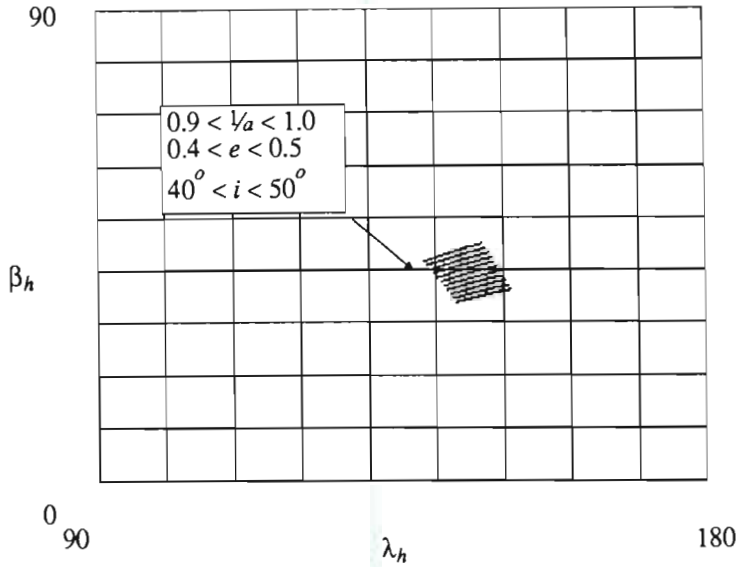

Figure 4-6 Example of the transformation from a region in orbital space to a region in heliocentric space.

A program was written to transform from orbital parameters to the ecliptical heliocentric distribution. The transformation was performed by digitizing the heliocentric celestial sphere into 5^o increments of λ_h and β_h. The region on the heliocentric celestial sphere corresponding to each cell of ($\Delta 1/a$, Δe, Δi) was calculated using the equations described in Section 4-2. The number of meteors, n ($\Delta 1/a$, Δe, Δi), in each cell, ($\Delta 1/a$, Δe, Δi), were distributed so that an even density distribution was obtained in each of the incremental regions, ($\Delta\lambda_h$, $\Delta\beta_h$). The relative contribution for each increment, ($\Delta\lambda_h$, $\Delta\beta_h$), was obtained for each transformation using the following expression:

$$n(\Delta\lambda_h, \Delta\beta_h) = n(\Delta 1/a, \Delta e, \Delta i) \frac{\cos \beta_{h_{\Delta\lambda_h \Delta\beta_h}}}{\sum_{\Delta\lambda_h \Delta\beta_h} \cos \beta_{h_{\Delta\lambda_h \Delta\beta_h}}} \qquad (4\text{-}6)$$

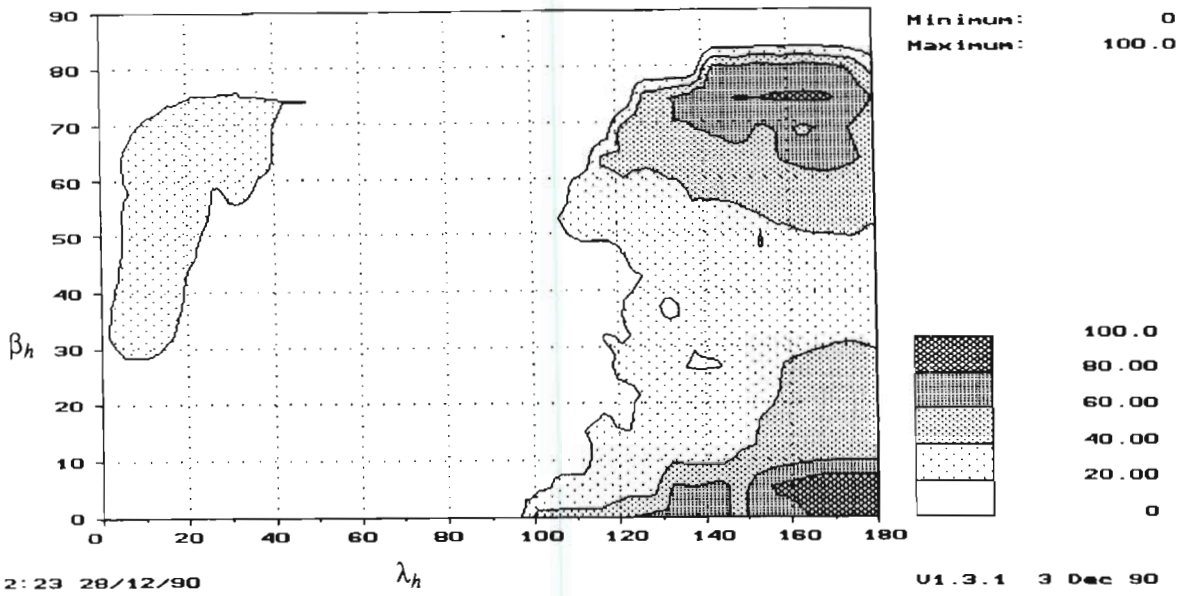

Figure 4-7 Contour plot of the approximated relative radiant density of meteors in heliocentric ecliptical coordinates.

Using the results given in Appendix A, $\dfrac{\cos \beta_{h_{\Delta\lambda_h \Delta\beta_h}}}{\sum_{\Delta\lambda_h \Delta\beta_h} \cos \beta_{h_{\Delta\lambda_h \Delta\beta_h}}}$ represents the fraction of the heliocentric region covered by a particular $(\Delta\lambda_h, \Delta\beta_h)$, which compensates for variation in the areas of particular regions, $(\Delta\lambda_h, \Delta\beta_h)$, over the celestial sphere.

The results of this transformation are presented in Figure 4-7, which is a contour plot of the relative radiant density of meteors in heliocentric ecliptical coordinates. It should be noted that, of necessity, symmetry has been assumed around the lines of longitude and latitude through $\lambda_h = 180^o$ and $\beta_h = 0^o$ respectively.

The transformation from a heliocentric density distribution to a geocentric density distribution will be postponed until the relevant theory has been described in the following sections.

4.3 Heliocentric to geocentric transformation

Using an involved method, Rudie developed a technique of transforming from a heliocentric to a geocentric radiant distribution. In order to put the method developed by Rudie into perspective, a more accurate and analytically simpler technique will first be described.

The transformation in meteor direction between the heliocentric and geocentric distributions may be simply derived with reference to Figure 2-2, *Lovell* [1954]. The relationship between the elongations of R_g and R_h is simply

$$\begin{aligned} \varepsilon_h &= \varepsilon_g + \Delta\varepsilon \\ &= \varepsilon_g + \sin^{-1}\left[\frac{V_e}{V_h}\sin\varepsilon_g\right] \end{aligned} \tag{4-7}$$

The relationship between elongation, ε, ecliptical longitude, λ, and ecliptical latitude, β, relative to the apex is

$$\cos\varepsilon = \cos\lambda\cos\beta\,. \tag{4-8}$$

The geocentric direction numbers of a meteor are

$$\begin{aligned} l_g &= \cos\lambda_g\cos\beta_g \\ m_g &= \sin\lambda_g\cos\beta_g \\ n_g &= \sin\beta_g \end{aligned} \tag{4-9}$$

Using simple vector addition, the heliocentric direction numbers are thus

$$\begin{aligned} l_h &= V_g\, l_g - V_e \\ m_h &= V_g\, m_g \\ n_h &= V_g\, n_g \end{aligned} \tag{4-10}$$

where from Figure 2-2 it may be seen that

$$V_g = \sqrt{V_e^2 + V_h^2 + 2\,V_e\,V_h \cos \varepsilon_h}\,, \text{ and} \tag{4-11}$$

$$\cos \varepsilon_h = \cos\left[\varepsilon_g + \sin^{-1}\left(\frac{V_e}{V_h} \sin \varepsilon_g \right)\right] \tag{4-12}$$

Using the heliocentric direction numbers, the heliocentric ecliptical longitude, λ_h, and ecliptical latitude, β_h, are thus

$$\lambda_h = \tan^{-1}\left[\frac{m_h}{l_h} \right], \text{ and } \beta_h = \tan^{-1}\left[\frac{n_h}{(m_h^2 + l_h^2)^{1/2}} \right]. \tag{4-13}$$

Equations 4-7 to 4-13 consist of a transformation in direction between a geocentrically referenced meteor radiant, λ_g, and, β_g, and a heliocentrically referenced meteor radiant, λ_h, and, β_h.

The transformation between geocentric and heliocentric distributions results in a radiant density transformation that may be described in terms of an area transformation. Figure 4-8 illustrates this change in area. Due to the effect of the direction transformation on each meteor, the same meteors seen emanating from an incremental surface on the celestial sphere, dS_h, in heliocentric coordinates, will appear to emanate from an incremental surface, dS_g, in geocentric coordinates.

By defining the incremental surfaces as being bounded by lines of constant elongation and by lines of longitude relative to the apex, as shown in Figure 4-8, it is possible to find the ratio between dS_g and dS_h. Using the theory shown in Appendix A, the ratio of these areas is:

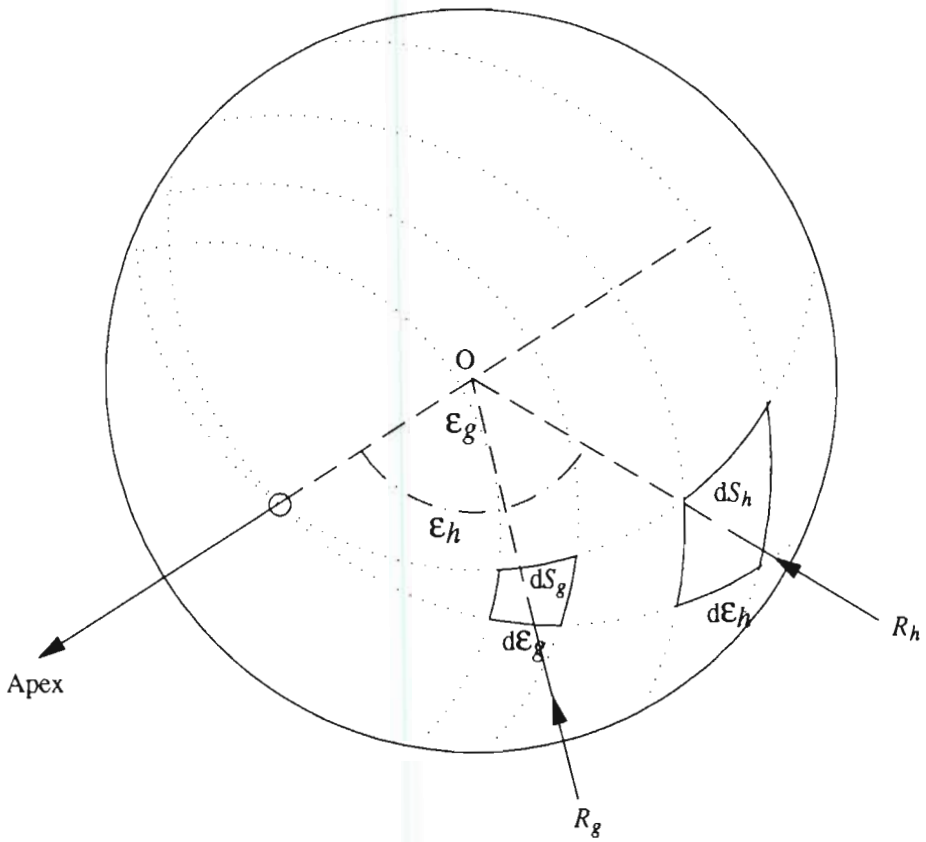

Figure 4-8 Diagram to illustrate the transformation from a heliocentric to a geocentric radiant density distribution.

$$\frac{dS_h}{dS_g} = \frac{d\varepsilon_h}{d\varepsilon_g} \cdot \frac{\sin \varepsilon_h}{\sin \varepsilon_g} \tag{4-14}$$

Differentiating Equation 4-14 and simplifying gives

$$\frac{d\varepsilon_h}{d\varepsilon_g} = 1 + \frac{V_e}{V_h} \frac{\cos \varepsilon_g}{\left[1 - \frac{V_e^2}{V_h^2} \sin^2 \varepsilon_g\right]^{1/2}}, \tag{4-15}$$

and from Figure 2-2

$$\frac{\sin \varepsilon_g}{\sin \varepsilon_h} = \frac{V_h}{V_g} . \tag{4-16}$$

Assuming that the radiant density of meteors at ε_h is δ_{ε_h} then the radiant density at ε_g is

$$\delta_{\varepsilon_g} = \frac{dS_h}{dS_g}\delta_{\varepsilon_h} = \frac{V_g}{V_h}\left[1 + \frac{V_e}{V_h}\frac{\cos \varepsilon_g}{\sqrt{1 - \frac{V_e^2}{V_h^2}\sin^2 \varepsilon_g}}\right] \cdot \delta_{\varepsilon_h} \quad \left[\frac{\text{meteors}}{\text{s m}^2}\right] \tag{4-17}$$

4.3.1 Rudie's technique

A more involved, yet equivalent method of calculating the geocentric to heliocentric direction transformation was developed by Rudie. Adapting Rudie's equations to the notation used in the previous section, the following are the direction transformation equations derived by Rudie:

$$\lambda_h = \tan^{-1}\left[\frac{1}{\cos^2 \lambda_h} - 1\right]^{1/2} \tag{4-18}$$

where λ_h, $\lambda_h + \pi$, $-\lambda_h$, and $-(\lambda_h + \pi)$ are the four possible values.

$$\cos^2 \lambda_h = \frac{-2ac + b^2 \pm b\sqrt{b^2 - 4c^2 - 4ac}}{2(a^2 + b^2)} \text{ , where} \tag{4-19}$$

$$a = V_h^2 l_g^2 - m_g^2 V_h^2 - V_e^2 n_g^2$$

$$b = 2 l_g m_g V_h^2$$

$$c = m_g^2 V_e^2 + n_g^2 V_e^2 - V_h^2 l_g^2 \text{, and}$$

$$\beta_h = \tan^{-1}\left[-\frac{n_g}{m_g}\sin \lambda_h\right] . \tag{4-20}$$

The correct choice of λ_h and β_h is determined by iterative testing to ensure that the following equations are satisfied:

$$\frac{l_g}{V_h \cos\beta_h \cos\lambda_h + V_e} = \frac{m_g}{V_h \cos\beta_h \sin\lambda_h}, \text{ and} \tag{4-21}$$

$$\frac{m_g}{V_h \cos\beta_h \sin\lambda_h} = \frac{n_g}{-V_h \sin\beta_h}. \tag{4-22}$$

Equations 4-18 to 4-22 are analytically equivalent to Equations 4-9 to 4-13.

Rudie developed an approximate method of transforming from an area, A_h, in heliocentric space to an equivalent area, A_g, in geocentric space.

In order to transform between heliocentric and geocentric space, Rudie defined an area, A_h, in heliocentric space as the area bounded by the lines on longitude and latitude that pass through the points

$$a_h = (\lambda_h - \frac{\Delta\lambda_h}{2}, \beta_h - \frac{\Delta\beta_h}{2}),$$

$$b_h = (\lambda_h - \frac{\Delta\lambda_h}{2}, \beta_h + \frac{\Delta\beta_h}{2}), \text{ and}$$

$$c_h = (\lambda_h + \frac{\Delta\lambda_h}{2}, \beta_h - \frac{\Delta\beta_h}{2})$$

on the celestial sphere.

Using the direction transformation described in Equations 4-18 to 4-22, Rudie found the points a_g, b_g,and c_g in geocentric space corresponding to the points a_h, b_h, and c_h in heliocentric space.

The angles, $\delta_{a_g b_g}$, and $\delta_{a_g c_g}$ between points a_g and b_g and points a_g and c_g respectively on the celestial sphere were found using Equations 4-21, 4-22, the vector dot product and the relationship

$$\tan\theta = \pm\left[\frac{1}{\cos^2\theta} - 1\right]^{1/2}, \text{ as} \tag{4-23}$$

$$\delta_{a_g b_g} = \tan^{-1}\left[\frac{1}{\left(\lambda_{g a_g}\lambda_{g b_g} + \mu_{g a_g}\mu_{g b_g} + \nu_{g a_g}\nu_{g b_g}\right)^2} - 1\right]^{1/2} \tag{4-24}$$

$$\delta_{a_g c_g} = \tan^{-1}\left[\frac{1}{\left(\lambda_{g a_g}\lambda_{g c_g} + \mu_{g a_g}\mu_{g c_g} + \nu_{g a_g}\nu_{g c_g}\right)^2} - 1\right]^{1/2} \tag{4-25}$$

where λ_{g*}, μ_{g*}, and ν_{g*} correspond to the geocentric direction cosines associated with $* = a_g$, b_g, or c_g.

Rudie then made the assumption that

$$A_g = \delta_{a_g b_g}\,\delta_{a_g c_g}. \tag{4-26}$$

This assumption is, however, only approximate, since, even as an approximation for small angles, the vectors, $\overline{a_g b_g}$ and $\overline{a_g c_g}$, formed by the points a_g, b_g and c_g are not necessarily mutually perpendicular.

A more accurate approximation of A_g for $\Delta \approx 0$ is

$$A_g = \left|\overline{a_g b_g} \times \overline{a_g c_g}\right| \tag{4-27}$$

Since an analytically more accurate technique has already been derived, the expansion of the above expression will not be performed.

4.3.2 Corrections due to the gravitational effect of the earth

The effect of the earth's gravitation on the path of a meteor may be described with reference to Figure 4-9, *Porter* [1952]. A meteor travelling in a straight line *MC* will be forced into a hyperbolic orbit, *MOM'*, due to the gravitational attraction of the earth. This effect results in the zenith angle of the radiant changing from ζ' to ζ relative to an observer at *O*. Since the meteor is always displaced towards the observer's zenith, this effect is known as *zenith attraction*. Porter has shown that the relationship between ζ and ζ' is :

$$\tan\frac{(\zeta-\zeta')}{2} = \frac{V_\infty - V_g}{V_\infty + V_g}\tan\frac{\zeta}{2} \qquad (4\text{-}28)$$

where $V_\infty = \sqrt{V_g^2 + 124.9}$ [km/s], is the actual speed with which the meteor enters the earth's atmosphere due to the gravitational attraction of the earth. As mentioned by Porter, the correction for zenith attraction is a maximum for when

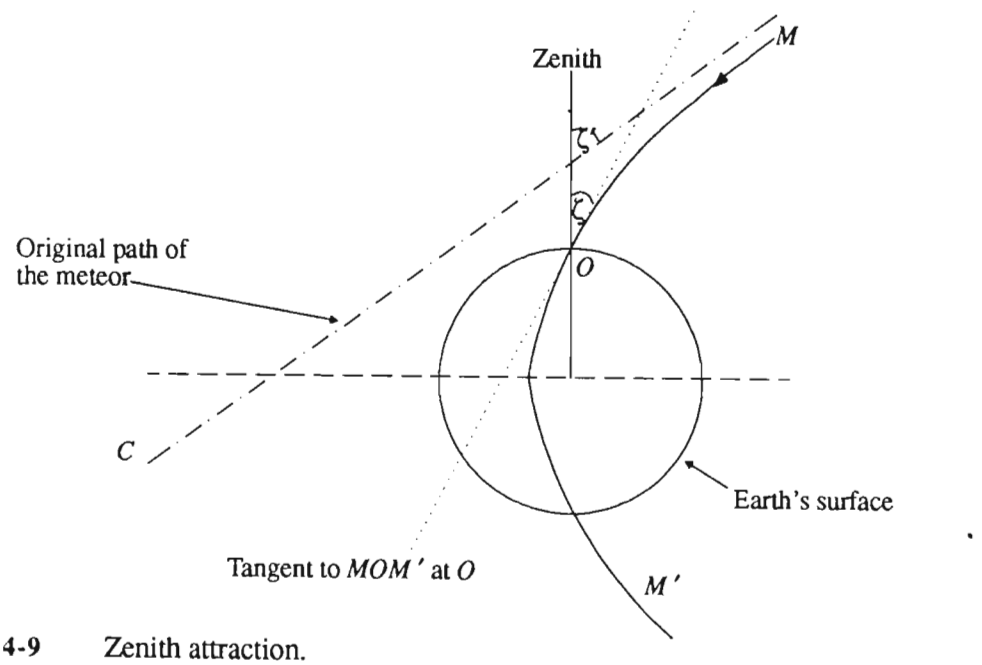

Figure 4-9 Zenith attraction.

the radiant lies near the horizon, and is near the antapex. The maximum correction under these circumstances will approach 17^{o}.

As shown by *Rudie* [1967] it is important to note that the effect of zenith attraction cannot be taken into account in the prediction of the influence of radiant distributions on the arrival rate of meteors due to the lack of information regarding the geocentric velocity of the incident meteors.

4.3.3 Other corrections

As mentioned by *Porter* [1952], and *Rudie* [1967], the effect of the earth's spin on the radiant of a meteor is negligible and may therefore be neglected. The deceleration of a meteor due to the earth's atmosphere results in a decrease in V_{∞} of between 0.5 to 1 kilometres per second in the meteor region. The effect of atmospheric deceleration may similarly be neglected.

4.4 Numerical simulation of the heliocentric to geocentric radiant density transformation

As shown by *Rudie* [1967] the transformation from heliocentric to a geocentric radiant distribution may be approximated using the transformation described in Section 4.3.1. Using the methods of Sections 4.3, the radiant density of any point in geocentric coordinates may be calculated by transforming to the corresponding radiant in heliocentric coordinates and calculating the density transformation of radiants at that point. This method thus involves "looking-up" the geocentric density distribution of meteors based on the known heliocentric distribution. The disadvantage of this technique is that multiple counting or omission of meteors from the heliocentric distribution will occur to a lesser or greater degree depending on the position of the radiants chosen to "look-up" in geocentric coordinates. The following numerical technique was developed to avoid multiple counting

and omission of meteors as well as to provide a potentially accurate density transformation:

The numerical simulation of the heliocentric to geocentric radiant density transformation is illustrated in Figure 4-10. The numerical transformation is performed by transforming the number of meteors in small regions over the entire heliocentric sphere to their appropriate region on the geocentric sphere. The heliocentric and geocentric spheres are projected in rectangular coordinates in Figure 4-10. As shown in Figure 4-10, the heliocentric and geocentric spheres are divided into small regions defined by incremental lines of longitude and latitude, $\Delta\lambda$ and $\Delta\beta$. The corresponding (on transformation) incremental region in geocentric coordinates is calculated for all the incremental regions in heliocentric coordinates, and the number of meteors in each of the incremental regions in heliocentric coordinates is added to the corresponding region in geocentric coordinates. As long as the incremental regions in heliocentric coordinates are far smaller that the regions in geocentric coordinates, the radiant density in each

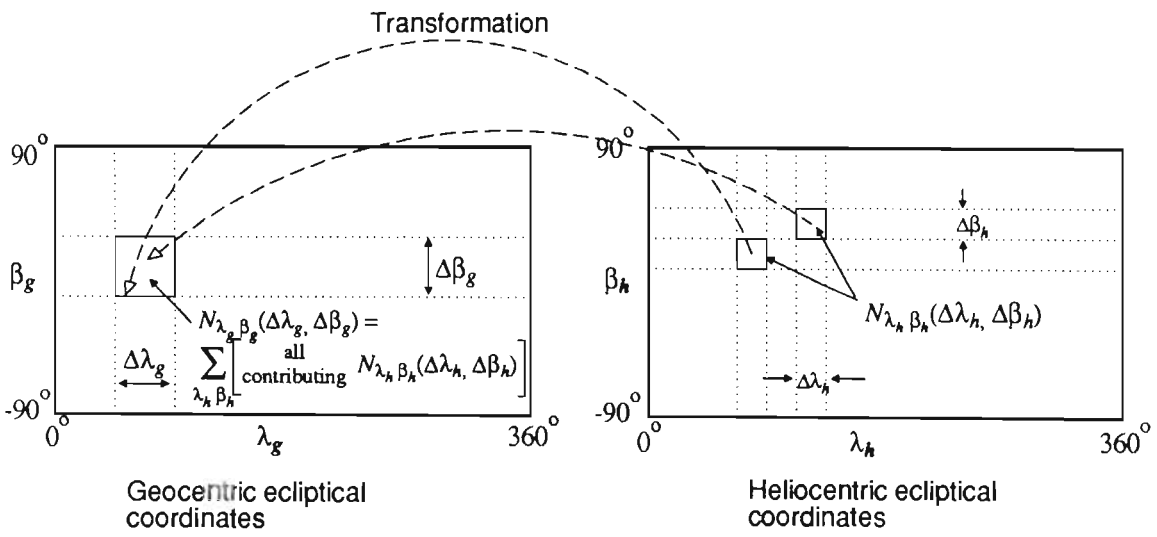

Figure 4-10 Diagram to illustrate the numerical method of simulating the heliocentric to geocentric radiant density transformation.

of the incremental regions in geocentric coordinates will be defined by the number of meteors divided by the area of the incremental region. Following this technique, the number of meteors, $N_{\lambda_g \beta_g}(\Delta\lambda_g, \Delta\beta_g)$, in each incremental region in geocentric coordinates, $(\Delta\lambda_g, \Delta\beta_g)$, is thus:

$$N_{\lambda_g \beta_g}(\Delta\lambda_g, \Delta\beta_g) = \sum_{\lambda_h \beta_h}\left[\begin{array}{c}\text{all}\\ \text{contributing}\end{array} N_{\lambda_h \beta_h}(\Delta\lambda_h, \Delta\beta_h)\right], \tag{4-29}$$

and the relative radiant density, $\delta_{g_{\lambda_g \beta_g}}$, at geocentric radiant, λ_g, β_g is

$$\delta_{g_{\lambda_g \beta_g}} = \frac{N_{\lambda_g \beta_g}(\Delta\lambda_g, \Delta\beta_g)}{\cos \beta_g}. \tag{4-30}$$

4.5 Approximation of Davies' observed radiant distribution

To complete the extraction of an observed radiant distribution based on Davies' orbital parameters alone, the heliocentric distribution approximated in Section 4.2.1 is transformed to a geocentric distribution. An estimation of the validity of the final results is then determined by a comparison with Davies' actual observed distribution. It should be remembered, however, that the heliocentric distribution derived in Section 4.2.1 was based on an extrapolation of Davies' orbital parameters and therefore the derived geocentric distribution will similarly only be an approximation. This exercise is undertaken to demonstrate the results of a more rigorous technique of deriving the geocentric distribution using Davies' orbital parameters exclusively.

Using the theory described in Section 4.3 and 4.4, the heliocentric radiant distribution shown in Figure 4-7 was transformed to a geocentric distribution. The results of this transformation are shown in Figure 4-11. As mentioned in Section 4.2, the lack of information about the argument of the perihelion results

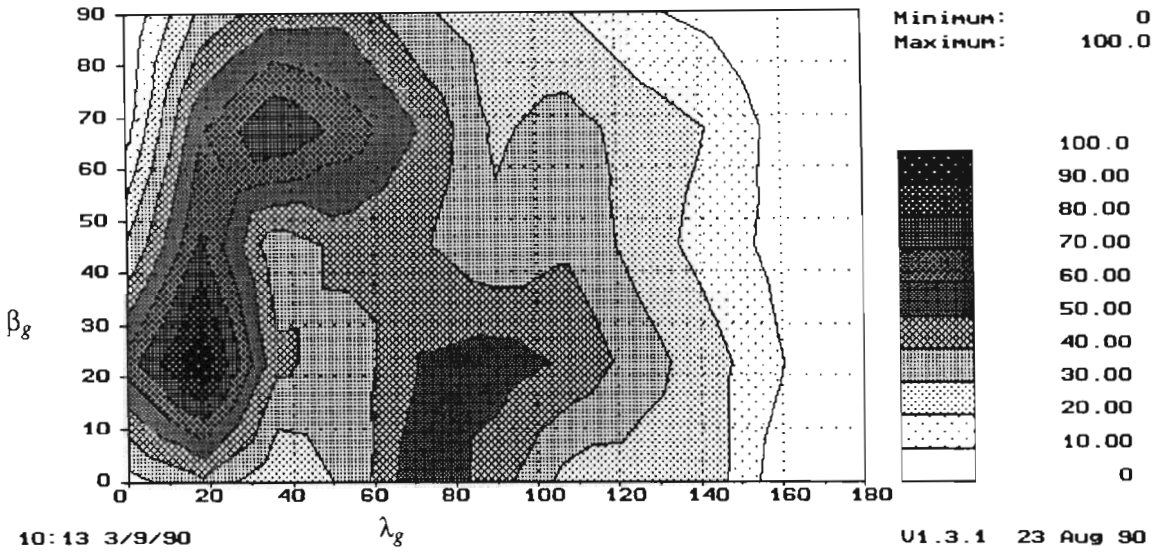

Figure 4-11 Observed radiant distribution of meteors obtained using an extrapolation of Davies' orbital parameters. Davies' observed radiant distribution was not used.

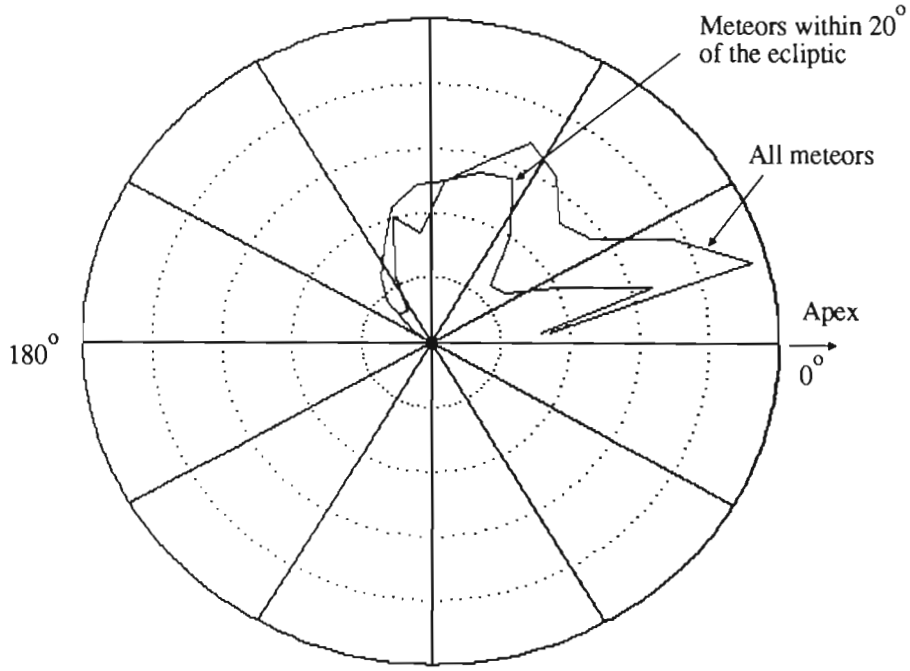

Figure 4-12 Polar plots of the approximated observed radiant distribution. Symmetry about the line of longitude through $\lambda_g = 180^o$ should be assumed.

in forced symmetry about $\lambda_g = 180^o$. In order to compare these results with the geocentric distribution observed by Davies in Figure 2-5, the transformed results are displayed in a form similar to that given by Davies in Figure 4-12. It is clear from a comparison between the two polar plots that the transformed results differ significantly from the actual results given in Figure 2-5.. It is clear therefore that an extraction of a geocentric radiant distribution, using Davies' orbital parameters alone, can only generate a rough approximation. The loss of information caused by the original assumptions described in Section 4.2.1, results in an inaccurate geocentric radiant distribution. The inaccuracy of this result serves to emphasize the fact that Rudie's orbital simulations were not based on the orbital parameters alone.

4.6 Rudie's simulated distribution in geocentric coordinates

In order to facilitate comparison between Rudie's orbital distribution of meteors and other geocentric distributions of meteors, Rudie's simulated orbital distribution has been transformed to geocentric ecliptical coordinates using the theory described by Rudie in Section 4.3 and is reproduced as a contour map of the geocentric density distribution of meteors in Figure 4-13. For the purposes of the transformation, an average heliocentric velocity of 35 kilometres per second was used.

The results obtained in Figure 4-13 are also presented as a polar plot of all sporadic meteor radiants versus ecliptical longitude in Figure 4-14. Davies' results for all sporadic meteor radiants from Figure 2-5 are also presented in Figure 4-14. It is interesting to note that the results of Rudie's transformation differ significantly from the results given by Rudie in Figure 2-25 (plot H). The comparison between Rudie's simulated and Davies measured results in Figure 4-13 actually show a far better correspondence than illustrated by Figure 2-25.

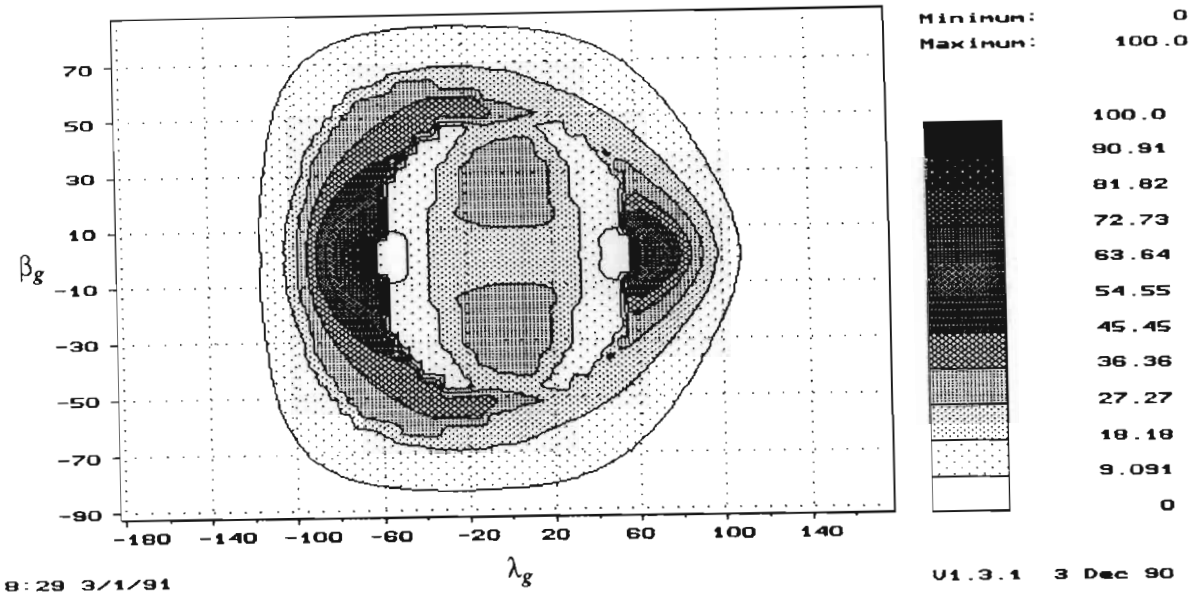

Figure 4-13 Contour map of the geocentric density distribution of meteors derived using Rudie's orbital simulation and transformation. An average heliocentric velocity of 35 kilometres per second was used.

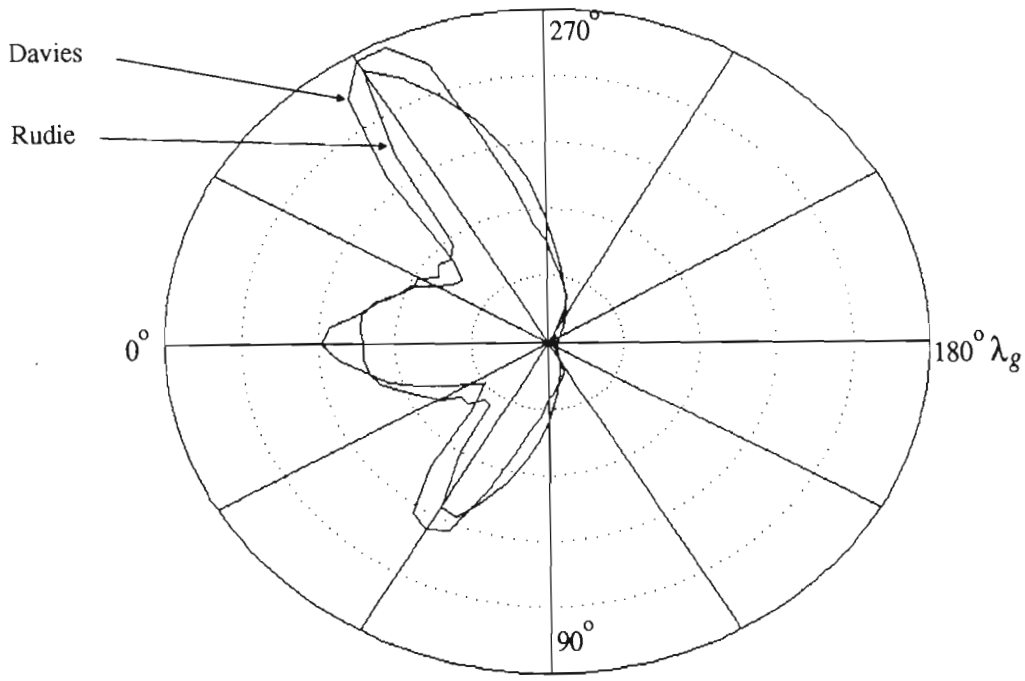

Figure 4-14 Comparison between Davies' polar plot of all sporadic meteors radiants versus the actual results obtained using Rudie's extrapolation (Compare with Figure 2-25.).

This seems to indicate that Rudie's plots reproduced in Figure 2-25 were only a rough representation of his actual results.

To test the validity of the approximations associated with Rudie's heliocentric to geocentric transformation, the orbital simulation given by Rudie has been transformed to geocentric coordinates using the more accurate numerical technique described in Section 4.4. Increments of λ_h and β_h of 0.25 degrees were used for the incremental regions on the heliocentric sphere and increments of λ_g and β_g of 5 degrees were used for the incremental regions on the geocentric sphere. Figure 4-15 is a contour map of the relative radiant density of meteors in geocentric coordinates obtained using the numerical transformation. Comparison between Figures 4-13 and 4-15 reveals some differences, which confirms that the transformation used by Rudie is only approximate. Since the original heliocentric distribution is only an approximation, however, the adoption of the

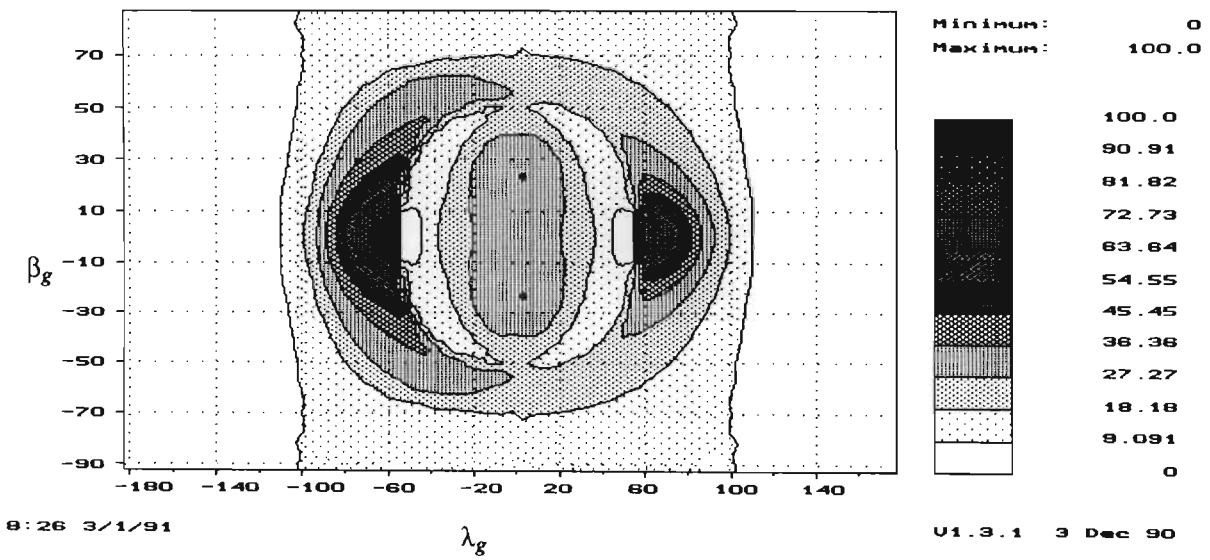

Figure 4-15 Contour map of the geocentric density distribution of meteors derived using the numerical transformation. An average heliocentric velocity of 35 kilometres per second was used.

geocentric distribution obtained using the slightly improved numerical transformation would probably be meaningless.

4.7 Extrapolation of Davies' observed distribution

It is possible to obtain an approximation of the observed radiant distribution in ecliptical coordinates by directly extrapolating Davies' results reproduced in Figure 2-5. A direct extrapolation of Davies' results provides a far simpler and possibly more accurate method of obtaining the observed distribution, and avoids the unnecessary complication of simulating a suitable heliocentric distribution that transforms to Davies' measured geocentric distribution.

As shown in Figure 2-5, the observed distribution of sporadic meteors is given as three polar plots: radiants within 20^{o} of the ecliptic; radiants within 40^{o} of the ecliptic; and all radiants. Due to the latitude at which the measurements were taken, radiants less than approximately -20^{o} were not observable. It is therefore possible to divide the data into three regions: $-20^{o} < \beta_g < 20^{o}$; $20^{o} < \beta_g < 40^{o}$; and $40^{o} < \beta_g < 90^{o}$. Due to the lack of data south of $\beta_g = -20^{o}$, it is necessary to assume symmetry about the ecliptic. Taking into account the respective areas of the three regions on the celestial hemisphere, it is thus possible to calculate the average radiant density in each region. An additional item of information for $40^{o} < \beta_g < 90^{o}$ is that, assuming a gradual change in density, the radiant density around the ecliptic poles should be similar. As a simple approximation a linear decrease in density may be assumed for $40^{o} < \beta_g < 90^{o}$ as β_g increases. Due to the poor resolution about the antapex an approximately uniform radiant density, based on the overall density, may be assumed as a first order approximation.

Figure 4-16 is a contour plot of the extrapolated results. Davies' polar plots were was graphically extracted in 5^{o} increments of λ_g. It is clear from Figure 4-16 that

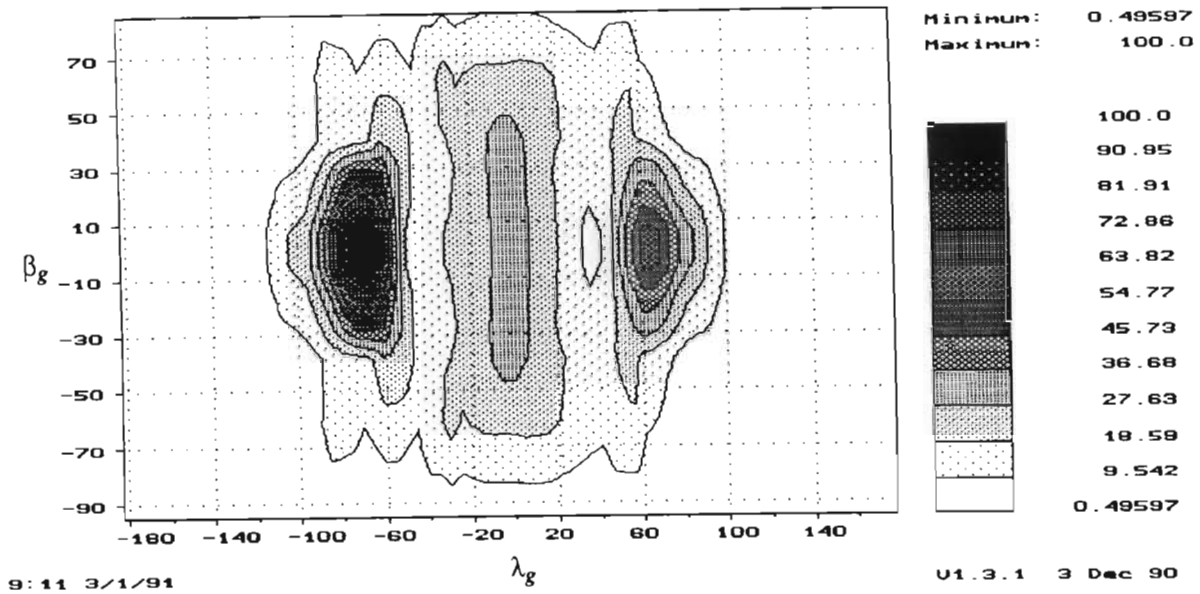

Figure 4-16 Contour map of the geocentric density distribution of meteors extrapolated directly from Davies' polar plots (Figure 2-5).

the extrapolated results show the expected concentrations at the apex, $\lambda_g = 65^o$, and $\lambda_g = 295^o$. Since Figure 4-16 is extrapolated directly from Figure 2-5, a polar plot of Figure 4-16 would be identical to Figure 2-5.

4.8 Summary of findings

Analysis of Davies' data has shown that Rudie's simulation was not based on the distributions of orbital parameters given by Davies. Although the technique used by Rudie to simulate a suitable orbital distribution is not completely clear, it is probable that Rudie's heliocentric distribution was derived from a transformation of Davies' geocentric distribution to heliocentric coordinates. Whether this was performed as an iterative process by selecting a suitable set of equations to simulate the heliocentric distribution that provided, on transformation, the correct geocentric distribution, or, whether this was performed by transforming some

form of the geocentric distribution directly to heliocentric coordinates and approximating the results as a set of equations, or whether this was performed as a combination of the two techniques, is unknown. Rudie obtained what was probably a reasonable approximation to Davies' measured results as a comparison between the results presented as polar plots and a comparison between directly extrapolated distributions and Rudie's geocentric distributions has shown.

The use of Rudie's simulation by *Weitzen* [1986], *Larsen and Rodman* [1988] and *Desourdis et al.* [1988] is indicative of the acceptance of Rudie's method of the simulation of Davies' results. The following quote by *Weitzen* [1986], pages 1012-1013, further demonstrates the acceptance of Rudie's technique:

> *"Next the empirical distribution of meteor orbits in ecliptic latitude and longitude, determined by Davies and approximated by Rudie as a series of closed form equations, is transformed to a distribution of meteor trail radiants observed at the earth. This transformation represents Rudie's significant contribution to meteor modeling and takes into consideration the effect of the Earth's orbital velocity on the direction and velocity of a meteor as the trail is formed."*

Since it has been shown that Rudie's simulation was simply an involved extrapolation of Davies' observed distribution and since Davies' observed distribution may be obtained by extrapolating Davies' results directly, it is doubtful that this was in fact Rudie's significant contribution to meteor modelling. It should also be remembered that Davies' measurements were based on a sample set of only 2400 radiants measured at high northern latitudes that implies that the resolution of the original measured distribution was probably not very detailed. It is therefore clear that a large number of existing meteor prediction models are probably based on an involved approximation of originally meagre data.

Chapter 5

Comparisons between predicted and measured arrival rates of meteors

In order to verify the validity of the radiant distributions presented in Chapter 2 and Chapter 4, comparisons between predicted and measured arrival rates of meteors for a forward-scatter link between Pretoria and Durban, South Africa are given in this chapter. The comparisons performed in this chapter represent the most detailed evaluation of the known radiant distributions of meteors presented to date, and answer some of the questions regarding the validity of the various distributions. Measured annual variations in the arrival rate of meteors are also presented and contrasted with previous measured and predicted results.

5.1 Measured results

A brief description of the measurement systems, the method of data capture, and data processing techniques used to extract the required data, is given here.

5.1.1 System description

Meteor trail reflection envelopes have been measured and recorded using two systems over a link between Pretoria and Durban, South Africa. Table 5-1 summarizes some of the important parameters of the two systems. Apart from the antenna configurations, the system parameters for the two systems are identical. One of the systems is designed to illuminate the meteor region between

Table 5-1 Midpath and endpath system parameters.

Transmitter Location	Irene, Pretoria, South Africa, Latitude $-25^{o}\ 43^{''}\ 58^{'}$, Longitude $28^{o}\ 12^{''}\ 00^{'}$
Receiving Site	Camperdown, Durban, South Africa Latitude $-29^{o}\ 49^{''}\ 01^{'}$ Longitude $31^{o}\ 00^{''}\ 57^{'}$
Path Length	532 km
Transmitter Power	350 W
Transmitter Frequency	50.050 MHz midpath 50.055 MHz endpath
Receiving System Noise Bandwidth	2 kHz
Receiving System Noise Figure	6 dB

Table 5-2 Midpath and endpath antenna configuration.

Antenna	**Midpath**	**Endpath**
Transmitting	11 element log periodic Horizontally polarized 3 metres high Maximum gain 15 dBi	11 element log periodic Horizontally polarized 8.5 metres high Maximum gain 15 dBi
Receiving	5 element yagi Horizontally polarized 3 metres high Maximum gain 13.5 dBi	3 element yagi Vertically mounted ½ metre high (reflector) Maximum gain 8 dBi

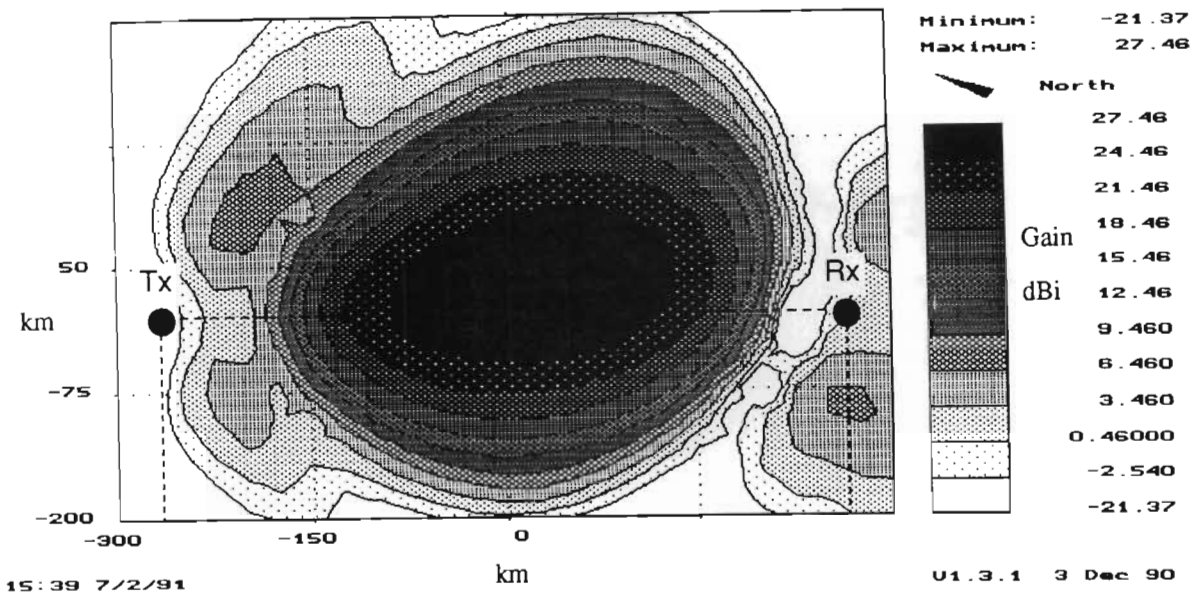

Figure 5-1 Contour plot of the combined predicted antenna illumination pattern of the meteor region for the midpath system. Tx and Rx are the transmitter and receiver locations respectively.

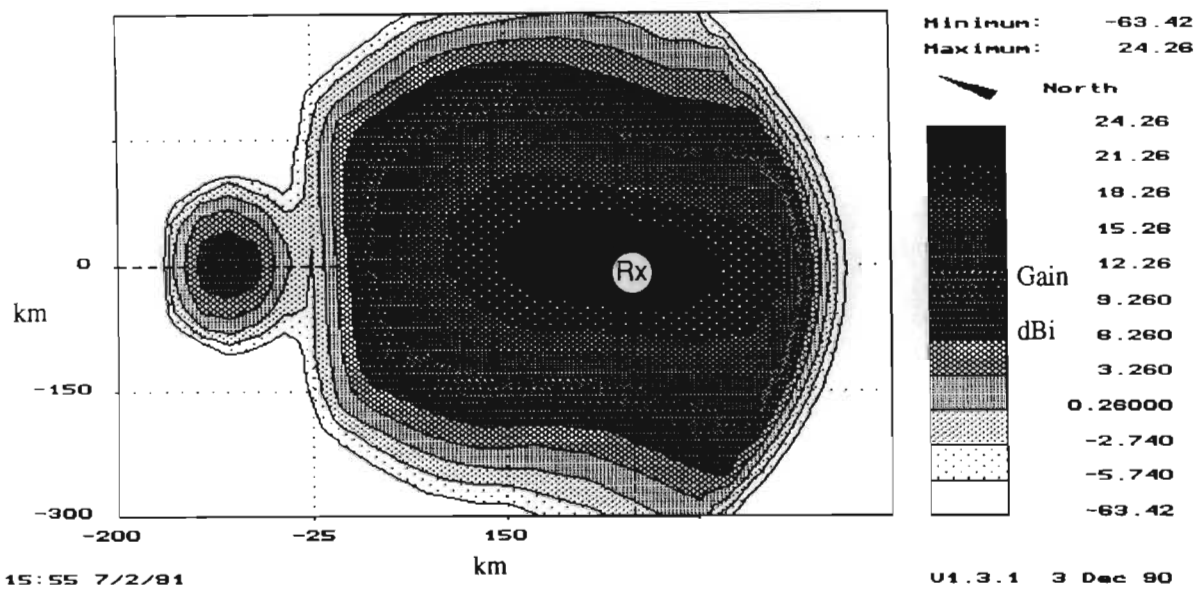

Figure 5-2 Contour plot of the combined predicted antenna illumination pattern of the meteor region for the endpath system. Rx is the receiver location.

the transmitter and receiver sites and is called the *midpath* system, whilst the other system is designed to illuminate the meteor region above the receiving site and is called the *endpath* system. Details of the midpath and endpath systems' antennas are given in Table 5-2. A contour plot of the combined predicted antenna illumination pattern of the meteor region for the midpath and endpath systems calculated using the technique used by *Larsen and Rodman* [1988] (See Section 3.4) is given in Figures 5-1 and 5-2 respectively.

5.1.2 Data capture, recording and processing

The received signal strength of meteor reflections is continuously recorded by the receiving systems. A continuous, unmodulated carrier signal is transmitted and each receiving system has the ability to discriminate between valid signals and unwanted noise bursts. Each receiving system is calibrated in one decibel steps from -140 to -80 dBm. Both the received signal and noise is converted to audio frequency, detected using a square-law device, logged and converted to dc for analogue-to-digital conversion. A detailed description of the analogue receiving system has been given by *Mawrey* [1988]. During the presence of a received trail reflection, the converted signal and noise voltages are sampled every five milliseconds and stored on magnetic disk for further analysis.

The digitized trail envelopes are further analysed and categorized according to the shape of the trail envelope (typed) using the trail classification scheme developed by *Melville et al.* [1989]. Summary information is then extracted from the classified trail envelopes. Using the summary information it is possible, for example, to extract the number of underdense trails received above a chosen signal level at a particular time.

Midpath and endpath data relevant to this thesis have been captured using the midpath system from October 1988 to November 1990. The endpath system has been operational from August 1989 to November 1990. Calendars of the days

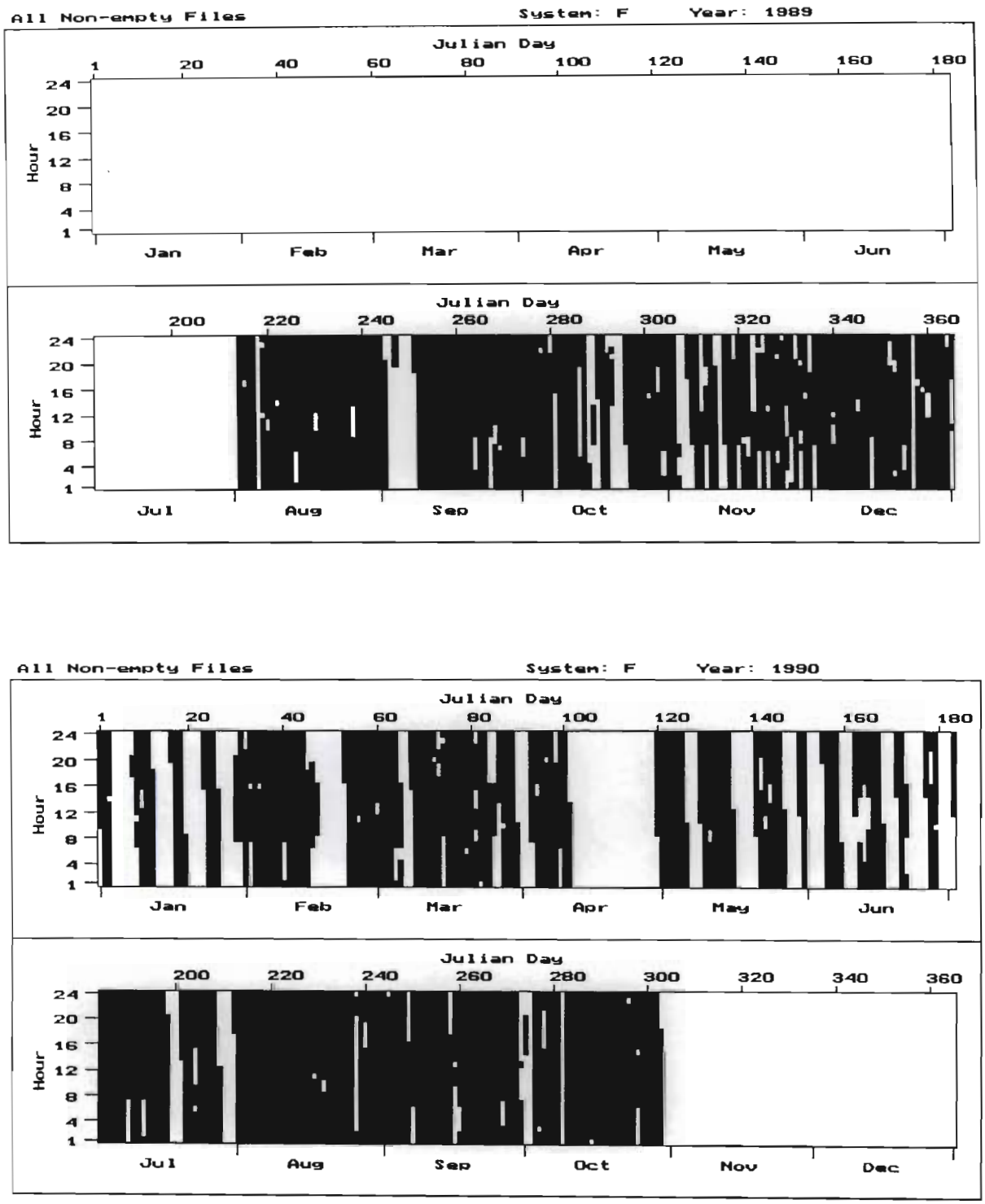

Figure 5-3 Days and hours during which data has been captured using the endpath system during 1989 and 1990.

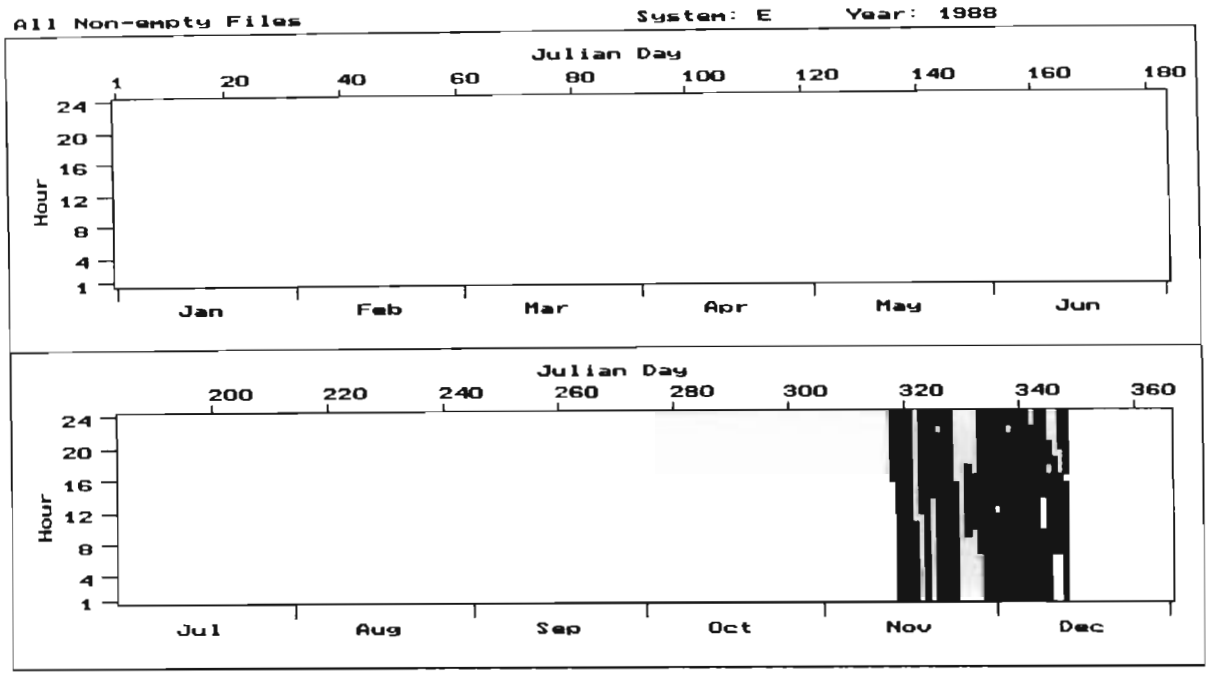

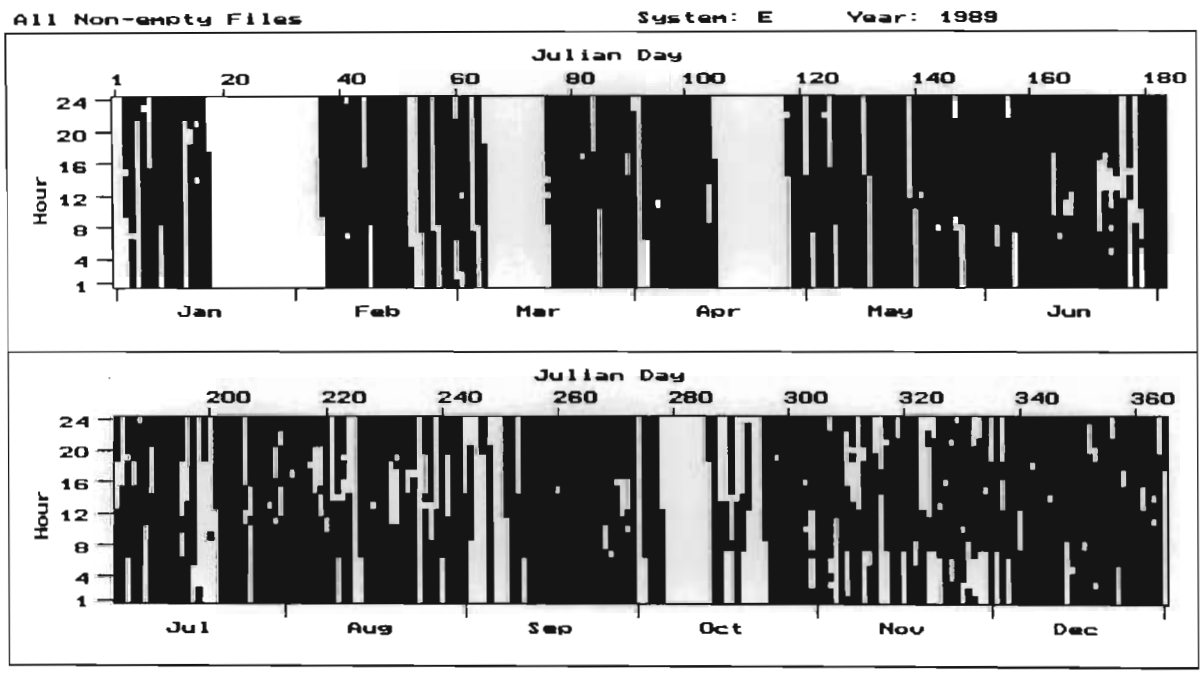

Figure 5-4 Days and hours during which data has been captured using the midpath system during 1988, 1989 and 1990 (for 1990 see next page).

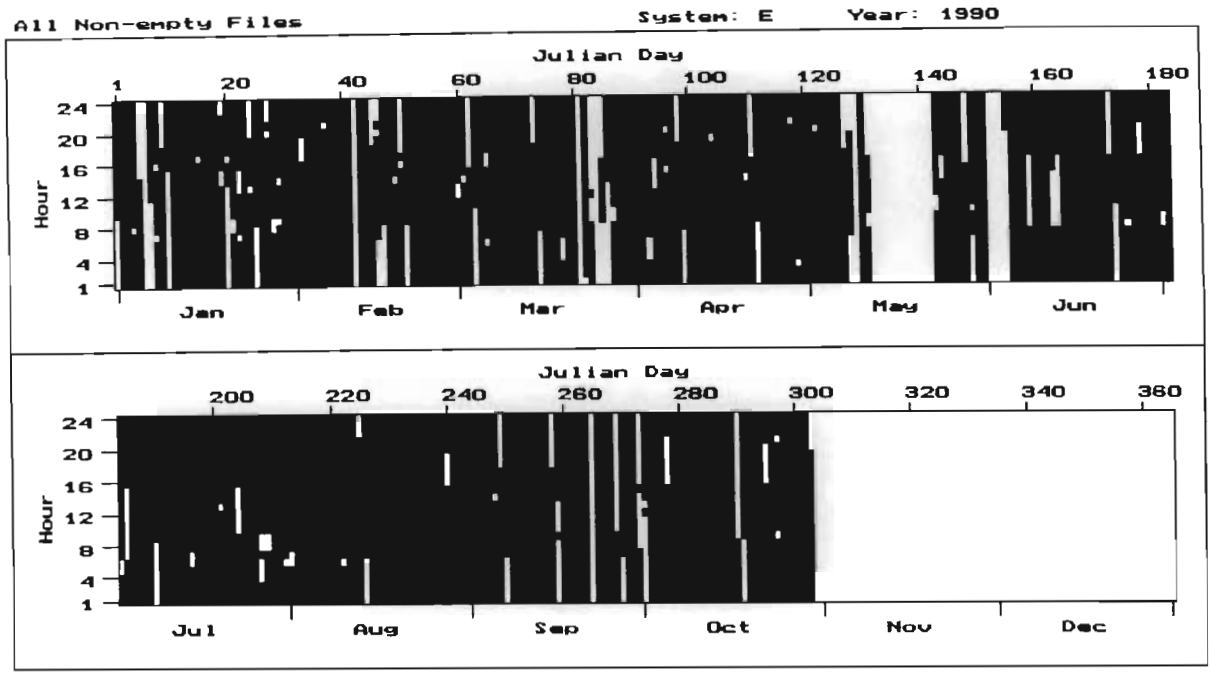

Figure 1-2 continued

and hours during which data have been captured using the midpath and endpath systems are given in Figures 5-3 and 5-4 respectively. The large gaps in the captured data throughout the year were caused by other tests being run that interfered with the midpath and endpath measurements.

5.2 Graphical technique of determining the relative contributions of regions in the celestial sphere to the arrival rate of meteors

The interaction between a particular radiant distribution of meteors and the arrival rate of meteors is typically illustrated as the relative contribution of parts of the meteor region to the arrival rate of meteors for a particular meteor-scatter link. An example of this is given in Figure 5-5. Figure 5-5 is a contour map of the contribution relative parts of the meteor region for the midpath system at 06h00

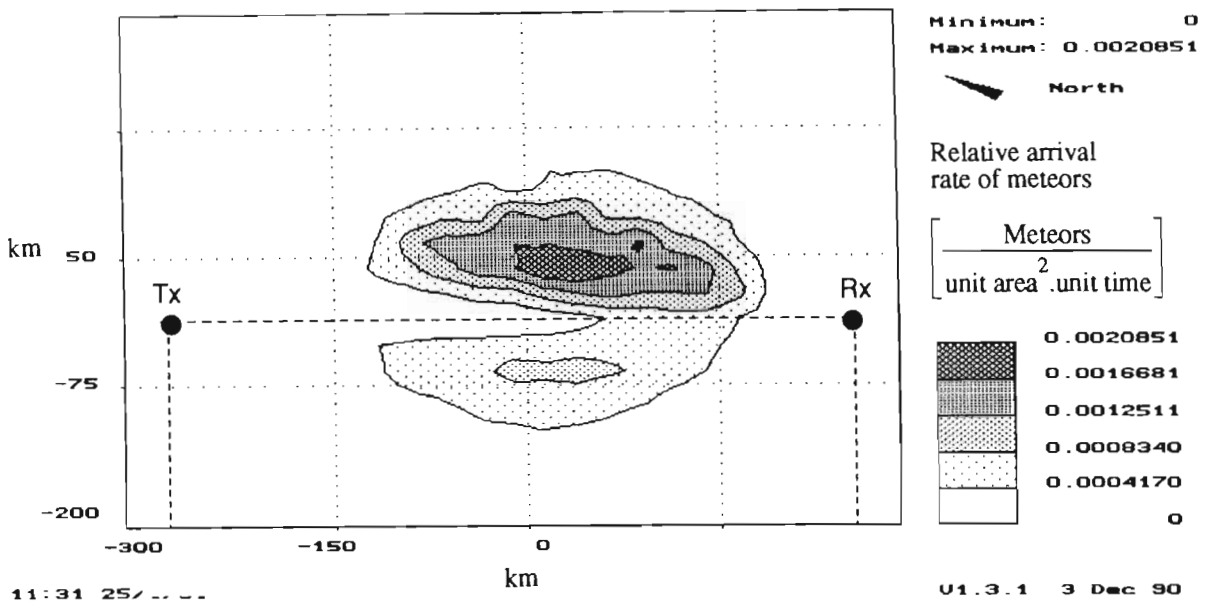

Figure 5-5 Contour map of the relative contribution of parts of the meteor region for the midpath system at 06h00 on 23 September using Rudie's radiant distribution of meteors

on 23 September using Rudie's radiant distribution of meteors. This method of illustrating the interaction between radiant distributions and the arrival rate of meteors, is ideally suited to displaying the relative contribution of parts of the meteor region to the arrival rate of meteors, when using a particular radiant distribution. Since the points of contribution of a particular radiant form a line when plotted on Figure 5-5, the interaction between the particular radiant distribution and the particular forward-scatter system is obscured.

Since every point of the meteor region is associated with a number of possible meteor radiants that may contribute to the arrival rate of meteors at that point, it is possible to calculate the regions of contribution of meteor radiants on the celestial sphere to the overall arrival rate of meteors for a particular meteor-scatter system. The contributions of parts of the celestial sphere to the arrival rate of

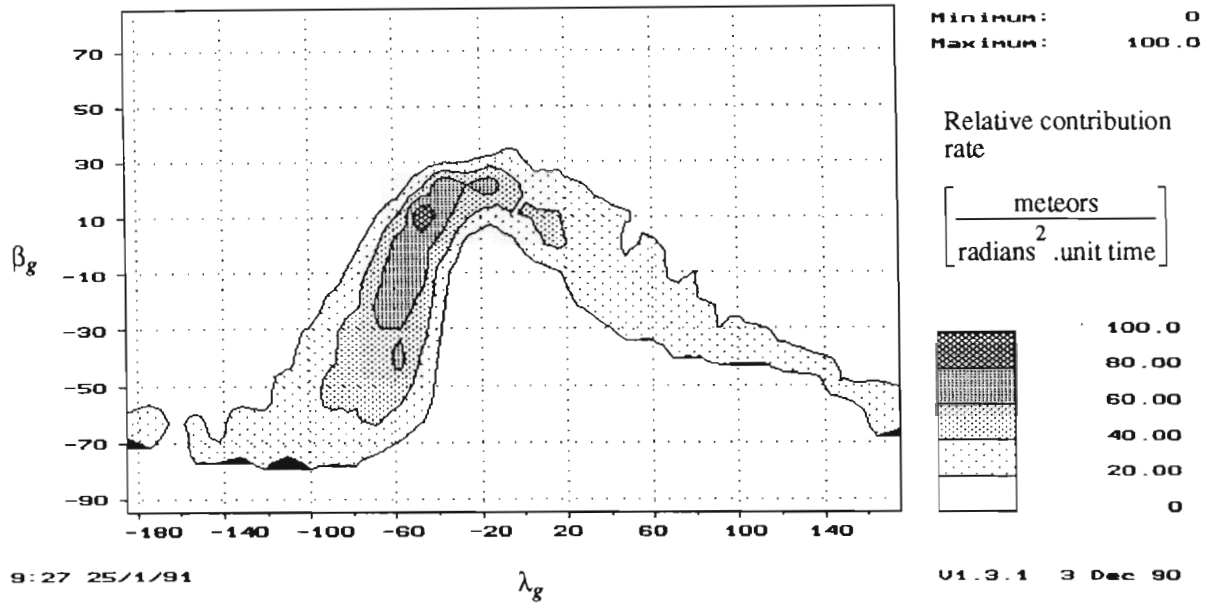

Figure 5-6 Relative contributions of parts of the celestial sphere to the arrival rate of meteors for the midpath system on 23 September at 06h00.

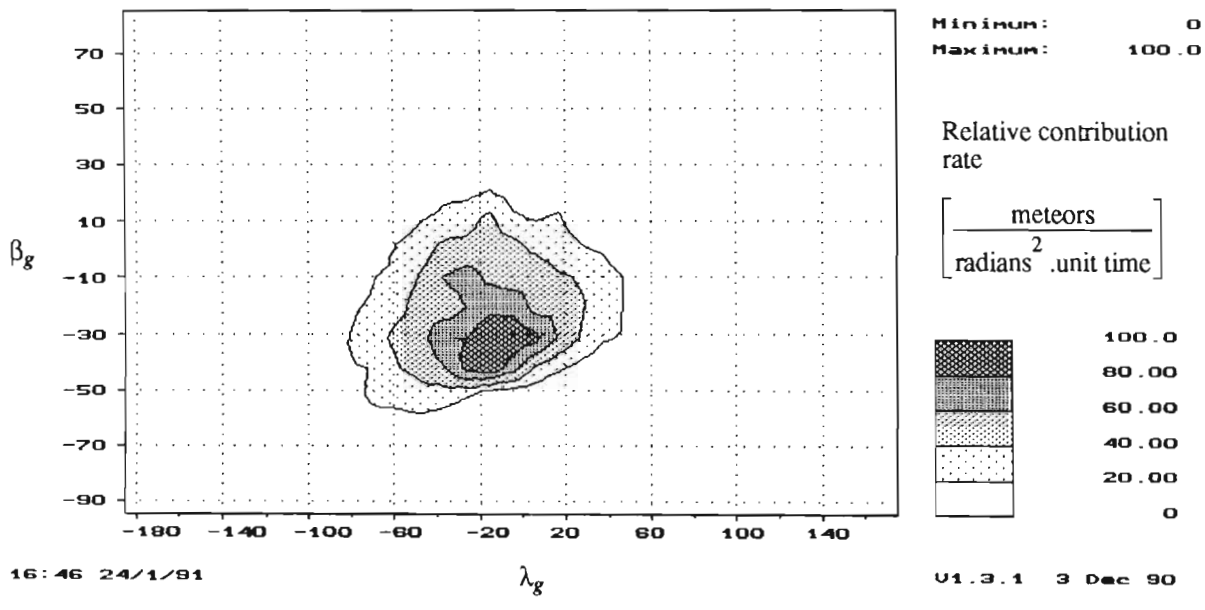

Figure 5-7 Relative contributions of parts of the celestial sphere to the arrival rate of meteors for the endpath system on 23 September at 06h00.

meteors for the midpath system on 23 September at 06h00 is contoured in Figure 5-6 in geocentric ecliptical coordinates. A uniform geocentric radiant density distribution of meteor radiants with an average heliocentric velocity of 35 kilometres per second was used to generate Figure 5-6. The geometrical requirements of forward-scatter, and the illumination pattern of the transmitter and receiver antennas, are the primary factors that determine the shape of the regions of contribution. For example, the illumination of the midpath between the transmitter and receiver and the geometrical tangential requirements of forward-scatter, which result in regions of high contribution at either side of the line between the transmitter and receiver as shown in Figure 5-5, also results in two "arms" of contribution in Figure 5-6. The effect of changing the antenna illumination pattern, as is the case with the endpath system, is illustrated in Figure 5-7. Figure 5-7 shows the relative contribution of radiants for the endpath system at the same time and date as the midpath system. As shown in Figure 5-7, the illumination of the meteor region above the receiver results in a different concentration of meteor radiants contributing to the arrival rate of meteors.

Since Figures 5-6 and 5-7 were generated using a uniform geocentric radiant distribution of meteors, the interaction between a particular radiant distribution of meteors and the arrival rate of meteors may be graphically illustrated by superimposing the contributions shown in Figures 5-6 and 5-7 with a particular non-uniform radiant distribution. For the purposes of this description Rudie's radiant distribution shown in Figure 4-13 may be used. Superposition of Figures 5-6 and 5-7 with Figure 4-13 illustrates the interaction between Rudie's radiant distribution and the arrival rate of meteors. The normalized midpath and endpath contributions of meteors on the celestial sphere using Rudie's distribution is given in Figures 5-8 and 5-9. Figures 5-8 and 5-9 are formed, in effect, by multiplication of the radiant contributions of Figures 5-6 and 5-7 with Rudie's distribution.

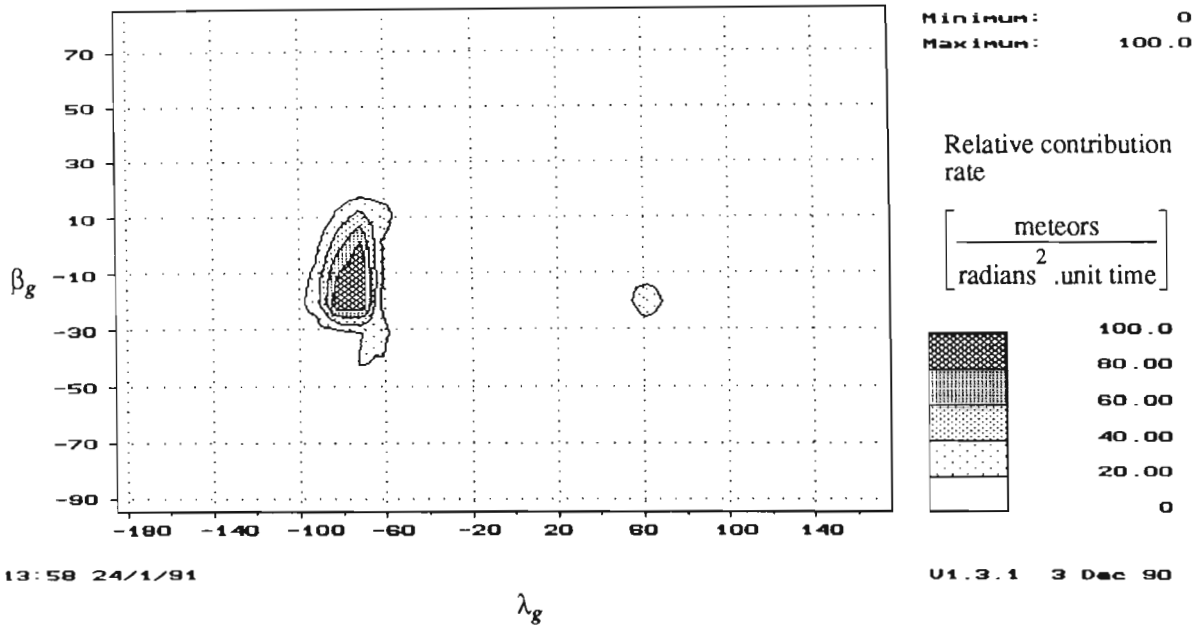

Figure 5-8 Relative contribution of meteors on the celestial sphere to the arrival rate of meteors for the midpath system on 23 September at 06h00 local time. Rudie's radiant distribution was used.

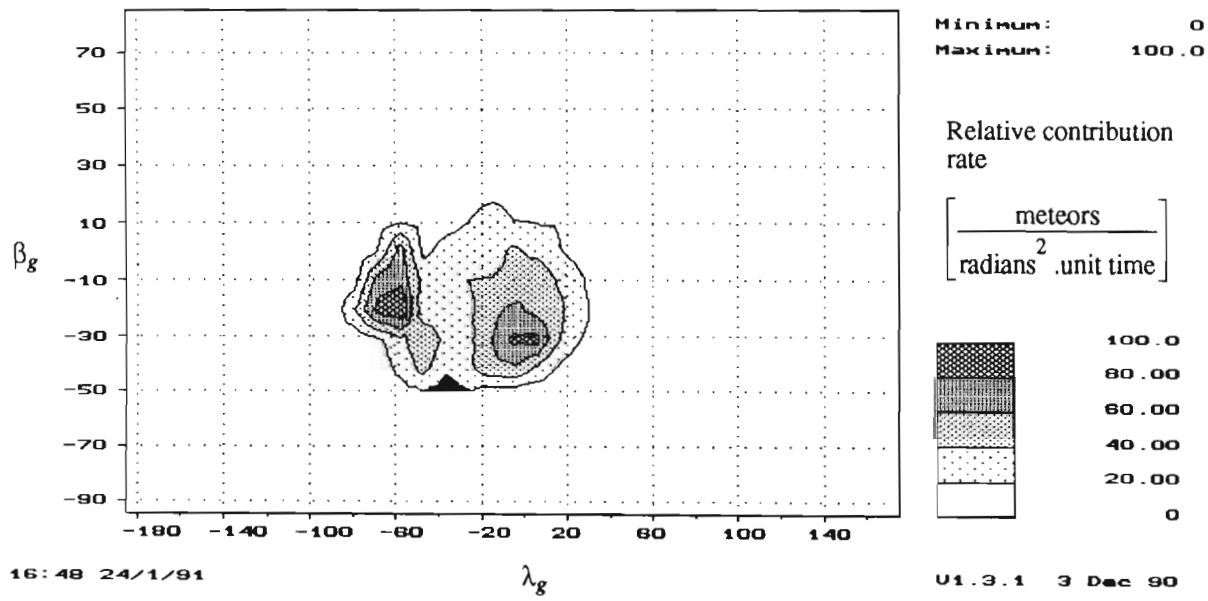

Figure 5-9 Relative contribution of meteors on the celestial sphere to the arrival rate of meteors for the endpath system on 23 September at 06h00 local time. Rudie's radiant distribution was used.

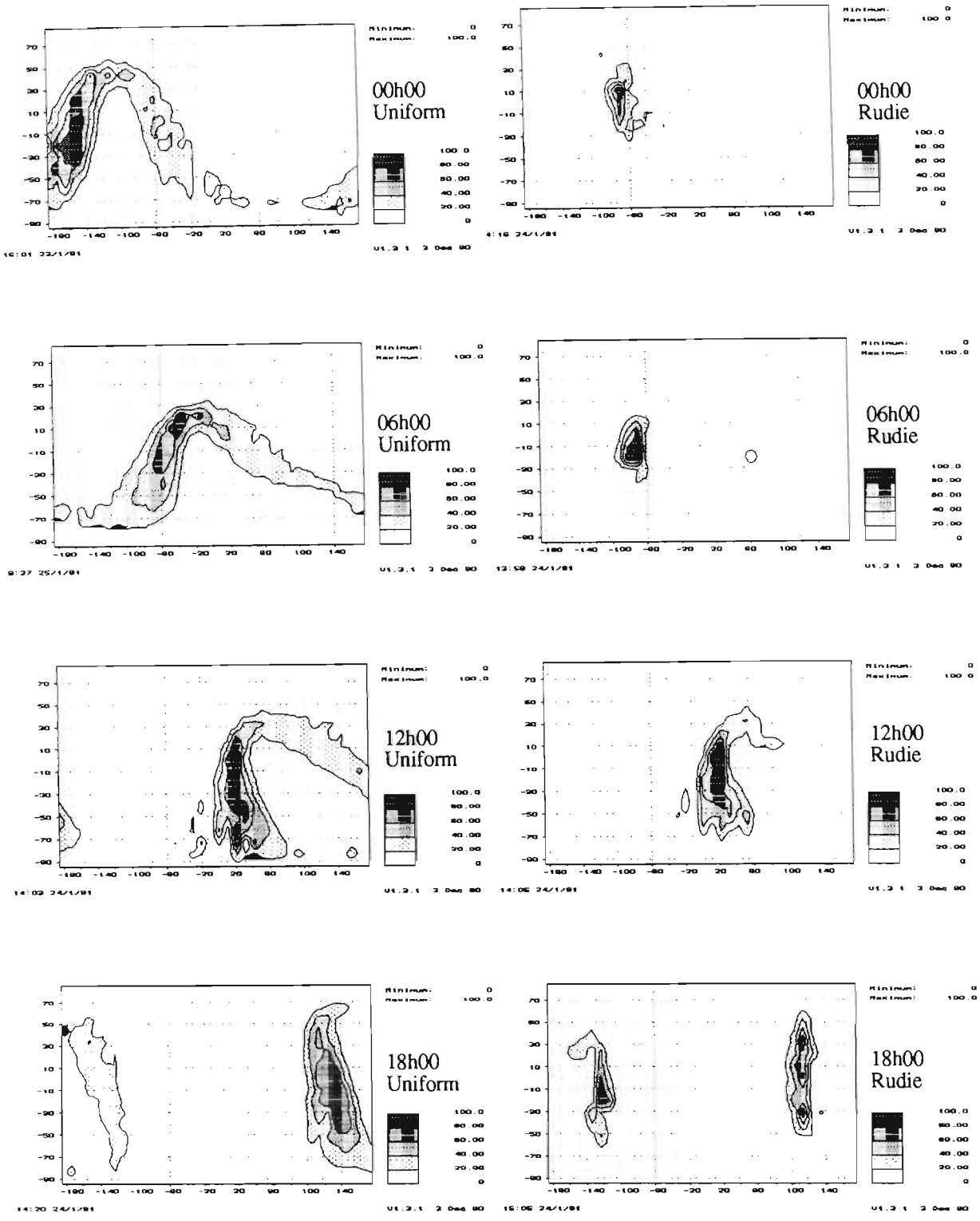

Figure 5-10 Contour plots of the midpath relative contributions on the celestial sphere for a uniform geocentric radiant distribution (Uniform) and for Rudie's radiant distribution (Rudie) for 23 September at 00h00, 06h00, 12h00 and 18h00 local time.

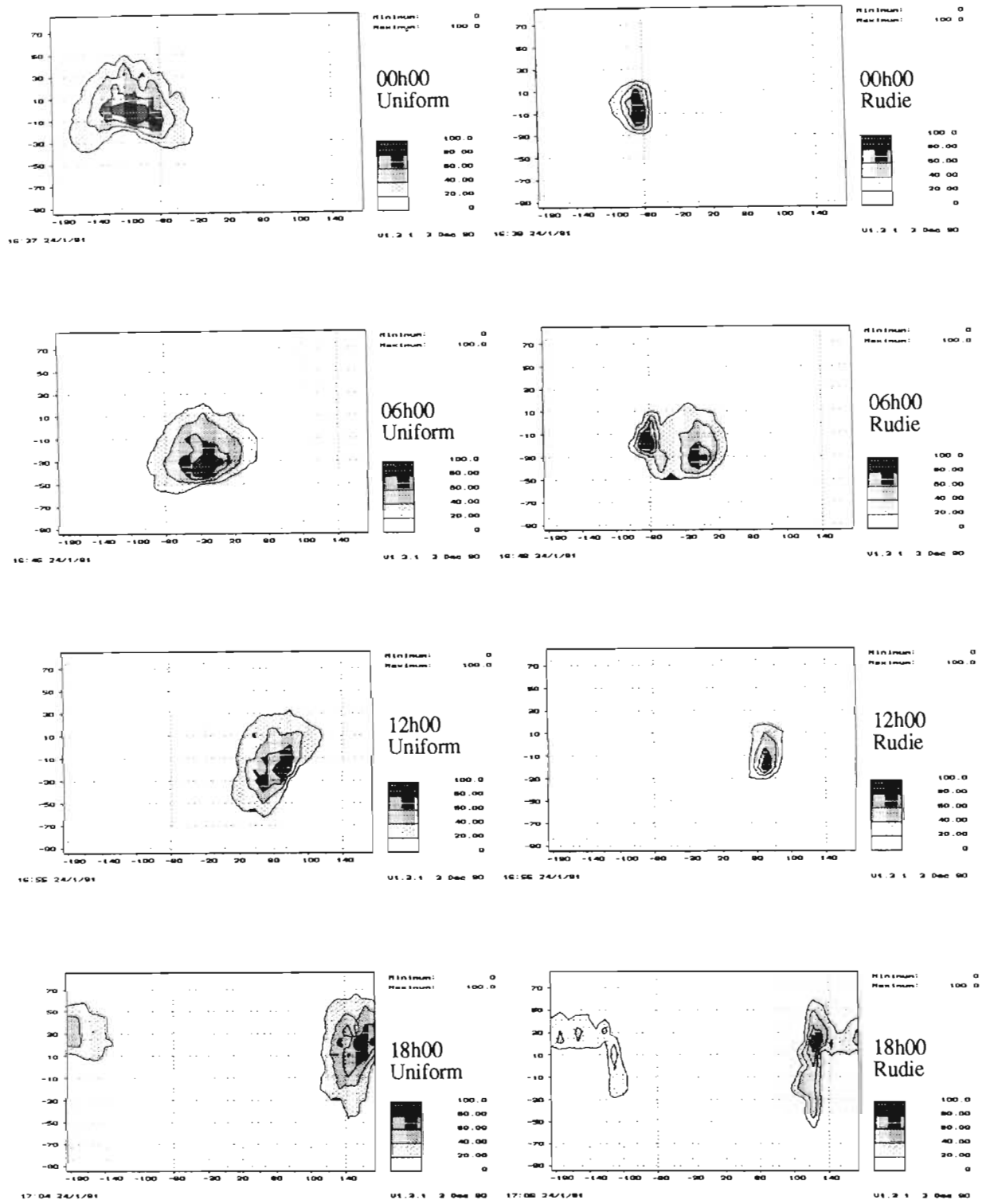

Figure 5-11 Contour plots of the endpath relative contributions on the celestial sphere for a uniform geocentric radiant distribution (Uniform) and for Rudie's radiant distribution (Rudie) for 23 September at 00h00, 06h00, 12h00 and 18h00 local time.

The daily variation in the arrival rate of meteors, caused by the interaction between a non-uniform radiant distribution of meteors and the axial rotation of the earth, may be clearly illustrated using the graphical technique described in this section. Figures 5-10 and 5-11, respectively, are contour plots of the midpath and endpath contributions for 23 September at 00h00, 06h00, 12h00 and 18h00 local time. Contributions assuming a uniform geocentric radiant distribution as well as the superposition using Rudie's distribution are shown. It should be noted that the contributions have been normalized for each contour plot and relative contributions between plots are not shown. Since most meteor radiants are concentrated about the apex hemisphere, the daily cycle in the arrival rate of meteors may clearly be illustrated by the interaction between the regions of meteor contribution on the celestial sphere and the non-uniform radiant distribution of meteors.

The annual variation in the arrival rate of meteors, caused by the axial tilt of the earth and the rotation of the earth about the sun, may also be illustrated. The longitudinal precession of regions of high contribution on the celestial sphere is illustrated in Figures 5-12 and 5-13. Figures 5-12 and 5-13, respectively, are the midpath and endpath contributions on the celestial sphere for 21 March, 21 June, 23 September and 22 December at 06h00 local time. As may be expected, the movement of regions of high contribution on the celestial sphere, caused by the earth's axial tilt and the earth's rotation about the sun, is far smaller than movement on the celestial sphere caused by the axial rotation of the earth.

One of the significant uses of this graphical technique is as an aid to the verification of radiant distributions. As will be shown in the following section, this graphical technique may be used in the comparison between predicted and measured arrival rates of meteors in order to determine the validity of various radiant distributions.

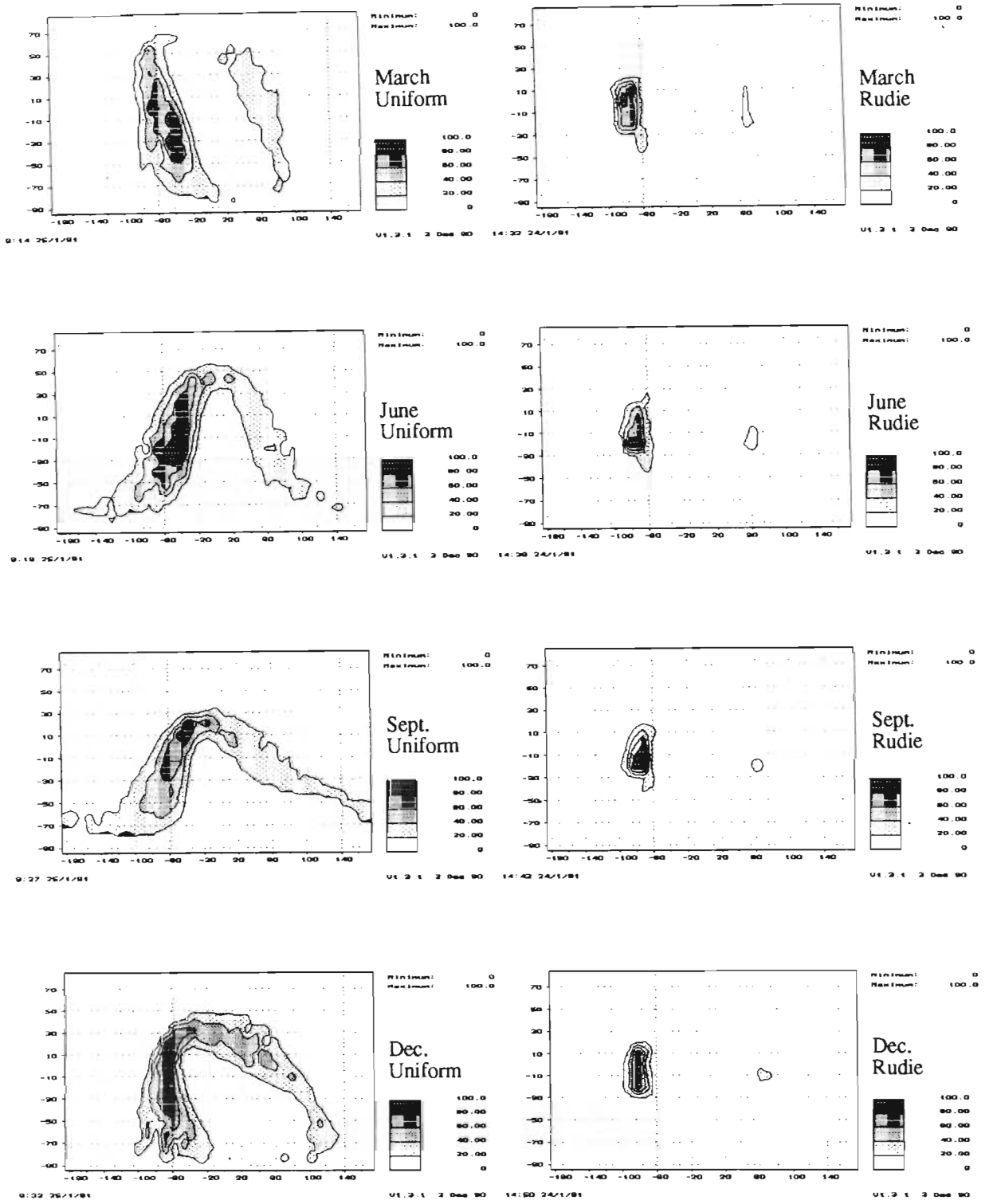

Figure 5-12 Contour plots of the midpath relative contributions on the celestial sphere for a uniform geocentric radiant distribution (Uniform) and for Rudie's radiant distribution (Rudie) for 21 March, 21 June, 23 September and 22 December at 06h00.

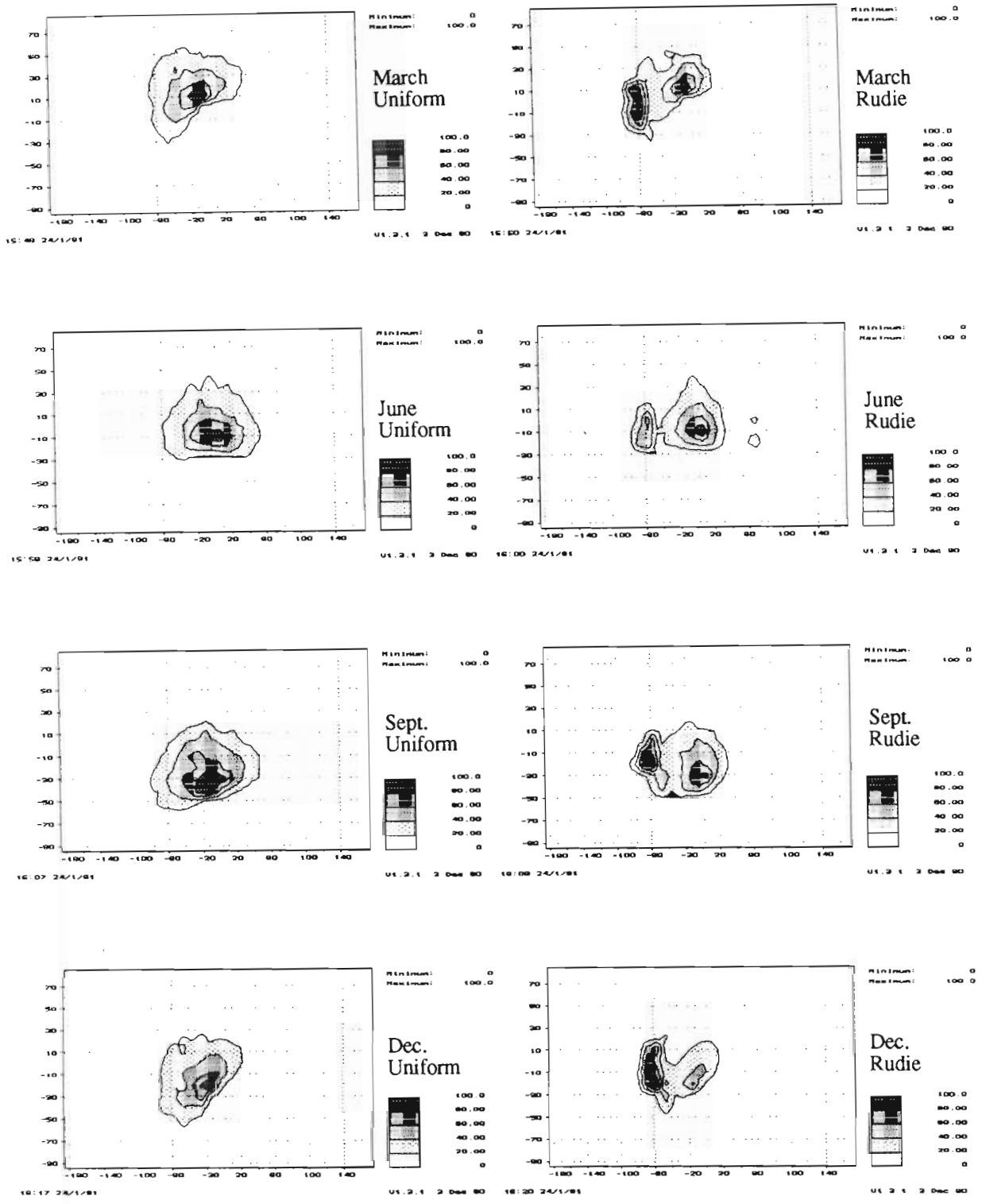

Figure 5-13 Contour plots of the endpath relative contributions on the celestial sphere for a uniform geocentric radiant distribution (Uniform) and for Rudie's radiant distribution (Rudie) for 21 March, 21 June, 23 September and 22 December at 06h00.

5.3 Comparison between measured and predicted arrival rates of meteors

In order to evaluate the validity of the various radiant distributions of meteors it was decided to compare variations in the predicted arrival rate of underdense meteors using a particular radiant distribution with the measured arrival rate of underdense meteors. The arrival rate of meteors was chosen rather than the duration because the arrival rate of meteors can be predicted more accurately than the duration of meteors. Furthermore, the arrival rate of meteors is more directly related to the density distribution of meteor radiants.

It was decided to compare the arrival rate of underdense meteors rather than overdense meteors, or even all meteor types, for three basic reasons. Firstly, the prediction of underdense meteor rates is better defined than the prediction of overdense meteors due to the fact that the underdense received power model is better defined than the overdense model. Secondly, owing to the well defined theoretical shape of the underdense trail envelope, the classification of measured underdense trails is also thought to be better defined than the overdense type classifications. Thirdly, the selection of only underdense trail types has the effect of eliminating other types of propagation such as sporadic E from the measured data.

In order to eliminate the effect of a varying noise threshold on the measured arrival rate of meteors, the measured results were extracted as underdense trails above a fixed signal level of -110 dBm, which was well above the measured background noise level. The predicted results were similarly generated assuming a constant background noise threshold.

Since the short term variation in the measured data can be large, and since the predicted results are inherently based on monthly- or yearly-averaged data, presentation of the results as monthly-averaged daily cycles of meteors was

chosen. Standard deviation error bars have been produced for the measured data to give an indication of the variation of the data. Owing to the large number and time intensive nature of the predictions, the results for only alternate months of the year, namely, January 1990, March 1990, May 1990, July 1990, September 1990 and December 1989, have been given. The omission of every alternate month is possibly only significant in the case of the predictions based on the monthly-averaged distributions, but, as will be shown later, since the yearly-averaged data seems more reliable and the difference in predictions from month to month using yearly-averaged distributions is not significant, the presentation of results for every alternate month was found to be adequate.

Monthly-averaged daily cycles of underdense meteors have been predicted for the midpath and the endpath system. Simulations have been performed using the following radiant distributions: Rudie's; Davies' extrapolated; Pupyshev's monthly-averaged; and Pupyshev's yearly-averaged. As may have been expected based on the form of the distributions shown in Chapter 2, simulations using Hawkins', McCrosky and Posen's, and the Harvard distributions confirmed that these distributions are a very poor representation of the real distribution of meteors in space. Predicted cycles for these distributions are therefore not presented here.

The simulated cycles have been compared with measured results by plotting measured and predicted results for each month. Since only relative rates are required, the measured and predicted results have been scaled so that the yearly-average for the measured and predicted results are the same. This enables any differences in the predicted and measured annual cycle of meteors to be seen.

5.4 Comparisons between measured and predicted results

Measured and predicted results for the midpath and endpath system using Rudie's, Davies' extrapolated, Pupyshev's yearly-averaged, and Pupyshev's

monthly-averaged radiant distributions are presented in Figures 5-14 to 5-17 and Figures 5-19 to 5-21 respectively. The vertical lines in the measured results represent the monthly-averaged standard deviation for the measured data.

The predicted results using Rudie's and Davies' extrapolated distributions are very similar. Although, as shown in Chapter 4, there appear to be significant differences between the two distributions, the averaging effect of a large area of contributing radiants tends to minimize the differences between the distributions. The similarity of the results from the two distributions, however, stands to reason since they are both based on Davies' data. Comparison between the measured and predicted midpath cycles using Rudie's or Davies' extrapolated distributions shows that there is a reasonable correlation between the results. Apart from the discrepancy during the July evening hours caused by showers, the only major error appears to occur from approximately 08h00 to 14h00 local time where the predicted results are almost consistently higher than the measured results. The regions of radiant contribution on the celestial sphere for the midpath system at 08h00, 10h00, 12h00 and 14h00 shown in Figure 5-22 illustrate the area on the celestial sphere where the distribution may be in error. Unfortunately, however, owing to the large region of contribution, it is not possible to localize the regions on the celestial sphere where the distributions may be in error in any more detail.

Midpath measured and predicted comparisons using Pupyshev's yearly- and monthly-averaged distributions show a far poorer correlation than Rudie's or Davies' extrapolated distribution. The shape and maximum-to-minimum variation for the yearly-averaged Pupyshev distribution differs significantly from the measured results and the monthly-averaged Pupyshev distributions provide even poorer results. Based on these results it is possible to conclude that the monthly-averaged distributions are probably poor and that Pupyshev's yearly-averaged

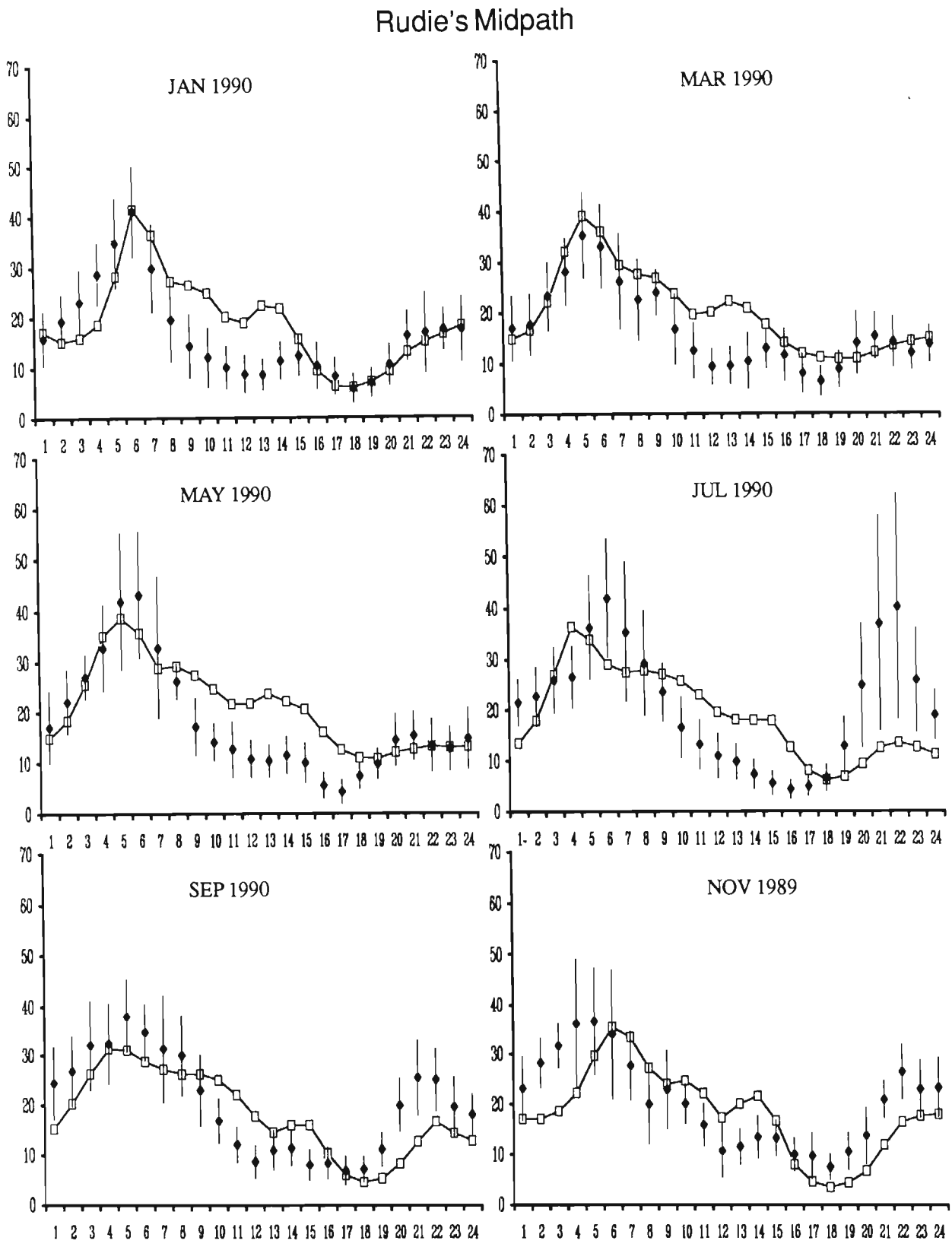

Figure 5-14 Comparison between measured (solid diamond) and predicted (square) monthly-averaged daily cycles of meteors for the midpath system using Rudie's distribution. (Trails per hour versus local time)

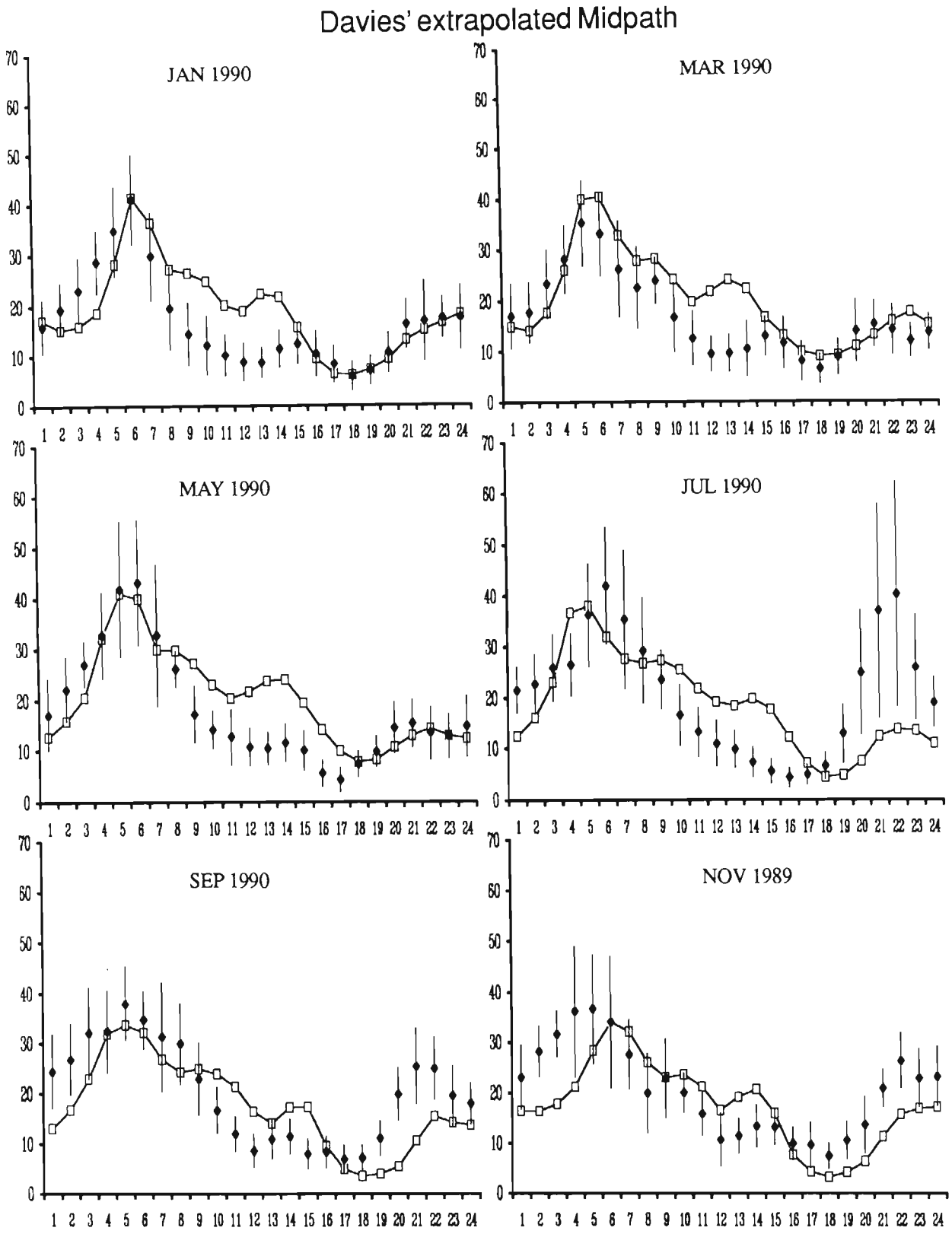

Figure 5-15 Comparison between measured (solid diamond) and predicted (square) monthly-averaged daily cycles of meteors for the midpath system using Davies' extrapolated distribution. (Trails per hour versus local time)

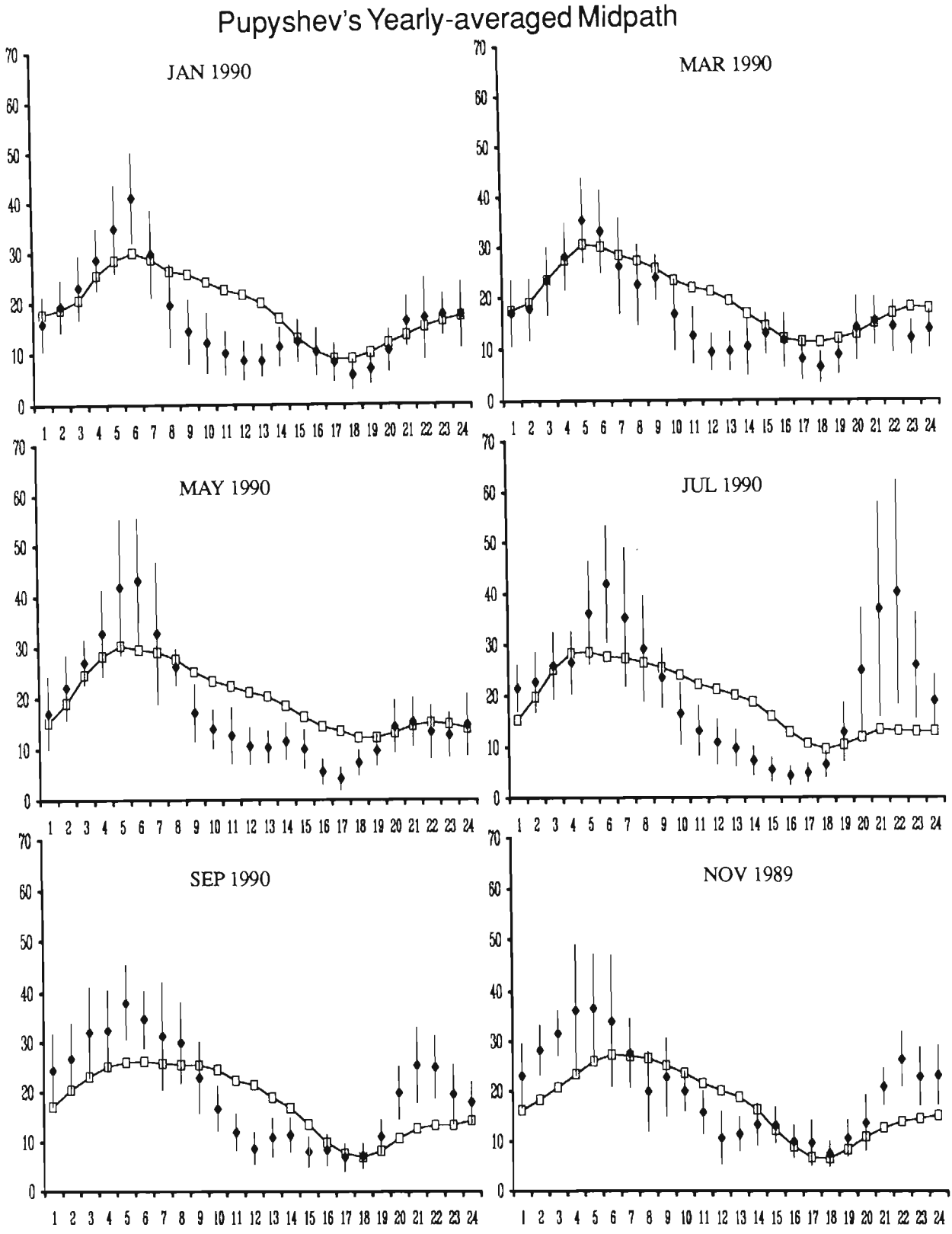

Figure 5-16 Comparison between measured (solid diamond) and predicted (square) monthly-averaged daily cycles of meteors for the midpath system using Pupyshev's yearly-averaged distribution. (Trails per hour versus local time)

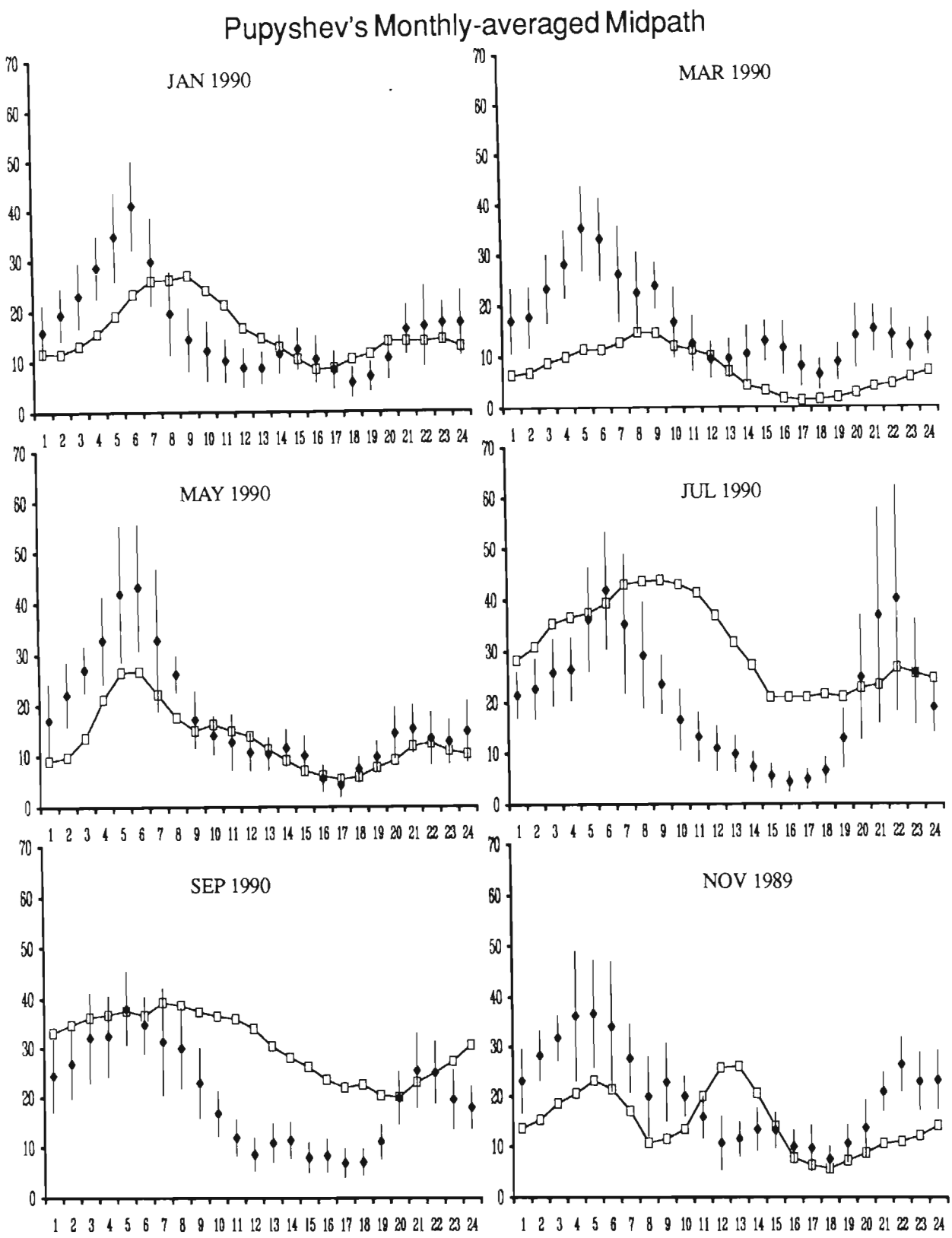

Figure 5-17 Comparison between measured (solid diamond) and predicted (square) monthly-averaged daily cycles of meteors for the midpath system using Pupyshev's monthly-averaged distribution. (Trails per hour versus local time)

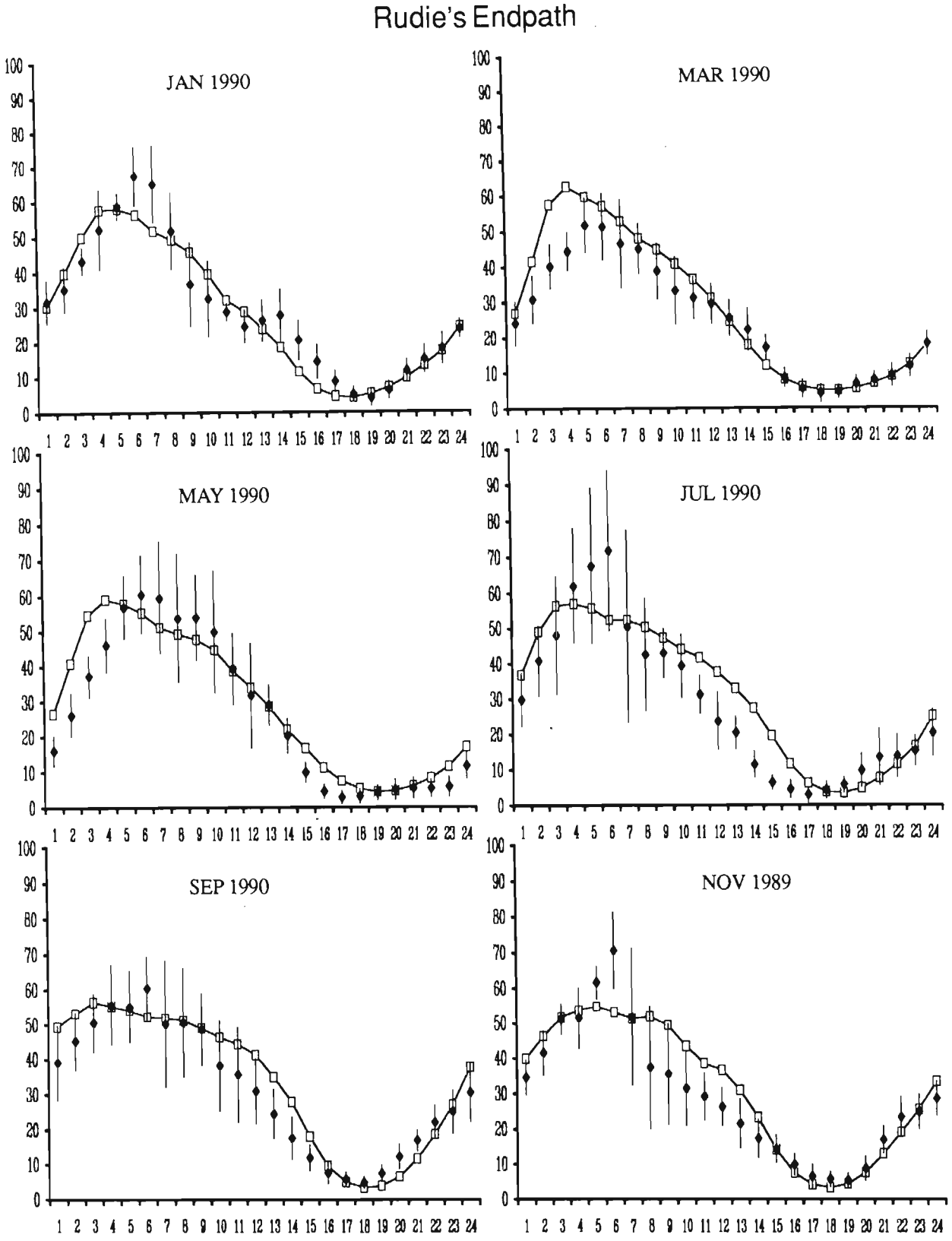

Figure 5-18 Comparison between measured (solid diamond) and predicted (square) monthly-averaged daily cycles of meteors for the endpath system using Rudie's distribution. (Trails per hour versus local time)

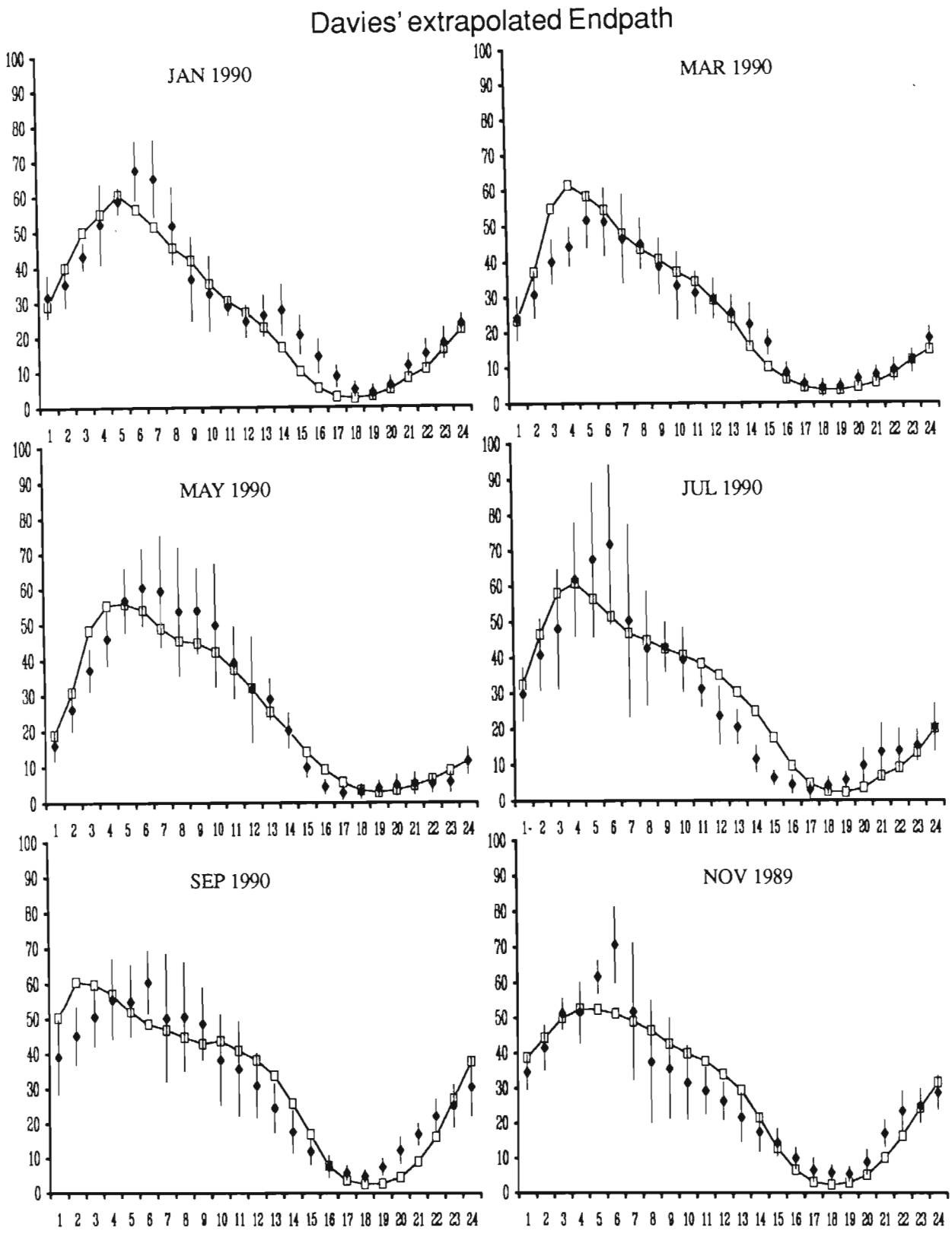

Figure 5-19 Comparison between measured (solid diamond) and predicted (square) monthly-averaged daily cycles of meteors for the endpath system using Davies' extrapolated distribution. (Trails per hour versus local time)

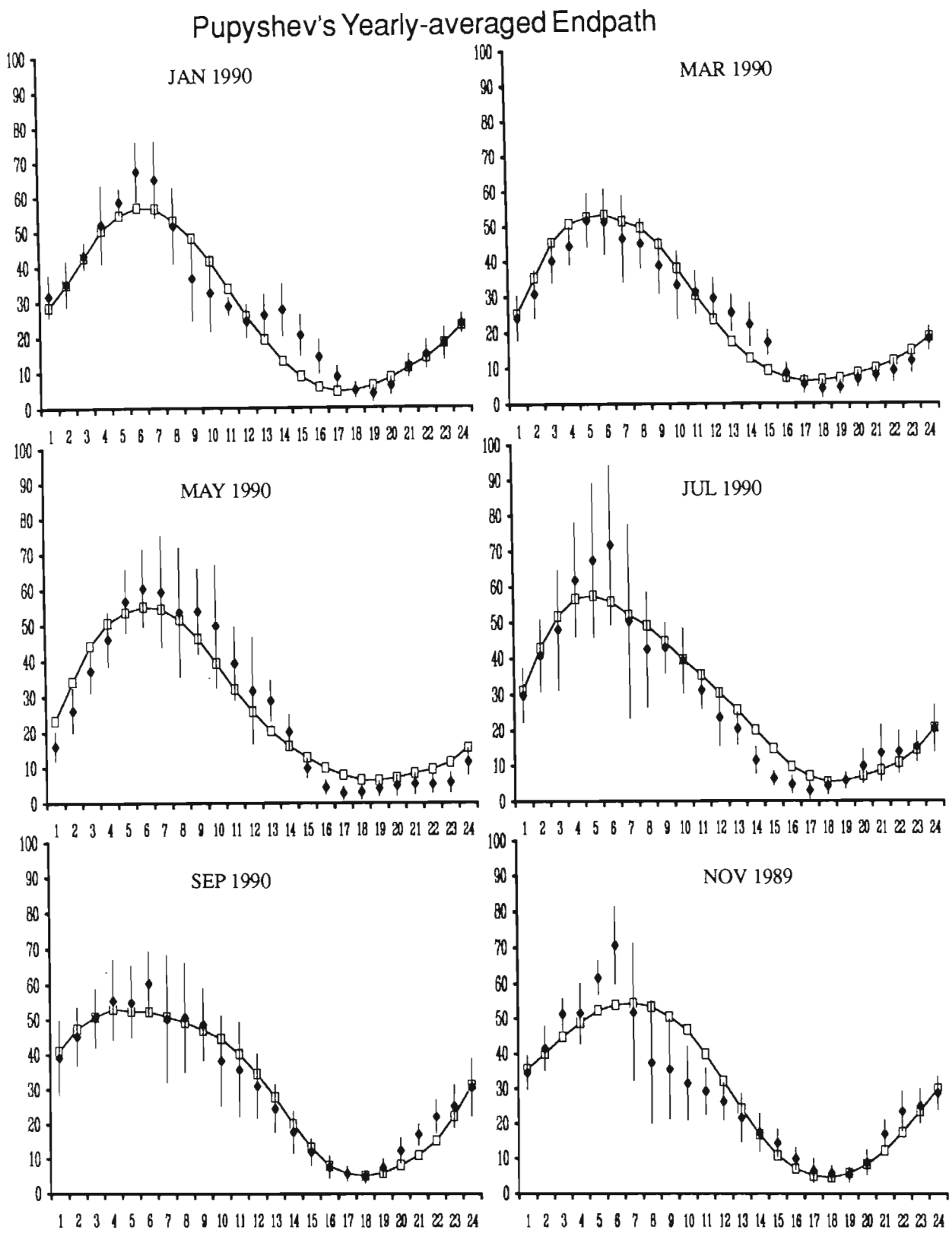

Figure 5-20 Comparison between measured (solid diamond) and predicted (square) monthly-averaged daily cycles of meteors for the endpath system using Pupyshev's yearly-averaged distribution. (Trails per hour versus local time)

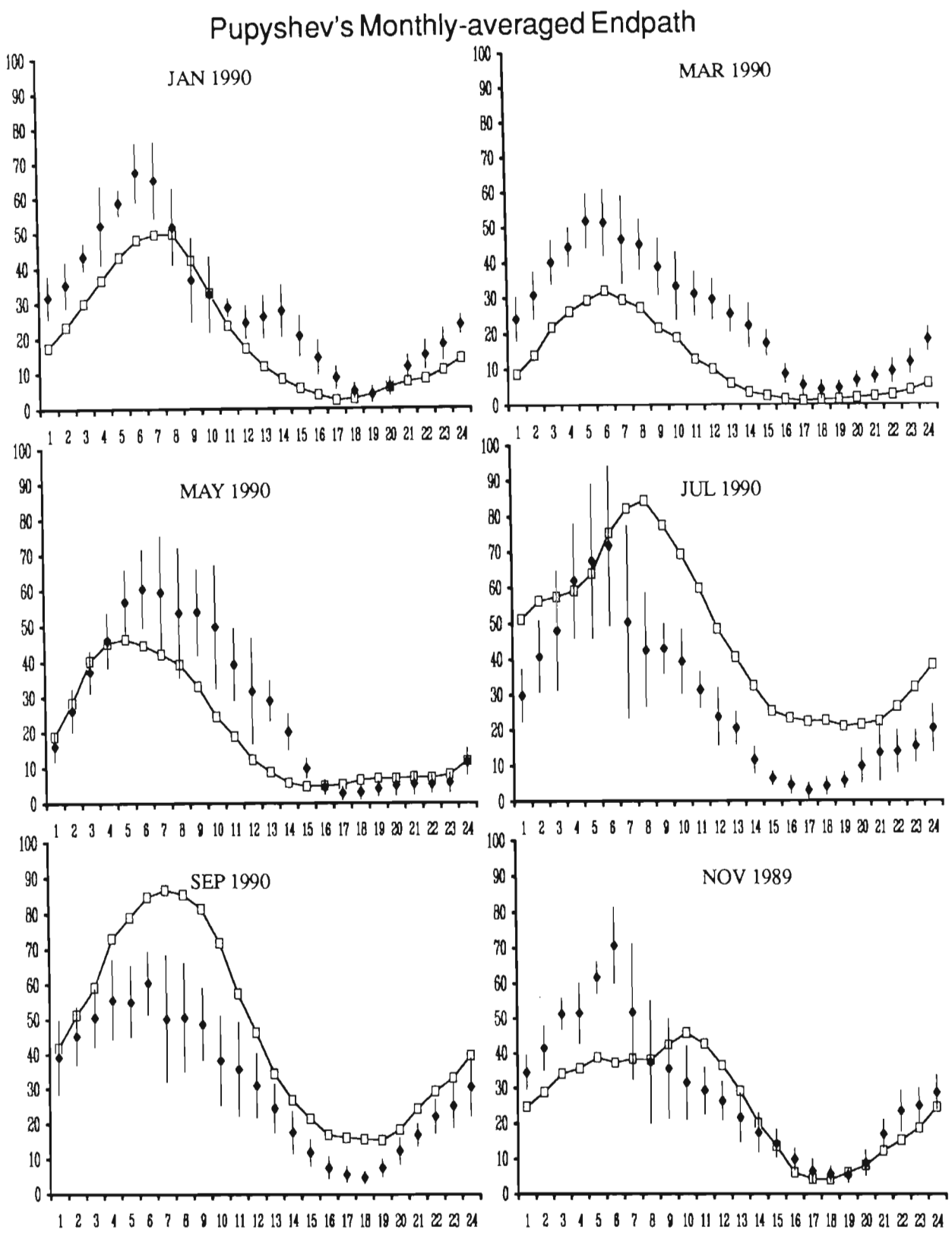

Figure 5-21 Comparison between measured (solid diamond) and predicted (square) monthly-averaged daily cycles of meteors for the endpath system using Pupyshev's monthly-averaged distribution. (Trails per hour versus local time)

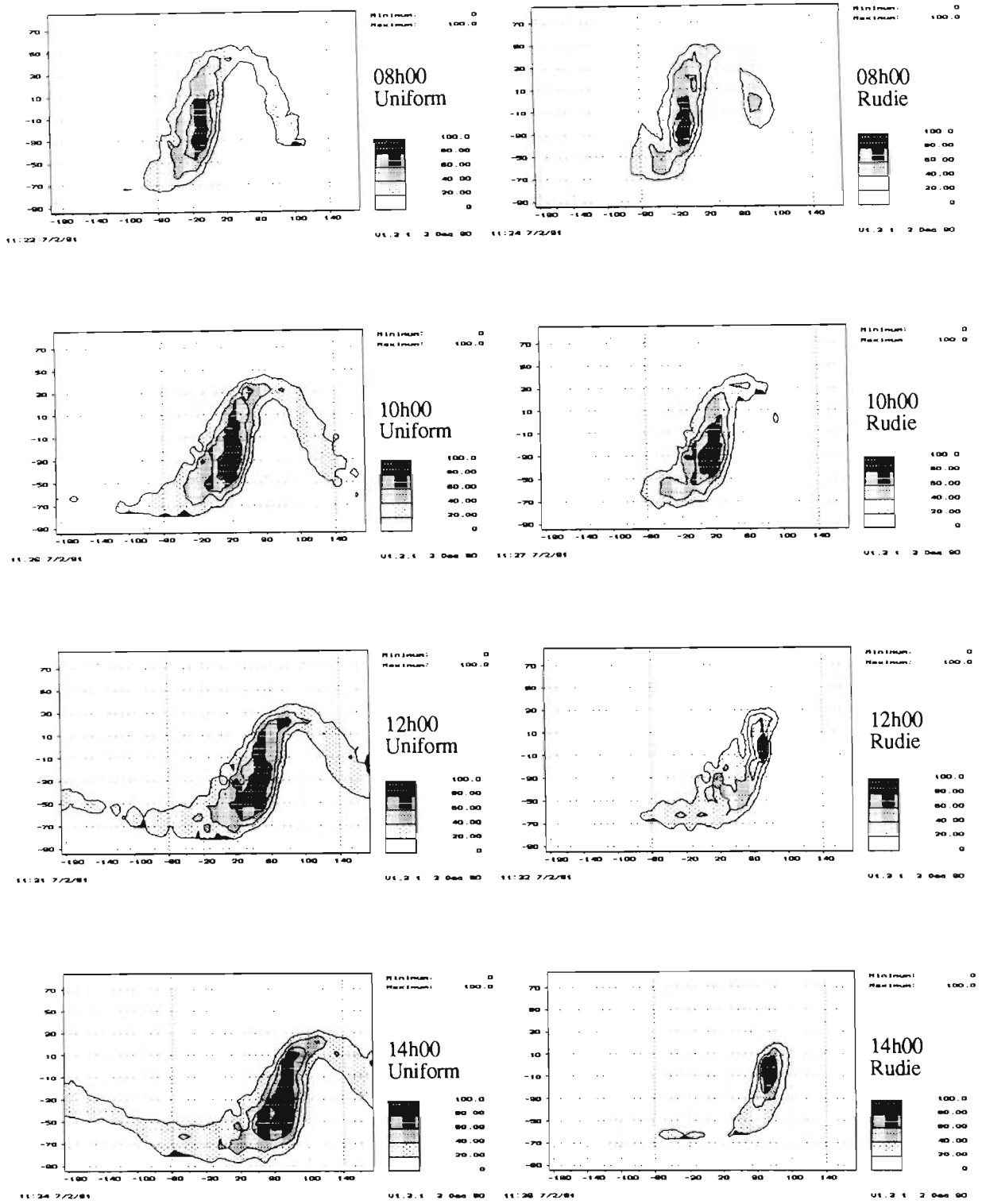

Figure 5-22 Contour plots of the endpath radiant contributions on the celestial sphere for a uniform geocentric radiant distribution (Uniform) and for Rudie's radiant distribution (Rudie) for March at 08h00, 10h00, 12h00 and 14h00 local time.

distribution produces poorer results than Rudie's or Davies' extrapolated distribution.

An examination of the endpath measured and predicted cycles, however, shows that predictions using Pupyshev's yearly-averaged distribution correlate better than the endpath predictions using Rudie's or Davies' extrapolated distribution, which appears to contradict the findings for the midpath predictions. An inspection of the regions of contribution on the celestial sphere for the midpath and endpath systems shown in Figures 5-10 to 5-13, along with an inspection of the radiant distributions, appears to offer a possible reason for this discrepancy. As shown in Section 5.2, the radiant contribution on the celestial sphere for the midpath system includes a greater concentration of radiants at higher latitudes than the endpath system. An inspection of Pupyshev's yearly-averaged distribution shows a greater contribution of radiants at high latitudes around the north and south ecliptic poles than Rudie's or Davies' extrapolated distribution. The contribution of the high latitude radiants on Pupushev's yearly-averaged midpath prediction results in higher predicted counts around 18h00 local time and therefore also distorts the shape of the midpath predicted cycle. Owing to the endpath radiant contributions occurring around the ecliptic and the good correlation obtained for the measured and predicted results using Pupyshev's yearly-averaged distribution, Pupyshev's distribution seems to be accurate about the ecliptic plane. Care should be taken, however, in the evaluation of the radiant distributions in this way, since it is clear that predictions using Rudie's, Davies' extrapolated, and Pupyshev's yearly-averaged distributions, all produced good correlation with the measured results and yet are different distributions. It is clear that the large area of the radiants on the celestial sphere that contribute to meteor count reduces the effect of differences between the distributions.

One notable observation from the comparison between the measured and predicted endpath cycles using Rudie's or Davies' extrapolated distribution is that a

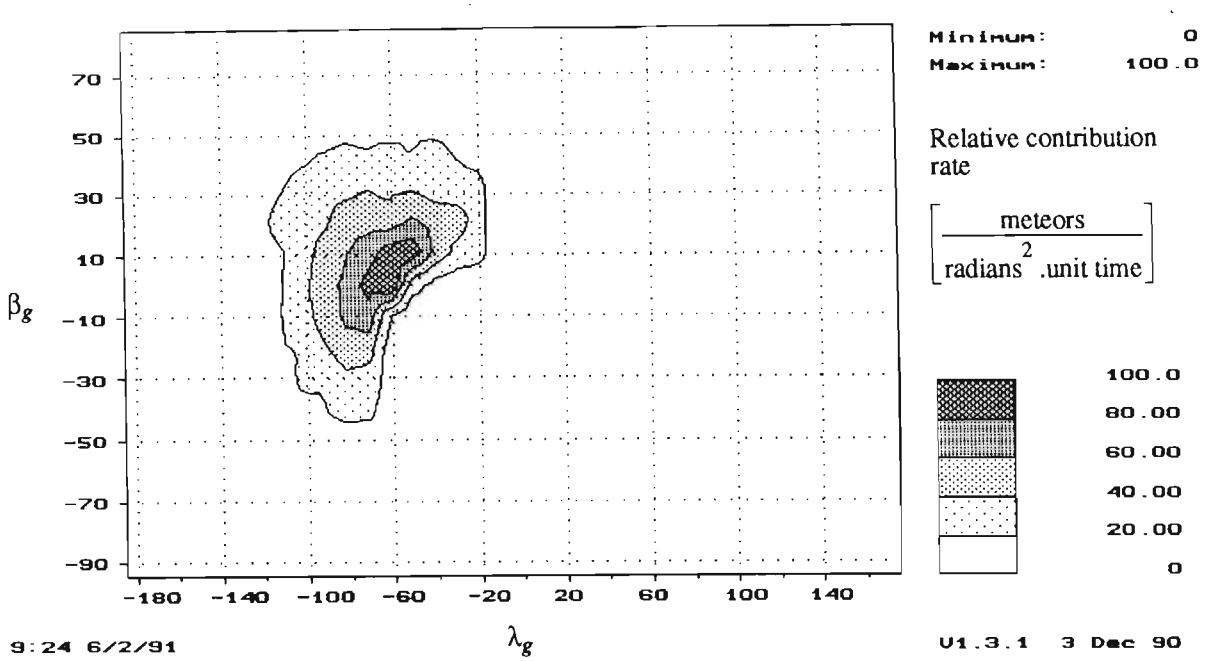

Figure 5-23 Regions of relative contribution of meteor radiants on the celestial sphere for the endpath system on 21 March at 04h00 local time

peak in meteor count is predicted earlier than the measured peak that typically occurs at 06h00 local time. The contribution of radiants on the celestial sphere for the predicted endpath March peak at 04h00 is shown in Figure 5-23, which shows that the peak is caused primarily by the anti-sun contribution. This seems to indicate that the position and/or amplitude of the anti-sun contribution relative to the apex contribution for Rudie's or Davies' extrapolated distribution may be incorrect. The low resolution of this technique of verifying the radiant distributions makes it difficult to determine the actual problem, but comparison between Rudie's or Davies' extrapolated and Pupyshev's yearly-averaged distribution seems to indicate that the relative amplitude of the radiant contributions about the apex for Rudie's or Davies' extrapolated distribution may be too low.

Finally, as was the case with the midpath system, an inspection of the measured and predicted results for the endpath system using Pupyshev's monthly-averaged

distributions show poor correlation. Although only half the monthly-averaged distributions have been presented here, the results are sufficient to show that Pupyshev's monthly-averaged data is poor. This result, and the fact that the yearly-averaged distributions give better results than the monthly-averaged distributions, confirms the observation that the monthly-averaged data appeared to have little resolution.

5.4.1 Annual variation

The measured results for both the midpath and the endpath system show that there is very little annual variation in the measured monthly-averaged arrival rate of meteors. As shown in Chapter 2, owing to the discrepancy between the various measured results, there is a high degree of uncertainty regarding the expected annual variation in the arrival rate of meteors. The results shown here contrast sharply with the large annual variation in the arrival rate of meteors adopted by Weitzen for example, based, apparently, on Hawkins' results. The variation in the space density of meteors with solar longitude has been estimated using similar techniques to those used by *Hawkins* [1956] and *Keay* [1963]. The space density of meteors with solar longitude has been estimated by comparing the measured and predicted results, using Rudie's or Davies' distribution, for the midpath and endpath system. Figures 5-24 and 5-25 are graphs of the normalized predicted and measured monthly-averaged annual variation in the arrival rate of meteors for the midpath and endpath system respectively. The annual variation in the space density of meteors has been estimated by finding the ratio of the measured to predicted results for the midpath and endpath systems as shown in Figure 5-26. The annual variation predicted using the midpath system is very similar to the variation predicted by *Keay* [1963] that is reproduced in Figure 2-35. The difference between the midpath and endpath results may possibly be due to their being a greater variation in the space density of meteors at higher ecliptical latitudes that would affect the midpath measurements more than the endpath

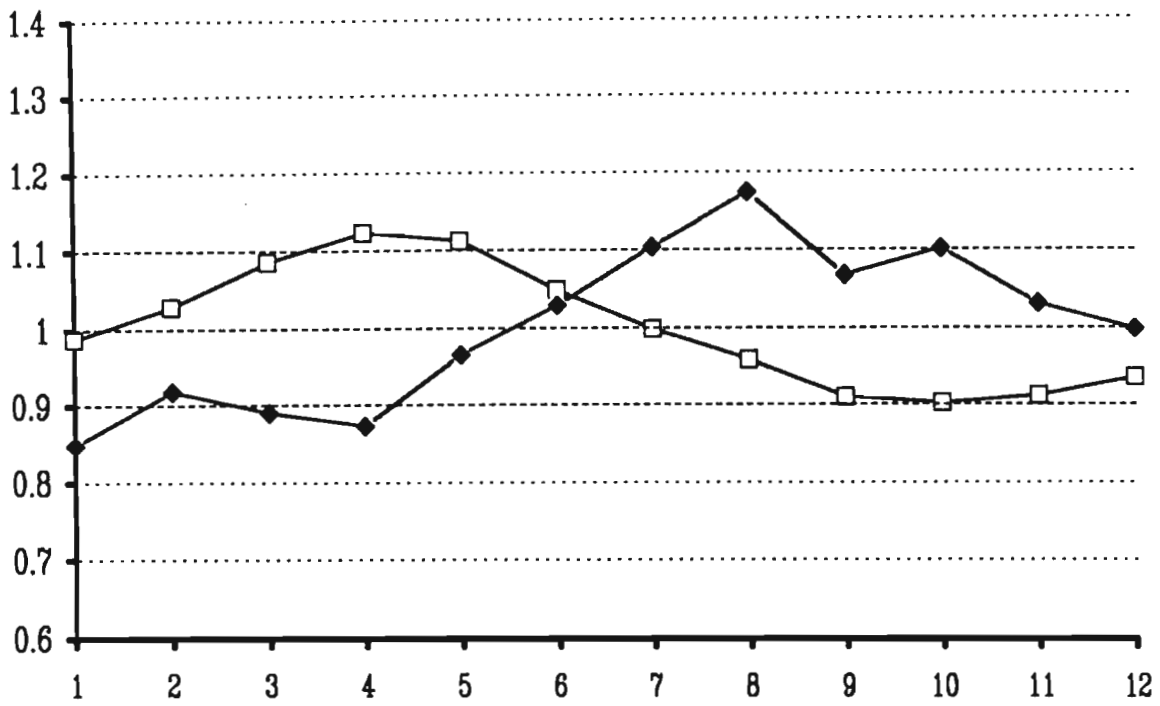

Figure 5-24 Normalised measured (solid diamond) and predicted (square) monthly-averaged annual variation in the arrival rate of meteors for the midpath system versus month of year.

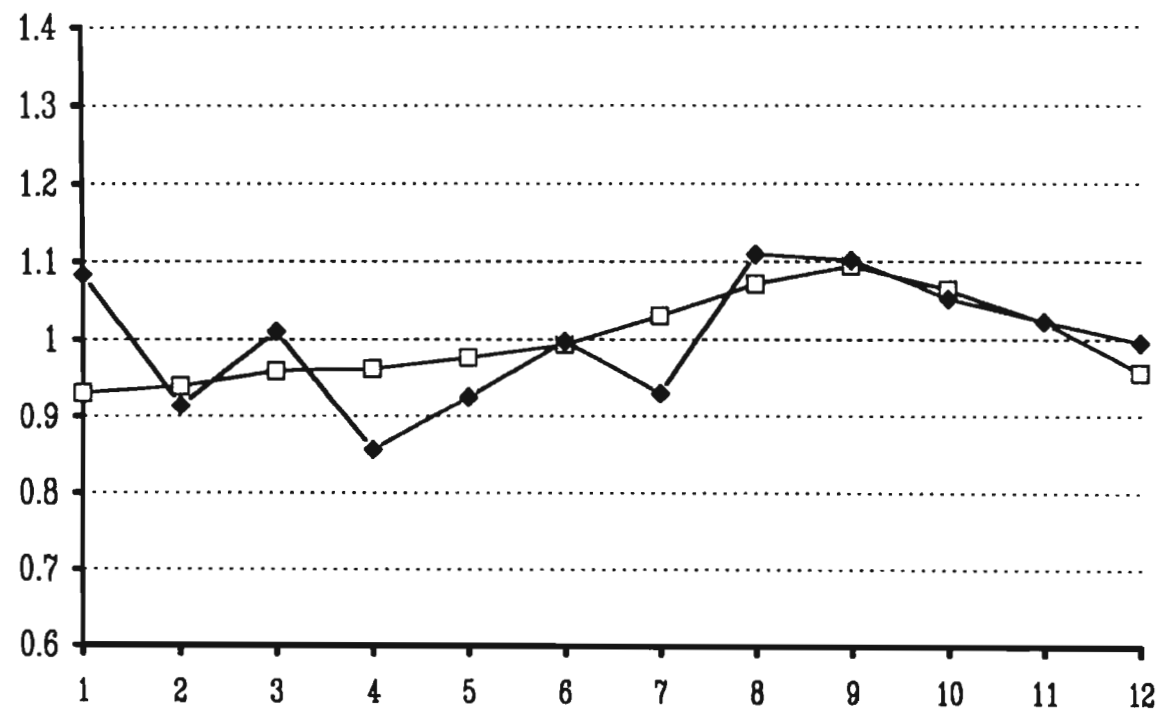

Figure 5-25 Normalised measured (solid diamond) and predicted (square) monthly-averaged annual variation in the arrival rate of meteors for the endpath system versus month of year.

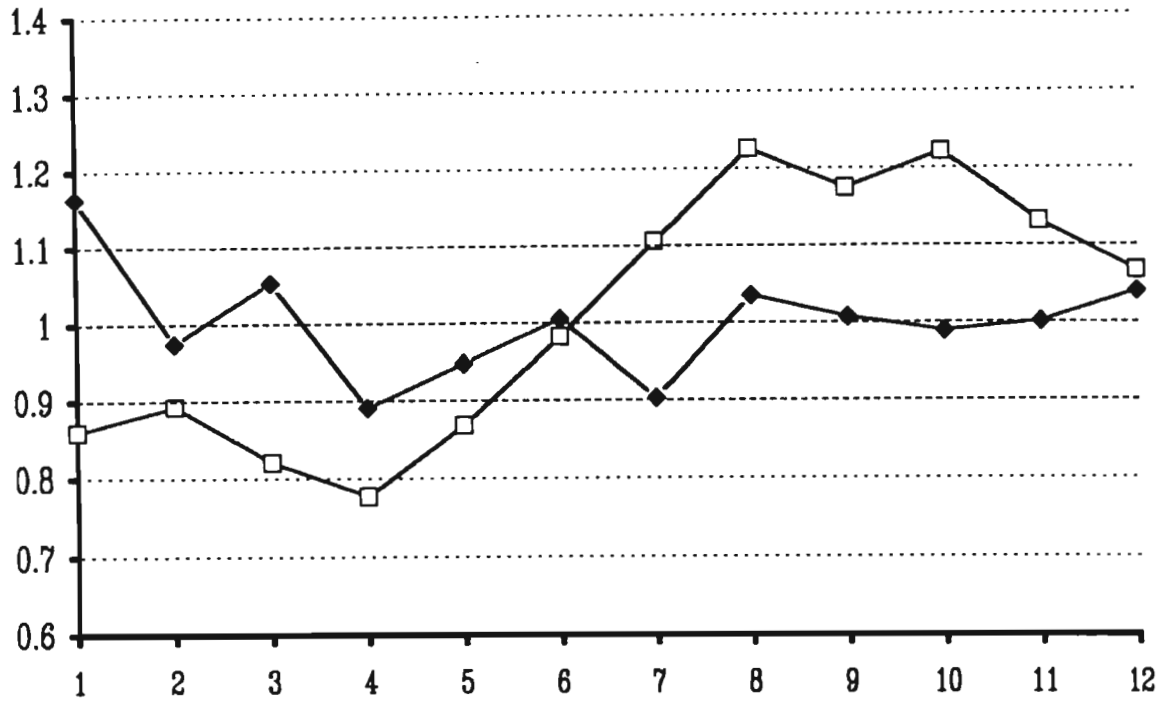

Figure 5-26 Apparant annual variation in the monthly-averaged space density of meteors estimated using the midpath (square) and the endpath (solid diamond) system. (Normalised variation versus month of year)

measurements. This would also account for the good correlation obtained with Keay's results, which were based on measurements taken at mid latitudes. The results presented here and by Keay confirm the probable error of Hawkins' space density variation. Since the space density variation of meteors does not appear to vary uniformly across the celestial sphere, the scaling of a yearly-averaged density distribution of meteors, in order to take into account the variation in space density of meteors, would not produce accurate predicted results.

5.5 Conclusions

Comparisons between measured and predicted annual variations of meteor counts shows that the predicted results are very close to the measured results, which indicates that a large variation in the space density of meteors with solar longitude does not occur. This result is in sharp contrast to the large variations

predicted by Hawkins, and indicates that the variation is even lower than the variation presented by *Keay* [1963].

Comparisons between predicted and measured results for both the midpath and endpath systems seem to indicate that Rudie's or Davies' extrapolated distributions provide the most accurate results overall. The good performance of Pupyshev's yearly-averaged distribution for the endpath system seems to indicate, however, that Pupyshev's yearly-averaged distribution is more accurate than Rudie's or Davies' extrapolated distribution around the ecliptic. The performance of Pupyshev's monthly-averaged distribution was poor, which indicates that the monthly-averaged distributions are not reliable.

Although the most reasonable results overall were obtained using Rudie's or Davies' distributions, the results obtained were by no means ideal. This is to be expected, since the measurements on which they are based are by no means comprehensive. It should also be remembered that the effect of integrating contributions of meteors over the meteor region tends to hide the fact that the actual relative distribution of meteors in the meteor region may not be accurate for a particular radiant distribution, although the integrated value may be. This has serious implications for the design of communication systems where the distribution of meteors across the meteor region needs to be known in order to optimize system parameters such as antenna polar patterns. Although the results of this chapter have shown that Rudie's or Davies' distributions produce reasonable results there is, therefore, still a need for a far more comprehensive set of radar measurements to determine the density, velocity and mass distributions of meteors intercepting the earth throughout the year.

Chapter 6

Conclusions

Questions regarding the origin of the heliocentric distribution presented by *Rudie* [1967] have been discussed in Chapter 4. A detailed investigation into the origin of the heliocentric distribution presented by Rudie has shown that Rudie's heliocentric distribution is simply an unnecessarily complicated extrapolation or approximation of a particular set of results presented by *Davies* [1957]. Furthermore it has been shown that distributions of orbital parameters of meteors presented by Davies could not have been used by Rudie to generate his heliocentric distribution of meteors directly. An alternative, far simpler extrapolation of Davies' results has been given in the form of a geocentric radiant distribution of meteors. A method of converting from a heliocentric to geocentric radiant distribution, which is slightly more accurate than the method given by Rudie, was also given in Chapter 4. Using either technique it was shown that very similar results were obtained for the transformation of Rudie's heliocentric distribution to geocentric coordinates. For the purposes of modelling the effect of radiant distributions on the arrival rate of meteors, theory developed in Chapter 3 has shown that the incorporation of radiant distributions presented in geocentric coordinates is analytically far simpler than the method used by Rudie of including the effect of a radiant distribution given in heliocentric coordinates.

Comparisons between measured and predicted monthly-averaged daily cycles of meteors have answered some of the questions surrounding the validity of the various radiant distributions presented in Chapters 2 and 4. Comparisons between

measured and predicted cycles have shown that, for the purposes of predicting arrival rates of meteors, Rudie's distribution and Davies' extrapolated distribution are very similar. Comparisons between predicted and measured midpath and endpath cycles have shown that Pupyshev's yearly-averaged distribution appears most accurate for radiants close to the ecliptic plane. The apparent approximate nature of Pupyshev's monthly-averaged distributions has also been confirmed, with the predicted cycles based on the monthly-averaged distributions producing poor results. Although the predicted endpath results using Pupyshev's yearly-averaged distributions produced the best correlation overall, on average, Rudie's distribution or Davies' extrapolated distributions produced the best results for both the midpath and endpath predictions.

Some of the confusion regarding the expected annual variation in the arrival rate of meteors has been resolved. Comparisons between measured and predicted annual variations in the arrival rate of meteors have shown that the apparent annual variation in the space density of meteors is small. The results presented in this thesis tend to agree with results presented by *McKinley* [1961] and *Keay* [1963] and are in sharp contrast to recent predictions by *Weitzen* [1986].

Since it is clear that Rudie's distribution or Davies' extrapolated distribution are the best available distributions at present and a comprehensive, new set of radar measurements is probably required to more adequately characterize the distribution of meteors intercepting the earth, modern computer-based meteor prediction models are limited by Davies' original measurements. The significance of this limitation to the modelling of communication systems depends, naturally, on the application. Comparisons between predicted and measured arrival rates of meteors in Chapter 5 have shown that reasonable results can be obtained. However, the limitations of the radiant distributions become apparent when more detailed resolution is required from the distributions. In situations where knowledge of the relative contribution of parts of the meteor region is required, for example,

as in the design of optimum antenna illumination patterns, the reliability of the predictions is still uncertain. Bearing in mind the limitations of particular regions of the radiant distributions described in this thesis can, however, aid in reducing this uncertainty.

Appendix A

Area on the surface of a sphere

Given a unit sphere in polar coordinates

$$r = \cos\beta\cos\lambda\,\hat{i} + \cos\beta\sin\lambda\,\hat{j} + \sin\beta\,\hat{j}$$

The area on the surface bounded by the lines of longitude and latitude that pass through the points: $\lambda - \frac{\Delta\lambda}{2}, \lambda + \frac{\Delta\lambda}{2}, \beta - \frac{\Delta\beta}{2}$, and $\beta + \frac{\Delta\beta}{2}$ is

$$A = \int_{\beta-\frac{\Delta\beta}{2}}^{\beta+\frac{\Delta\beta}{2}} \int_{\lambda-\frac{\Delta\lambda}{2}}^{\lambda+\frac{\Delta\lambda}{2}} \left| \frac{\partial \boldsymbol{r}}{\partial\lambda} \times \frac{\partial \boldsymbol{r}}{\partial\beta} \right| d\lambda\, d\beta$$

$$= \int_{\beta-\frac{\Delta\beta}{2}}^{\beta+\frac{\Delta\beta}{2}} \int_{\lambda-\frac{\Delta\lambda}{2}}^{\lambda+\frac{\Delta\lambda}{2}} |\cos\beta|\; d\lambda\, d\beta$$

$$= \Delta\lambda \left| \sin\beta \right|_{\beta-\Delta\frac{\beta}{2}}^{\beta+\Delta\frac{\beta}{2}}$$

$$= 2\,\Delta\lambda \sin\Delta\beta\cos\beta$$

For $\Delta\beta \approx 0$, $\sin \Delta\beta = \Delta\beta$

Hence

$$A = 2\,\Delta\lambda\,\Delta\beta\cos\beta$$

References

Andrianov, N. S. and Pupyshev, Yu. A., 1972 "The Distribution of the Geocentric Velocities of Sporadic Meteors over the Celestial Sphere", Translation of *"Meteornoye Rasprostraneniye Radiovoln (Meteoric Propagation of Radio Waves)*, No. 7, Kazan' University Press, Kazan', 1970", NTIS N72-26720, pp 1-18.

Babadzhanov, P. B., Bibarsov, R. Sh., Getman, V. S., and Kolmakov, V. M., 1985, "The Incident Flux Density of Meteors According to Observations in Dunshanbe", *Solar System Res.*, Vol. 19, No. 4, pp 217-222.

Barton, M. and Burke, M., 1977, "SNOTEL: An Operational Data Acquisition System using Meteor Burst Technology", *Western Snow Conference*, April 18-21, 1977, Albuquerque, New Mexico, pp 1-10.

Brown, D. W. and Williams, H. P., 1978, "The performance of Meteor-Burst Communications at Different Frequencies", *AGARD Conference Proceedings*, Vol. 244.

Brown, D. W., 1985, "A Physical Meteor-Burst Propagation Model and Some Significant Results for Communication System Design", *IEEE Journal on Selected Areas in Communications*, Vol. SAC-3, No.5, pp. 745-755.

Burke, G. J. and Pogio, A. J., 1981, "Numerical Electromagnetic Code (NEC) - Method of Moments", *Lawrence Livermore Laboratory*, NOSC, Technical Document 116.

Cook, A. F., Flannery, M. R., Levy, H. II, McCrosky, R. E., Sekanina, Z., Shao, C. -Y, Southworth, R. B., and Williams, J. T., 1972, "Meteor Research Program", *Smithsonian Astrophysical Observatory*, NASA CR-2109.

Danby, J. M. A., 1970, "Fundamentals of Celestial Mechanics", *The MacMillian Company*, 866 Third Avenue, New York, New York, Third Printing 1970.

Davies, J. G., 1957, "Radio Observations of Meteors", *Advances in Electronics and Electron Physics*, Vol. 9, pp. 95-128.

Davies, J. G., Greenhow, J. S., and Hall, J. E., 1959, "The Effect of Attachment on Radio Echo-Observations of Meteors", *Proc Roy Soc A, Vol. 253, pp 130.*

Desourdis, R. I. Jr., Merrill, S. C., Wojtaszek, J. H. and Hernandez, K., 1988, "Meteor Burst Link Performance Sensitivity to Antenna Pattern, Power Margin and Range", *IEEE MILCOM 88*, pp 257-263.

Ellyett, C. D., 1977, "Solar Influence on Meteor Rates and Atmospheric Density Variations at Meteor Heights", *Journal of Geophysical Research*, Vol. 82, pp 1455-1462.

Ellyett, C. D. and Keay, C. S. L., 1961, "Southern Hemisphere Meteor Rates", *Monthly Notices of the Royal Astronomical Society*, Vol. 125, pp. 325-346.

Ellyett, C. D. and Keay, C. S. L., 1964, "Meteors: An Unexpected Increase in 1963", *Science*, Vol. 146, p 1458.

Ellyett, C. D. and Kennewell, J. A., 1980, "Radar Meteor Rates and Atmospheric Density Changes", *Nature*, Vol. 287, No. 5782, pp. 521-522.

Eshleman, Von R. and Manning, L. A., 1954, "Radio Communication by Scattering From Meteoric Ionization", *Proceedings of the IRE*, Vol. 42, pp. 530-536.

Eshleman, Von R., 1955, "Theory of Radio Reflections from Electron-Ion Clouds", *IRE Transactions on Antennas and Propagation*, pp 32-39.

Felber, F., Davis, H., Stahl, R., Wheeler, R. and Wright, D., 1985, "Concepts for Near Continuous Reception of VHF (Very High Frequency) Signals Using Meteor Burst Propagation", *JAYCOR*, San Diego, CA., Report No. JAYCOR-J200-85-875/2393.

Forsyth, P. A., Vogan, E. L., Hansen, D. R. and Hines, C. O.,1957, "The Principles of JANET - A Meteor-Burst Communication System", Proceedings of the IRE, Vol. 45, pp 1642-1657.

Haakinson, E. J., 1983, "Meteor Burst Communications Model", *NTIA Report 83-116*, US Department of Commerce, Springfield, VA.22161.

Hawkins, G. S., 1956, "Radio Echo Survey of Sporadic Meteor Radiants", *Monthly Notices of the Royal Astronomical Society*, Vol. 116, No. 1, pp 92-104.

Hines, C. O., 1955, "Diurnal Variations in the Number of Shower Meteors Detected by the Forward-Scattering of Radio Waves. Part I. Theory.", *Canadian Journal of Physics*, Vol. 33, No. 9, pp. 493-503.

Hines, C. O., 1956, "Diurnal Variations in Forward-Scattered Meteor Signals", *Journal of Atmospheric and Terrestrial Physics*, Vol. 9, No. 4, pp. 229-232.

Hines, C. O.and Pugh, R. E., 1956, "The Spatial Distribution of Signal Sources in Meteoric Forward-Scattering", *Canadian Journal of Physics*, Vol. 35, pp. 703-711.

Hines, C. O. and Forsyth, P. A., 1957, "The Forward-Scattering of Radio Waves from Overdense Meteor Trails", *Canadian Journal of Physics*, Vol. 35, pp 1033-1041.

James, J. C. and Meeks, M. L., 1956, "On the Relative Contributions of Various Sky Reqions to Meteor-Trail Communications", *Georgia Institute of Technology*, Atlanta, Georgia, Engineering Experiment Station, Naval Research Contract No. NOnr-991(02), Technical Report No. 1.

James, J. C., 1958, "The Influence of Meteor Radiant Distributions on Radio Echo Rates", *Georgia Institute of Technology*, Atlanta, Georgia, Engineering Experiment Station, Naval Research Contract No. NOnr-991(02), Technical Report No. 3, pp 1-105.

Kaiser, T. R., 1953, "Radio Echo Studies of Meteor Ionisation", *Phil. Mag.*, Vol. 2, pp 495-544.

Keay, C. S. L., 1963, "The Distribution of Meteors around the Earth's Orbit", *Monthly Notices of the Royal Astronomical Society*, Vol. 126, pp 165-176.

Keay, C. S. L. and Ellyett, C. D., 1968, "Southern Hemisphere Meteor Rates Final Report", NASA-CR-105828, NTIS N69-37252, 94p.

Kresákova, M. and Kresák, L., "On the Activity of Telescopic Meteors and Some Related Problems", *Contr. Astron. Obs. Skalnate Pleso*, Vol. 1, pp 40-77.

Larsen, J. D. and Rodman, P. J., 1988, "Study into Meteor Scatter Communication Systems", *Salbu (Pty) Ltd.*, P O Box 109, Irene, South Africa, Project IV, Part II, Vol.2.

Larsen, J. D., Melville, S. W. and Mawrey, R. S., 1990, "Adaptive Data Rate Capacity of Meteor-Burst Communications", *1990 IEEE Military Communications Conference*, Monterey California, Vol. 2, pp 863-867.

Linblad, B. A., 1967, "Solar Cycle Variations in Atmospheric Density as Deduced from Meteor Observations", *Space Research VII* (North Holland Publ. Co., Amsterdam), pp. 1029-1043.

Lovell, A. C. B., 1954, "Meteor Astronomy", *The International Series of Monographs on Physics*, Oxford University Press, London.

Mawrey, R. S., 1988, "A Meteor Scatter Measurement System", *M.Sc. Eng. Thesis*, University of Natal, Durban, South Africa.

Mawrey, R. S., 1990, "A Comparison between Predicted and Measured Annual Cycles of Meteors", *The Third South African IEEE Conference on Theoretical and Practical Work in Communications and Signal Processing (COMSIG 90)*, Johannesburg, IEEE Catalog No. 90TH0314-5, pp 32-37.

McCrosky, R. E. and Posen, A., 1961, "Orbital Elements of Photographic Meteors", *Smithsonian Contributions to Astrophysics*, Vol. 4, No. 2, pp 15-84.

McIntosh, B. A. and Simek, M., 1969, "Mass Distributions of Meteoroids Determined by Radar Observations of Underdense Meteor Trails", *Canadian Journal of Physics*, Vol. 47, No. 1, pp. 7-22.

McKinley, D. W. R., 1961, "Meteor Science and Engineering", McGraw-Hill, New York.

Melville, S. W., Larsen, J. D., Letschert, R. Y., and Goddard, W. D., 1989, "The Classification of Meteor Trail Reflections by a Rule-Based System", *Transactions of the South African Institute of Electrical Engineers*, Vol. 80, No. 1, pp 104-116.

Millman, P. M. and McIntosh, B. A., 1964, "Meteor Radar Statistics I", *Canadian Journal of Physics*, No. 42, pp. 1730-1742.

Millman, P. M. and McIntosh, B. A., 1966, "Meteor Radar Statistics II", *Canadian Journal of Physics*, No. 44, pp. 1593-1602.

Murakami, T., 1955, "On the Annual Variation of Sporadic Meteors. I and II", *Publ. Astron. Soc. Japan*, Vol. 7, pp 49-64.

Porter, F. G., 1952, "Comets and Meteor Streams", *The International Astrophysical Series*, Vol. 2, Chapman & Hall Ltd., London.

Pupyshev, Yu. A., Filimonova, T. K., and Kazakova, T. V., 1980, "Charts of the Distribution over the Entire Sky of the Visible Density of Radiants of Sporadic Meteors", taken from the book *Meteornoye Rasprostraneniye Radiovoln*, Kazan', Kazan' University Press, 112 pp.

Rodman, P. J., 1989, "A Microcomputer-based Meteor Burst Communications Prediction Modelling System", User Manual IBM PC Version 1.3, *Salbu (Pty) Ltd.*, P O Box 109, Irene, South Africa.

Rudie, N. H., 1967, "The Relative Distribution of Observable Meteor Trails in Forward-Scatter Meteor Communications ", *Ph.D. Thesis*, Montana State University.

Sachs, D., 1984, "Improvement of VHF (MB) Model", *Science Applications International Corporation*, La Jolle, CA., Report No. SAIC-84/1634.

Sekanina, Z., 1970 "Statistical Model of Meteor Streams 1. Analysis of the Model", *Icarus 13*, pp 459-474.

Sinno, K., 1979, "A Role for Metallic Ions of Meteor Origin in VHF Ionospheric Forward-Scattering and Further Contribution to the Formation of Sporadic-E", *Journal of The Radio Research Laboratories*, Vol. 26, No. 120/121, pp. 101-116.

Southworth, R. B. and Hawkins, G. S., 1963, "Statistics of Meteor Streams", *Smithsonian Contributions to Astrophysics*, Vol. 7.

Southworth, R. B. and Sekanina, Z., 1975, "Physical and Dynamical Studies of Meteors", *Smithsonian Institution*, Cambridge, Mass. 02138, NASA CR-2615.

Srirama Rao, M., Ratnam, S. R., Krishna Rao, D. A. V. and Bhagiratha Rao, E., 1983, "Survey of Meteor Signal Rates Observed over a VHF Forward-Scatter Link Between Waltair & Dehra Dun", *Indian Journal of Radio and Space Physics*, Vol. 12, No. 2, pp. 50-52.

Steffancin, W. and Brown, D., 1986, "CSC (Computer Sciences Corporation) Meteor Burst Model Enhancement Test Report", *Computer Sciences Corp.*, Falls Church, VA., Contract No. DCA100-84-C-0030, pp 1-51.

Sugar, G. R., 1964, "Radio Propagation by Reflection from Meteor Trails", *Proceedings of the IEEE*, Vol. 52, pp 116-136.

Svetashkova, N. T., 1987, "Density Variations of Meteor Flux along the Earth's Orbit", *Middle Atmosphere Program. Handbook for Map*, Vol. 25, NTIS N88-14545, pp 311-315.

Taylor, R. E., 1973, "136-MHz/400-MHz Radio-Sky Maps", *Proceedings of the IEEE (Letters)*, April, pp 469-472.

Verniani, F., 1965, *Smithsonian Contributions to Astrophysics*, Vol. 8, pp 141.

Vogan, E. L. and Cambell, L. L., 1957, "Meteor Signal Rates Observed in Forward-Scatter", *Canadian Journal of Physics*, Vol. 35, pp. 1176-1189.

Weiss, A. A., 1957, "Meteor Activity in the Southern Hemisphere", *Australian Journal of Physics*, Vol. 10, No. 2.

Weitzen, J. A., 1983, "Feasibility of High Speed Digital Communications on the Meteor Scatter Channel", *Ph.D. Thesis*, The University of Wisconsin - Madison.

Weitzen, J. A., 1986, "Predicting the Arrival Rate of Meteors Useful for Meteor Burst Communication", *Radio Science*, Vol. 21, No. 6, pp 1009-1020.

Yavus, D. Y., 1990, "Meteor Burst Communications", *IEEE Communications Magazine*, September, pp 40-48.